UCRL 231

UNIVERSITY OF CALIFORNIA

Radiation Laboratory

FOR REFERENCE

NOT TO BE TAKEN FROM THIS ROOM

BERKELEY, CALIFORNIA

DISCLAIMER

This document was prepared as an account of work sponsored by the United States Government. While this document is believed to contain correct information, neither the United States Government nor any agency thereof, nor the Regents of the University of California, nor any of their employees, makes any warranty, express or implied, or assumes any legal responsibility for the accuracy, completeness, or usefulness of any information, apparatus, product, or process disclosed, or represents that its use would not infringe privately owned rights. Reference herein to any specific commercial product, process, or service by its trade name, trademark, manufacturer, or otherwise, does not necessarily constitute or imply its endorsement, recommendation, or favoring by the United States Government or any agency thereof, or the Regents of the University of California. The views and opinions of authors expressed herein do not necessarily state or reflect those of the United States Government or any agency thereof or the Regents of the University of California.

UNIVERSITY OF CALIFORNIA
Radiation Laboratory

Cover Sheet
Do not remove

INDEX NO. UCRL-231
This document contains 61 pages
and 50 plates of figures.
This is copy 82 of 93 Series A

UNCLASSIFIED

[redacted]

Classification

Issued to UCRL

Each person who receives this document must sign the cover sheet in the space below

Route to	Noted by	Date	Route to	Noted by	Date

UCRL-231

Physics-General

UNIVERSITY OF CALIFORNIA

Radiation Laboratory

Contract No. W-7405-eng-48

PHYSICS DIVISION

QUARTERLY REPORT AUGUST 1, 1948 TO NOVEMBER 1, 1948

Classification changed to UNCLASSIFIED
by authority of Local Dedass RK Wakerling
on 4-3-52 B. Foskett
Date Person making change

November 30, 1948

CAUTION

This document contains information affecting the National Defense of the United States. Its transmission or the disclosure of its contents in any manner to an unauthorized person is prohibited and may result in severe criminal penalties under applicable Federal Laws.

Berkeley, California

Standard Distribution	Copy Nos.
Argonne National Laboratory	1-8
Armed Forces Special Weapons Project	9
Atomic Energy Commission, Washington	10-11
Battelle Memorial Institute	12
Brookhaven National Laboratory	13-20
Bureau of Ships	21
Carbide & Carbon Chemicals Corp. (K-25 Plant)	22-25
Carbide & Carbon Chemicals Corp. (Y-12 Plant)	26-29
Columbia University (Dunning)	30
General Electric Company, Richland	31-34
Hanford Operations Office	35
Iowa State College	36
Knolls Atomic Power Laboratory	37-40
Los Alamos	41-43
Mound Laboratory Destroyed 44A. 9-8-49	~~44~~-45
National Bureau of Standards	46-47
Naval Radiological Defense Laboratory	48
NEPA Project	49
New York Operations Office	50-51
North American Aviation, Inc.	52
Oak Ridge National Laboratory	53-60
Patent Advisor, Washington	61
Sandia Base	62-63
Technical Information Division, OROO	64-78
UCLA Medical Research Laboratory, (Warren)	79
University of California Radiation Laboratory	80-84
University of Rochester	85-86

Further distribution, University of California Radiation Laboratory

E. O. Lawrence ✓	87
Patent Department ✓	88
Chemistry Department ✓	89
J. G. Hamilton ✓	90
E. Segre ✓	91
J. H. Lawrence ✓	92
~~R. Ball~~ ns	~~93~~

~~B. Moyer~~ 12 Dest. 10-1-53

Total 93

Information Division
Radiation Laboratory
University of California
Berkeley, California

TABLE OF CONTENTS

I GENERAL PHYSICS RESEARCH

1.	Cloud Chamber Program	Page 4
2.	Film Program	6
3.	Theoretical Physics	11
4.	Nuclear Cross Sections for High Energy Neutrons as Measured with Bismuth Fission Chambers	13
5.	High Energy Particles Emitted During Neutron Bombardment of Various Nuclei	15
6.	90 Mev Neutron Differential Scattering Cross Section	16
7.	High Energy Gamma Rays from Cyclotron Target	17
8.	Isotope Analysis	18
9.	Scattering and Other Studies	22
10.	P-P Scattering Experiments in the Linear Accelerator	23
11.	Short Half Life Investigations in Linear Accelerator	24
12.	Inelastic Scattering of Protons	25
13.	The Detection of Light and Heavy Mesotrons Outside the Tank of the 184-inch Cyclotron	26

II ACCELERATOR AND CALUTRON OPERATION AND DEVELOPMENT

1.	184-inch Cyclotron	28
2.	60-inch Cyclotron	30
3.	Synchrotron	60
4.	Linear Accelerator	61
5.	Isotope Separation (In Supplement)	62

I. GENERAL PHYSICS RESEARCH

1. Cloud Chamber Program

Evans Hayward

Neutral Meson Experiment

An experiment was undertaken to try to detect the neutral meson which, according to some theories, should be produced as often as positive or negative π-mesons. This meson is supposed to have a life of about 10^{-12} seconds in which it decays into a pair of γ-rays, each carrying about 80 Mev. We have tried to detect such a pair of γ-rays with a cloud chamber. The 380 Mev deflected α-particle beam of the 184-inch cyclotron was directed at a carbon target in the center of a cloud chamber (Fig. 1). Presumably mesons, charged and neutral, were made in this target. A 1/4" lead plate was placed on either side of the target so that the γ-rays would each produce a small shower in the lead. Several runs were made but nothing that could be clearly described as a pair of high energy γ-rays was observed. The main difficulty seems to be that the α-particle beam produces secondaries in and near the cloud chamber. These are observed as electrons and protons near the plates from which it was hoped that the electron showers would come. This experiment has been abandoned until higher energy particles are available.

Delayed Neutrons

The measurement of the energy distribution of the delayed neutrons from O^{17} has been completed. When bombarded with 195 Mev deuterons, the elements just above oxygen in the period table yield delayed neutrons with a period of 4 seconds. The 4 second period is the half-life of the β-decay of N^{17}. Following the decay of N^{17}, O^{17} is left in an excited state. It immediately emits a neutron and becomes O^{16}. The width of the energy level in O^{17} may be determined by measuring the neutron energies. This has been done by measuring the ranges and scatter angles of their recoil protons in a hydrogen-filled cloud chamber. Neutron energies less than 0.5 Mev were not included nor were events that involved scatter angles greater than 30°.

Tracks of all ages have been included. The width of a track gives a rough estimate of its age. It has been assumed that all "new" tracks, those less than 0.1 cm wide, were produced by protons that traversed the cloud chamber after the expansion and that all those wider than 0.1 cm passed through before the expansion. In obtaining the energy from the proton range the expanded pressure was used for all "new" tracks and the compressed pressure for all the rest. This seems justifiable because if the data are divided into groups corresponding to different ages, all give essentially the same energy distribution. Figure 2 shows the neutron energy distribution for the old and for the new tracks; the dotted histogram represents sharp tracks. More weight should be attached to the new tracks than to the old, since their scatter angles can be measured to $\pm 1°$ whereas the old tracks were measured to only $\pm 3°$. The errors in the neutron energies have been estimated to be $\pm 6\%$ for diffuse tracks and $\pm 2\%$ for sharp ones.

Figure 3 is a histogram showing the actual numbers of neutrons in each energy interval, the total number being 391. Figure 4 shows the energy distribution after being corrected for the variation of the scattering cross section with energy. The curve looks as ugh the neutron has an energy of about 1 Mev but it should be pointed out that the high energy tail is real since it comes from proton recoils that have energies as high as 1.7 Mev. See Figure 5. The conclusion is that the most probable energy for this neutron is 1.06 Mev but that it can have as much as 1.7 Mev. The lower energy end of the curve is not so clearcut since the recoils responsible for it may be produced by neutrons that scatter first from the walls of the chamber

t re producing the knock-on in the gas. The energy level in O^{17} is either 0.7 Mev wide or there is indeed more than one level from which the neutrons may come.

Deuterons

Some of the counter experiments of H. F. York led us to suspect that deuterons may be produced when the 90 Mev neutrons interact with nuclei. Some of the cloud chamber pictures taken in connection with the n-p scattering experiment were examined. The curvatures of those tracks that originated in the 5 mil aluminum window and were directed within $\pm 15^{\circ}$ of the neutron beam were measured. The histogram in Figure 6 shows the energy distribution of 186 particles under the assumption that they are all protons. The energy distribution of the incident neutrons that was obtained in the n-p scattering experiment cannot explain the peak near 150 Mev. These particles have been identified as deuterons, because their curvatures are too small for protons knocked on by neutrons of this energy and also because they appear to be slightly more heavily ionizing than other high energy tracks in the same region of the cloud chamber. This group makes up 20% of the total number of particles.

In order to make certain that deuterons were being observed, another experiment has been started to measure the energy and angular distribution of the ionizing particles that come out of carbon when it is bombarded by high energy neutrons. A 1/8" carbon target and a 1/4" glass absorber were placed eight inches apart in a 22 inch cloud chamber (Fig. 7). The particles that come out of the carbon and go into the absorber are being investigated. If they have enough energy to traverse the plate, then their mass is determined by their curvature on either side of the absorber. The magnetic field is 21,700 gauss so that errors in curvature measurement are small. Only a few photographs have been analyzed but these indicate that protons and deuterons come out in practically equal numbers. There is also some evidence that H^3, He^3, and α-particles are also emitted.

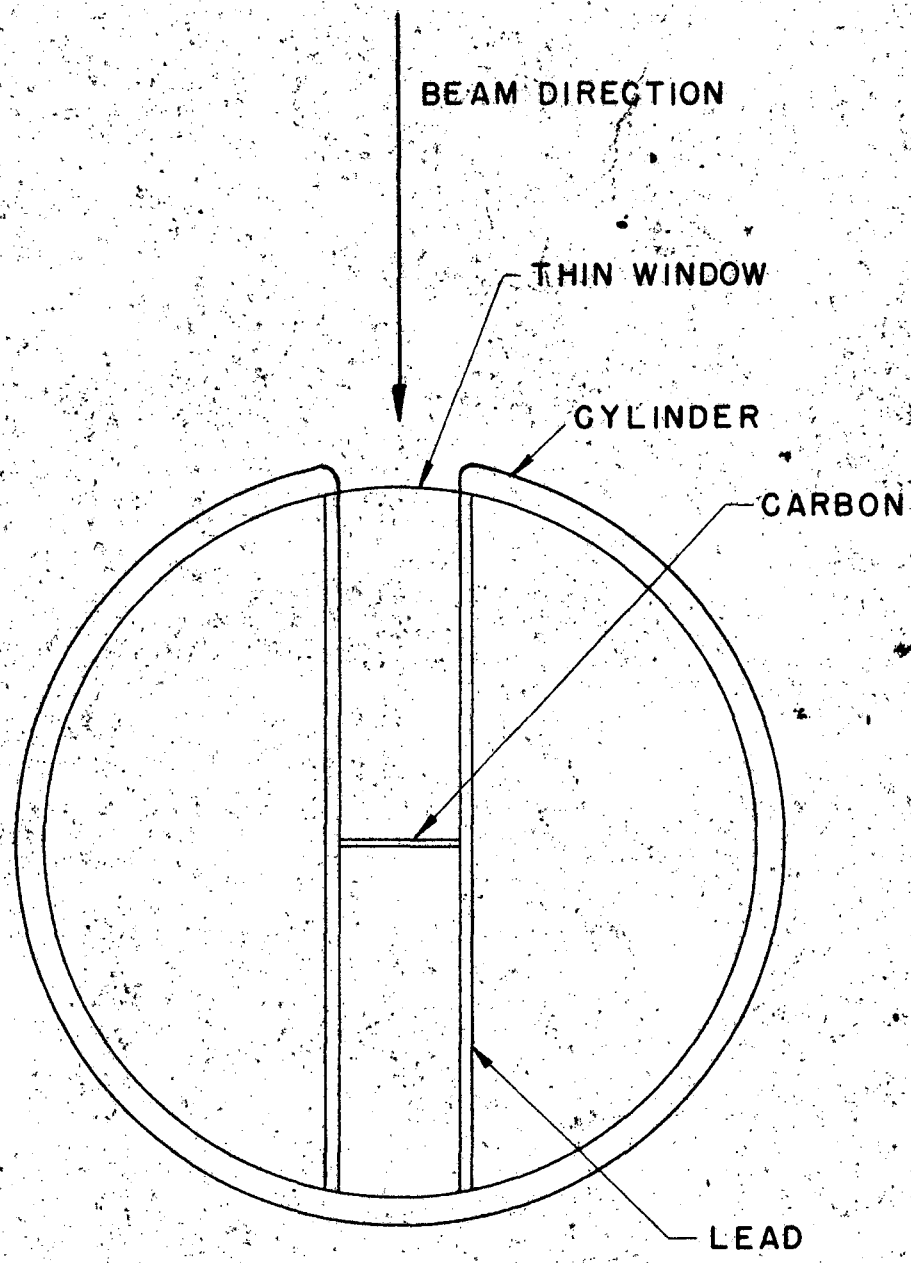
BEAM DIRECTION
THIN WINDOW
CYLINDER
CARBON
LEAD

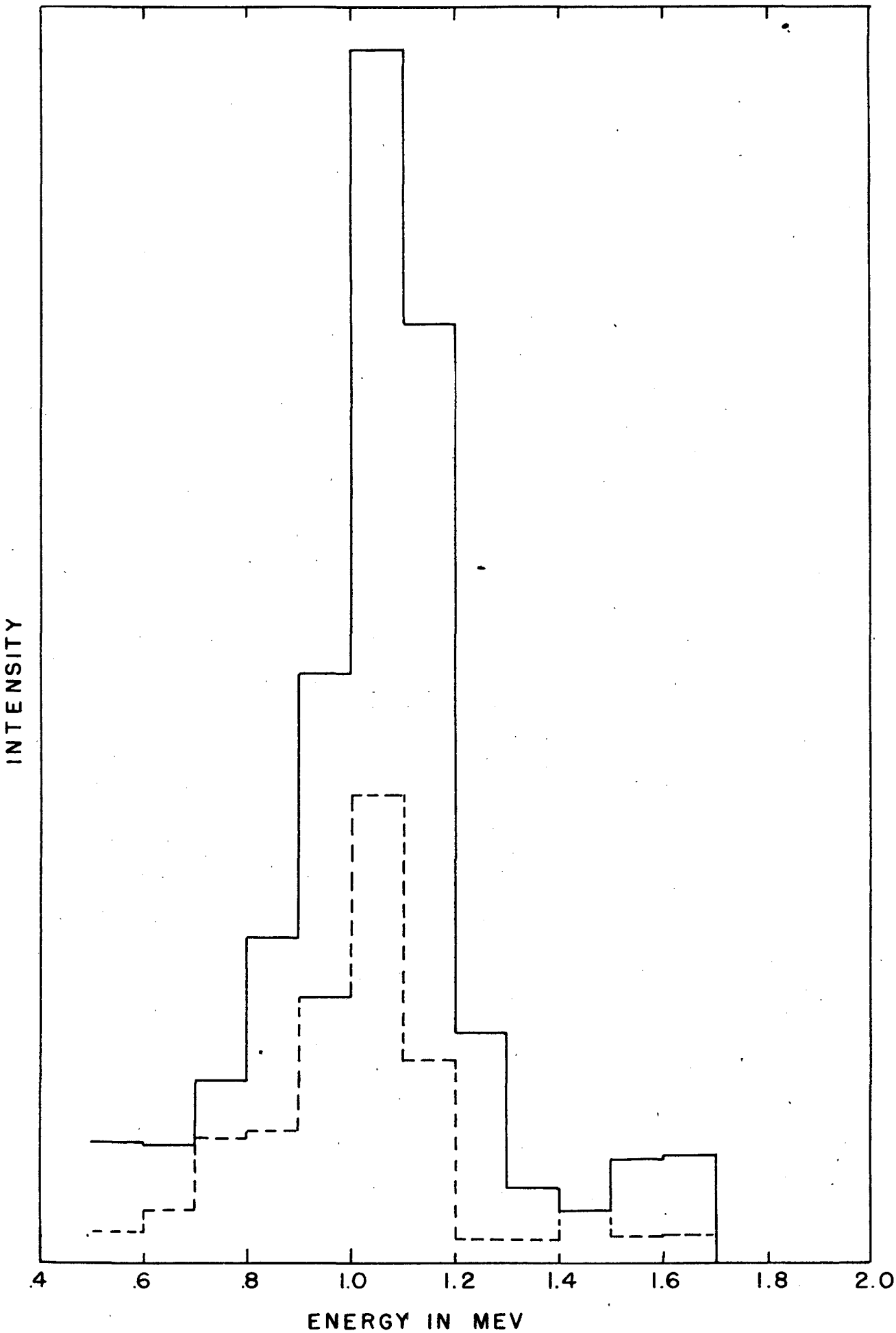

FIG. 2

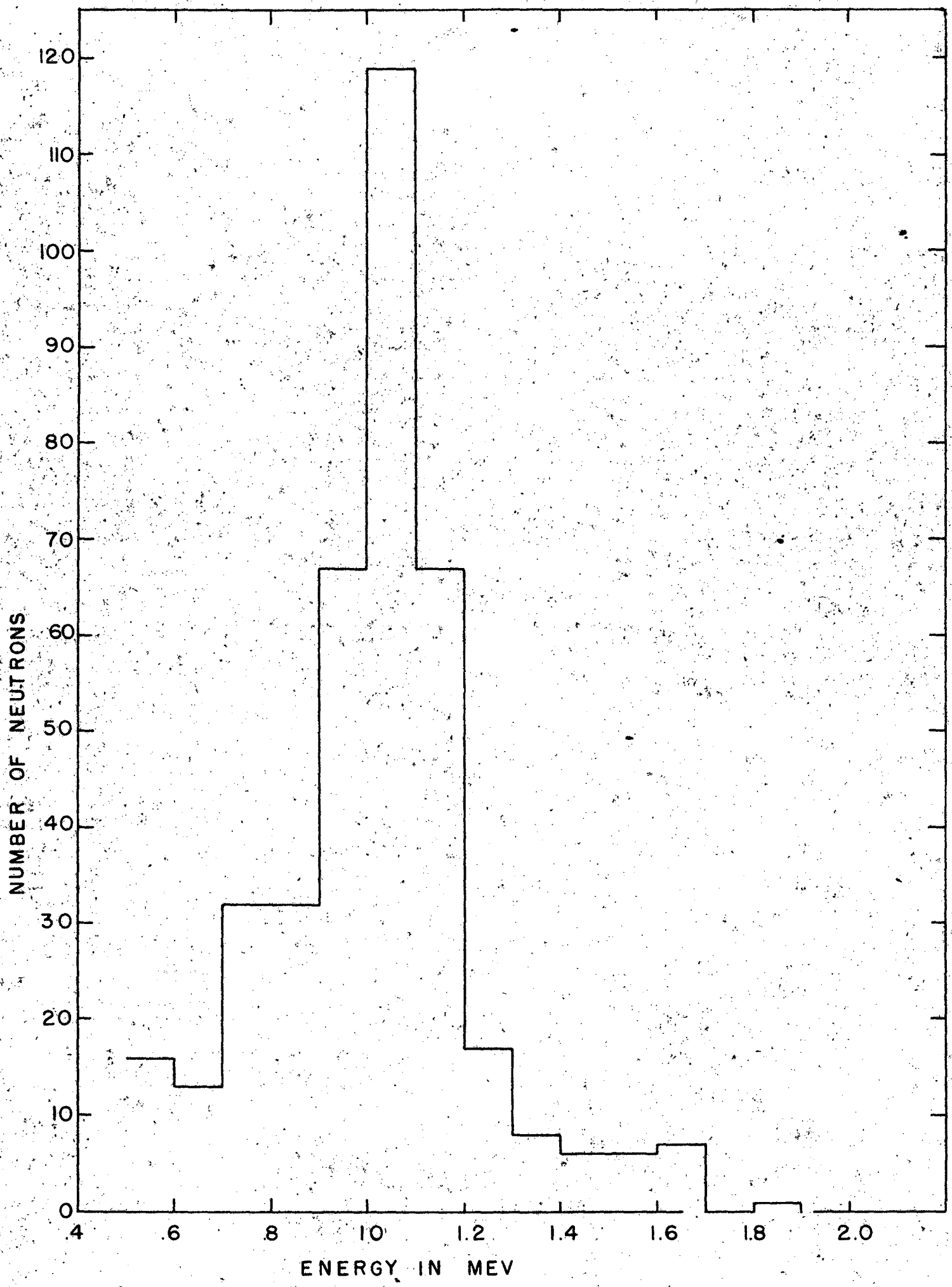
NUMBER OF NEUTRONS
0
10
20
30
40
50
60
70
80
90
100
110
120
.4
.6
.8
1.0
1.2
1.4
1.6
1.8
2.0
ENERGY IN MEV

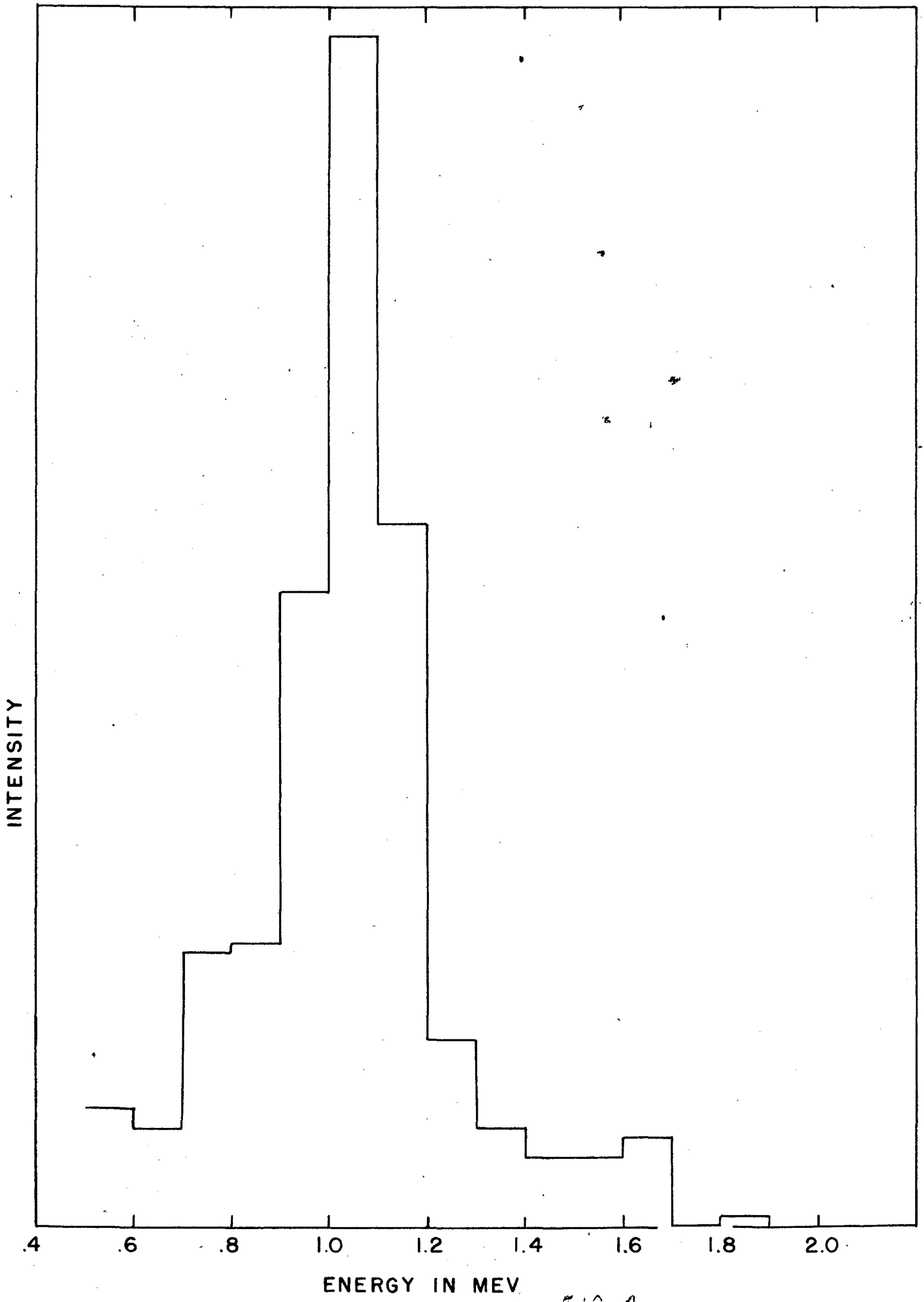

FIG. 4.

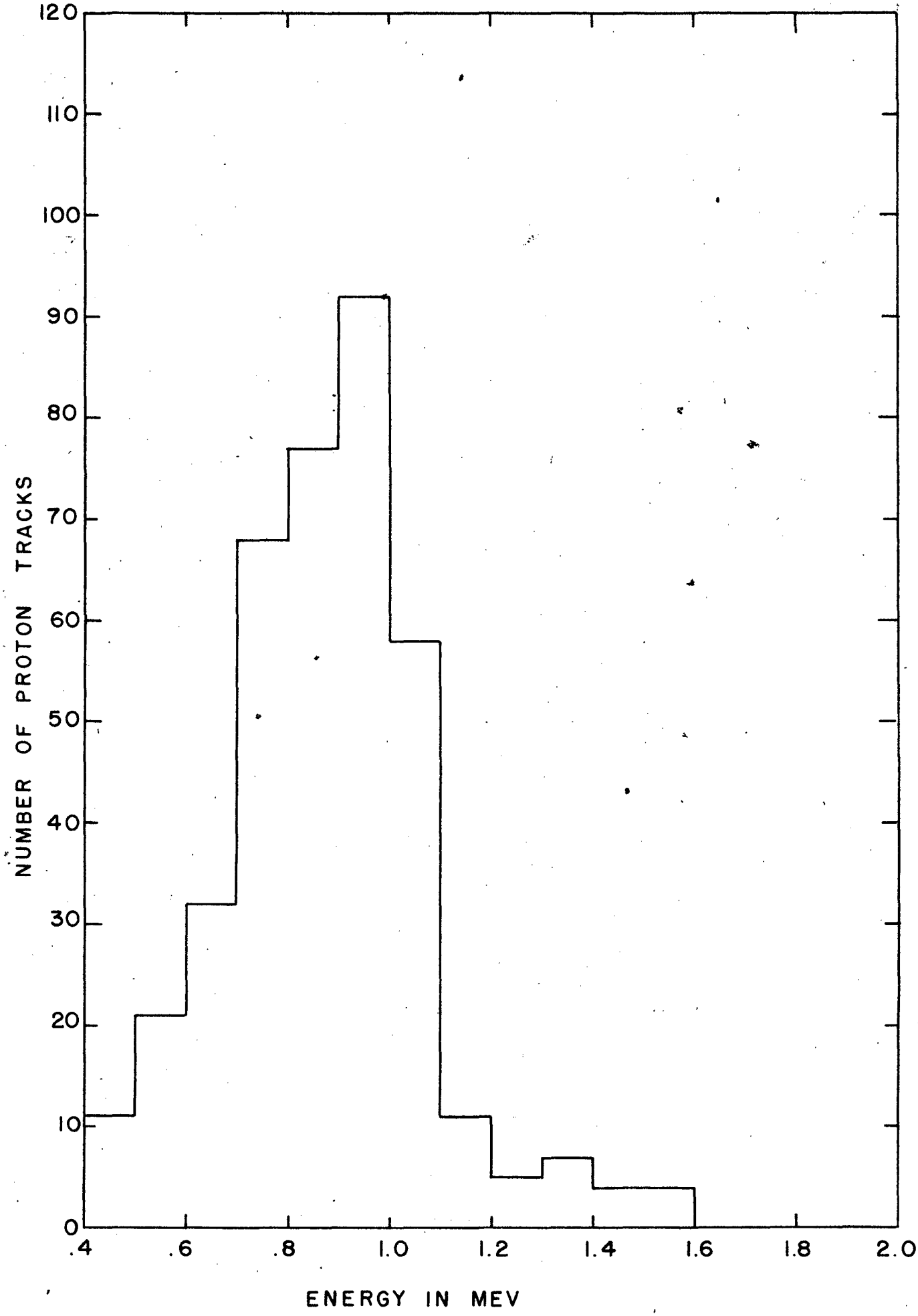
120
110
100
90
80
70
60
50
40
30
20
10
0
NUMBER OF PROTON TRACKS
.4
.6
.8
1.0
1.2
1.4
1.6
1.8
2.0
ENERGY IN MEV

FIG. 5

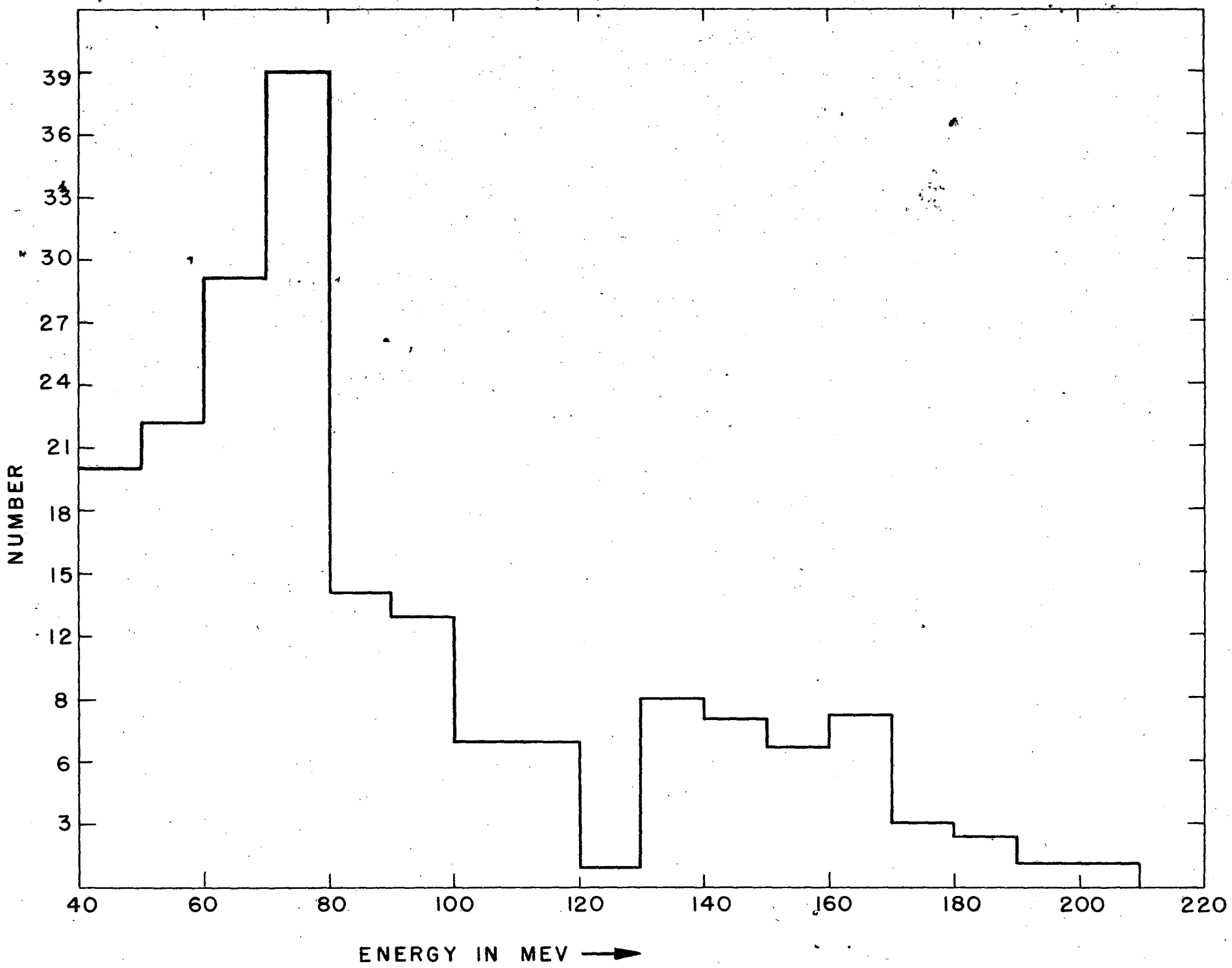
NUMBER
39
36
33
30
27
24
21
18
15
12
8
6
3
40
60
80
100
120
140
160
180
200
220
ENERGY IN MEV

FIG 6

13100

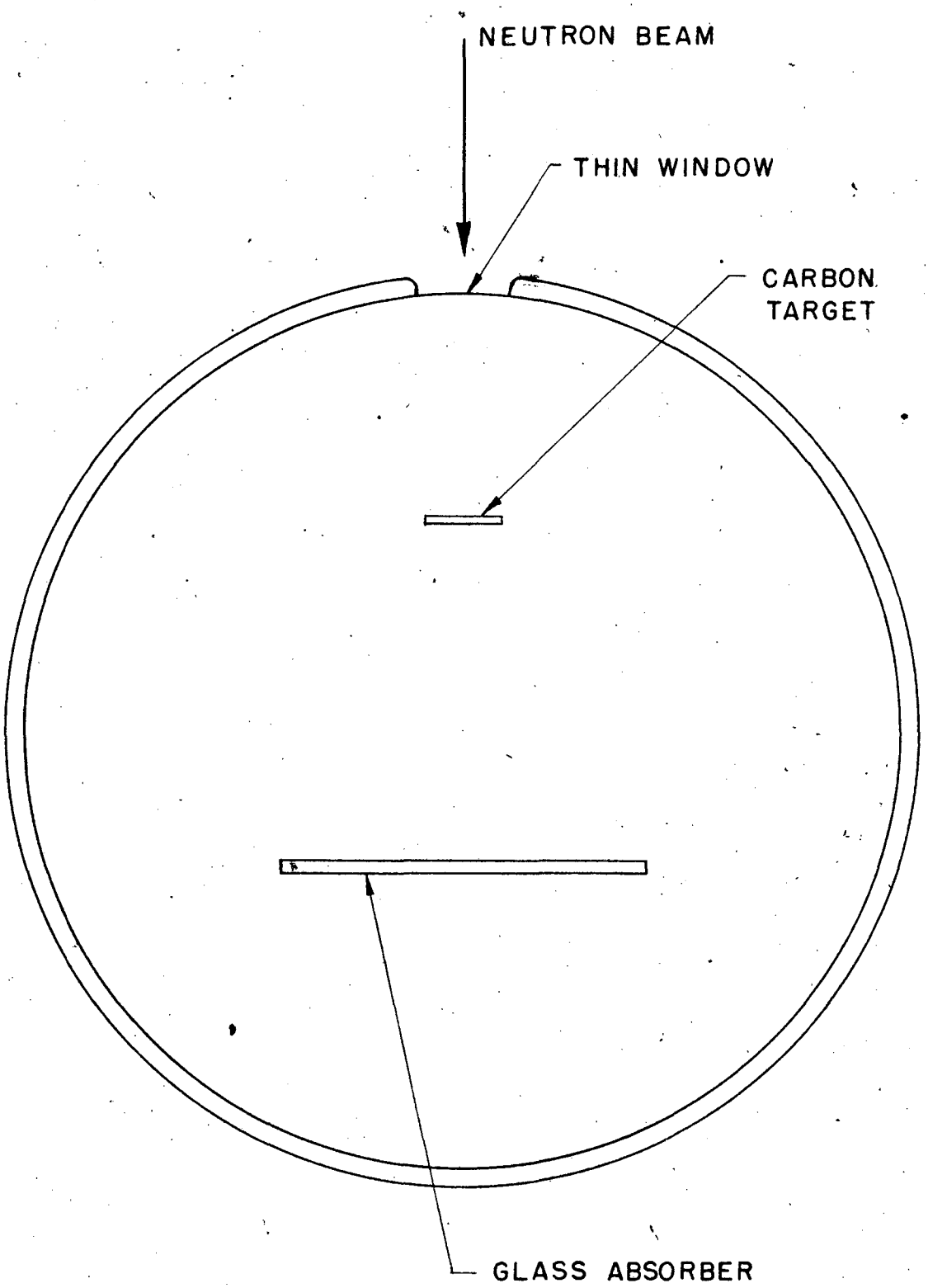

FIG. 4

13102-1

2. Film Program

Eugene Gardner

Meson Mass Measurements

A study is now in progress to find the masses of mesons produced by 380 Mev alpha-particles in the 184-inch Berkeley cyclotron. Although the work has not yet been completed, we can describe the method and the apparatus and give some preliminary mass values.

The method consists of measuring the radius of curvature of a meson trajectory in the magnetic field of the cyclotron and the range of the meson in photographic emulsion. If we assume that the meson has a charge of one electron charge, then the classical formula for the energy in terms of the radius of curvature in the magnetic field is

$$E = \frac{e^2}{2mc^2}(H\rho)^2 \qquad (1)$$

For the range in photographic emulsion there is an empirical range-energy relation of the form

$$E = k\, m^{1-n} R^n \quad . \qquad (2)$$

The values of k and n in this equation have been found by extrapolation from the values given by Lattes, Fowler and Cüer[1]. From Equations (1) and (2) it is possible to find values of E and m, since all other quantities are known or measurable. A small relativistic correction is applied to the result.

Description of Apparatus

The mesons are produced when the circulating beam of 380 Mev alpha-particles strikes an internal target. The position of the target in the cyclotron is shown in Fig. 1. Photographic plates are placed as shown in Figs. 2 and 3. The target shown in Fig. 2 is a "flat" target used in early experiments. It was usually made of carbon 1/16 inch thick. This type of target has been superseded by the "ribbon" target shown in Fig. 3. The objection to the flat target is that the distance from the plate to the point at which the meson originates is not known accurately. The results given in this paper are based on plates exposed with ribbon targets. Ordinarily the ribbon targets are made of beryllium and have a cross section of 1/32 inch by 1/16 inch, the 1/16 inch dimension being in the direction of the beam.

The radius of curvature of a meson trajectory is calculated from the position on the plate at which the track is found and the direction which the track makes with the normal to the edge of the plate. In Fig. 4, if AB is the distance from the target to the point at which the meson track is found, then the radius of curvature ρ, is given by

$$\rho = \frac{AB}{2 \cos \theta} \qquad (3)$$

For an error $\Delta\theta$ in the measurement of θ, the corresponding fractional error in ρ is given

$$\frac{\Delta\rho}{\rho} = \tan\theta\, \Delta\theta \quad . \qquad (4)$$

Thus the error in ρ is smallest for small θ, and the best tracks to use for mass determination are those which are approximately normal to the edge of the plate. Another advantage in using tracks of small θ is that the corrections for the non-uniformity of the magnetic field are easier to make.

A convenient arrangement for rejecting mesons whose trajectories make angles greater than about 10° with the normal to the edge of the plate is shown in Fig. 5. When the plates are exposed in this "channel" plate holder all of the meson tracks found can be used for mass measurements and it is not necessary to study large numbers of tracks in order to find a few which will be suitable. The channel serves only to reject unwanted mesons; its dimensions do not enter the calculation of radii of curvature.

For mass measurements of positive mesons, the apparatus was arranged as shown in Fig. 6. Mesons are received which leave the target in a direction opposite to beam direction, the arrangement being similar to that described in an earlier paper[2]. As with the experiments with negative mesons, a channel was used which accepted only those mesons whose trajectories made small angles with the normal to the edge of the plate. It was found that masses of both heavy and light mesons could be measured with this apparatus.

In the early experiments it was customary to wrap the photographic plates in black paper or aluminum foil to prevent exposure to light. The mass measurements based on wrapped plates are unsatisfactory for the following reasons:

(1) If the mesons are scattered in the wrapping material, the measurement of θ as shown in Fig. 4 will be in error, and hence there will be an error in the value of ρ calculated from Equation (3).

(2) When the plates are wrapped, the position of the plates with respect to the target is not known with precision. There is an uncertainty in the position of the plates inside the package, and there is also an uncertainty in the position of the package as a whole with respect to the target.

(3) In the case of the black paper the thickness is variable; and there is no way to tell whether the meson went through a thick part or a thin part. This contributes to the error in the measurement of the range.

For the measurements described in this paper the plates were used without wrapping. The plates were put into the cyclotron while the room was nearly dark, the only source of illumination being a photographic safelight. The concrete shielding of the 184-inch cyclotron provides a convenient enclosure which admits little light from the outside. We had very little trouble with light-struck plates; apparently neither the arc of the cyclotron ion source nor the random discharges from the dee provides enough light to spoil the plates.

The method of measuring the distance from the target to the meson track is to put a fiducial mark on the plates at a known distance from the target. Distances are then measured from the meson tracks to the fiducial mark. The fiducial mark is put on by means of a "marker" shown in Fig. 7. The marker has a slit with a small light globe behind it. A metallic contact point C is at a known fixed distance from the slit. When the point C makes electrical contact with the ribbon target, the light globe is turned on for a few seconds. After the plates have been developed and are viewed under a microscope, the fiducial mark is seen as a dark line.

Two different arrangements of plates have been used in connection with plate holders of the type shown in Figs. 2, 3, 5, and 6:

(1) Stacks of plates with each plate horizontal, as shown in Fig. 8. The mesons enter the edge of the emulsion. A piece of plain glass is ordinarily placed on the top of the stack in order that the top emulsion will have a glass covering.

(2) Plates inclined at angles of 5° or 10°, arranged so that mesons strike the top of the emulsion. This is illustrated in Fig. 9.

In order to show the order of magnitude of the numbers of tracks found per plate we have listed in Table I approximate values for the various types of exposures. The numbers given correspond to the use of plates with emulsion thickness 100 microns and an exposure time of 10 minutes with an alpha-particle current of the order of 0.1 microampere. Exposures are ordinarily limited to about this length in order that the background of proton and alpha-particle tracks will not interfere seriously with the study of the meson tracks.

Study of the Plates

The plates were examined under the microscope with a 2 mm apochromatic objective (oil immersion) and an X6 eyepiece. Meson tracks are distinguished by a characteristic grain density change along the track and a characteristic wandering associated with small angle scattering. This wandering makes it necessary to measure the length of the track in sections. The lengths of sections of the track are measured by comparing them with a scale in the eyepiece, which is calibrated by means of a stage micrometer. Successive measurements of the range of the same track are consistent within about 1 per cent.

When exposures are made with the plates inclined as shown in Fig. 9 the mesons enter the emulsion through the upper surface, and there is no difficulty in deciding where the tracks start. When the plates are exposed in a stack as shown in Fig. 8 the mesons enter the emulsion at the edge, and a difficulty arises from the fact that the edge of the emulsion suffers a contraction during processing. This contraction, illustrated in Fig. 10, results in a deformation of the meson track. The straight track ABC is distorted into the track ABD. The portion BC is of the order of 50 or 20 microns, respectively, for the emulsions of thickness 100 or 50 microns. For the measurements made for this paper we used the following convention. The length of the meson is measured up to where the deformation starts. Then, by placing the scale parallel to the direction of the track in the last non-deformed part of the track the range is extrapolated on the assumption that the meson entered the emulsion at the point where the scale crosses the edge of the glass. It is assumed that before processing the emulsion actually was uniform up to the edge of the glass. A comparison of results obtained with plates of different emulsion thickness confirms the correctness of this assumption. The inclined plates avoid difficulties associated with the edges of the emulsion, and hence are more satisfactory for range measurements than the stacked plates. The results given in this paper are all taken from inclined plates. The advantage of the stacked plates is that the mesons are concentrated at the edge of the plate and are therefore easier to find. The density of mesons is about ten times as large as for the inclined plates. This makes the stacked plates useful for survey experiments and order of magnitude estimates.

For plates run in the inclined position, the angle which the meson trajectory makes with the normal to the edge of the plate is measured by setting a cross-hair in the eyepiece parallel to the meson track at the point of entrance into the emulsion. The angle is then read on a goniometer. For stacked plates the angle is measured in the non-deformed region. The results of successive measurements of the same track are consistent to within about 1°.

Preliminary Mass Values

Preliminary values for the meson masses are as follows:

Heavy negative meson: 285 m_e
Heavy positive meson: 286 m_e
Light positive meson: 216 m_e

where m_e is the mass of the electron. The value of 285 m_e for the mass of the heavy negative

ion supersedes the value of 313 ± 16 m_e given in an earlier paper[3]. When this study is completed, it is hoped that the probable error of the mass determinations will be as low as ± 2 per cent; however, the preliminary values given above do not have this accuracy.

The ratio of masses of heavy positive to light positive mesons is 1.31. This ratio is consistent with the assumption that a light particle (e.g., a neutrino or a gamma-ray) is given off when a heavy positive meson decays into a light one.

References

1. C. M. G. Lattes, P. H. Fowler, P. Cüer, Proc. Phys. Soc., 59, 883 (1947).

2. J. Burfening, E. Gardner, and C. M. G. Lattes, Phys. Rev., Jan. 15, 1949.

3. E. Gardner and C. M. G. Lattes, Science 107, 270 (1948).

Table I. Numbers of Mesons Found in Various Types of Exposures

Type of Exposure	Diagram	Radii of Sides of Channel	Area of Plate Used	Number of Mesons Per Plate
Heavy negative mesons without channel	Fig. 3	-	3 inches x 1 mm (leading edge of plate)	100-200
Heavy negative mesons with channel Stacked plates	Fig. 5 Plates stacked as shown Fig. 8	2-1/2 inches 3-1/2 inches	1 inch x 1 mm (leading edge of plate)	5-10
Heavy negative mesons with channel Inclined plates	Fig. 5 Plates inclined as shown Fig. 9	2-1/2 inches 3-1/2 inches	1 inch x 1 inch (surface of plate)	100-200
Total heavy positive and light positive mesons without channel	Fig. 6 without channel	-	3 inches x 1 mm (leading edge of plate)	10-20
Total heavy positive and light positive mesons with channel	Fig. 6	1-3/4 inches 2-3/4 inches	1 inch x 1 mm (leading edge of plate)	1/2-1

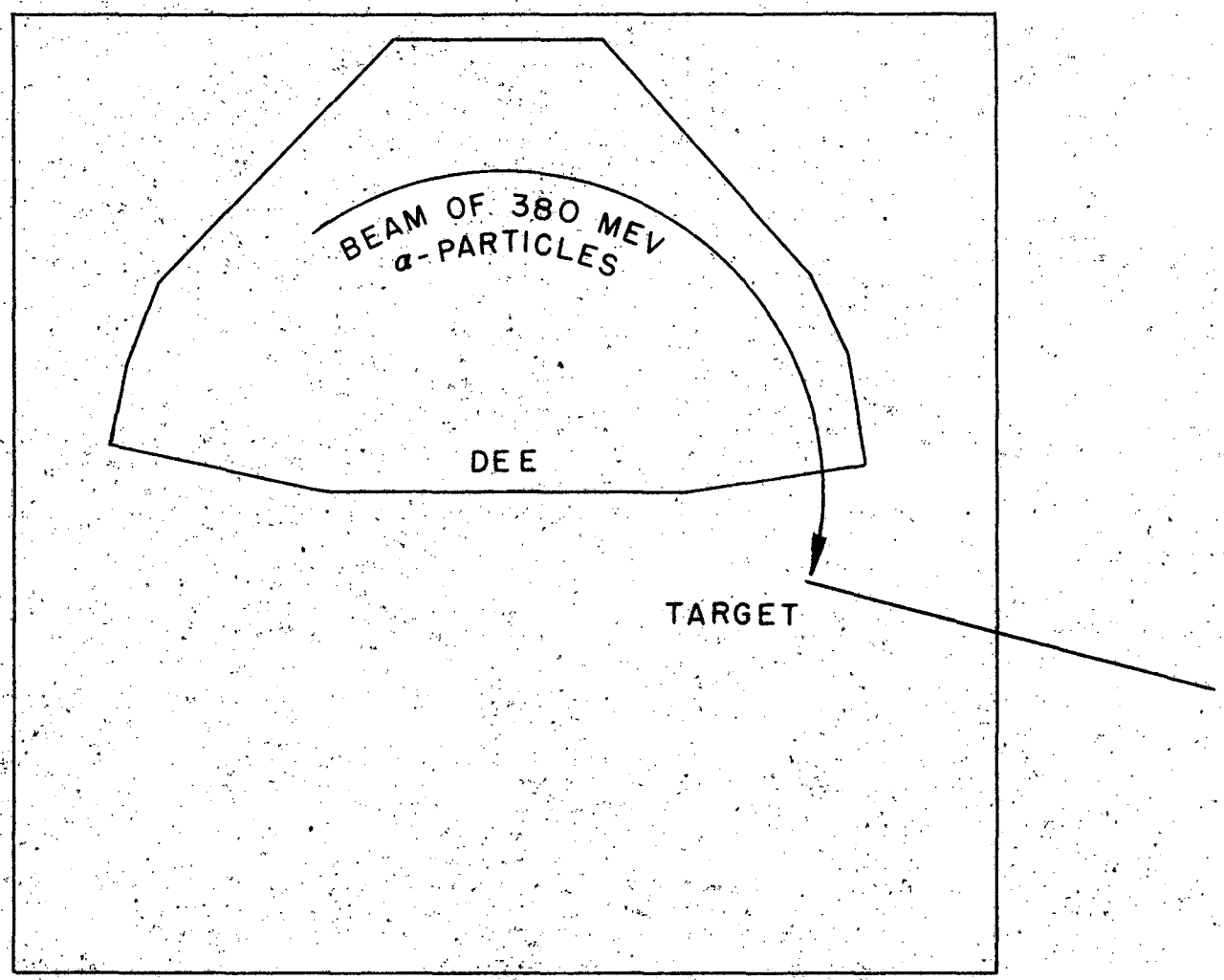

PLAN VIEW OF CYCLOTRON

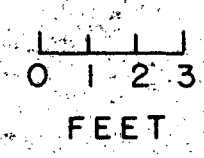

FIG 1

12972-1

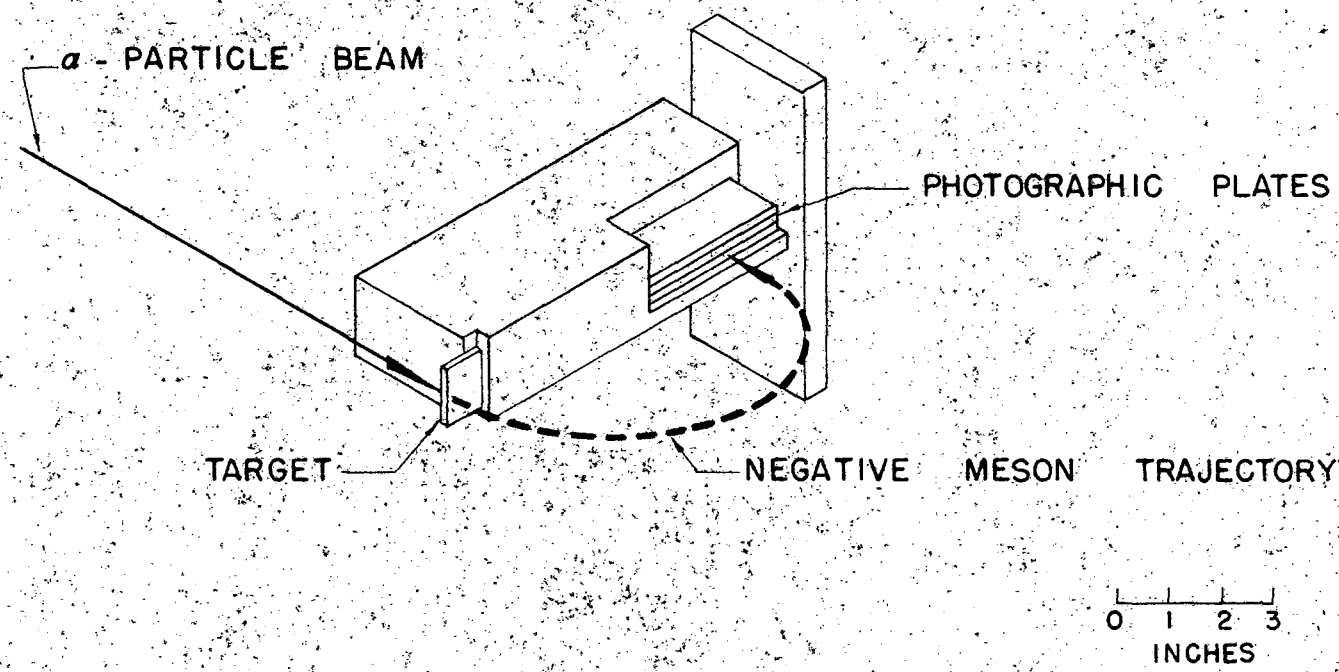
α - PARTICLE BEAM
PHOTOGRAPHIC PLATES
TARGET
NEGATIVE MESON TRAJECTORY
0 1 2 3
INCHES

FIG 2

13093-1

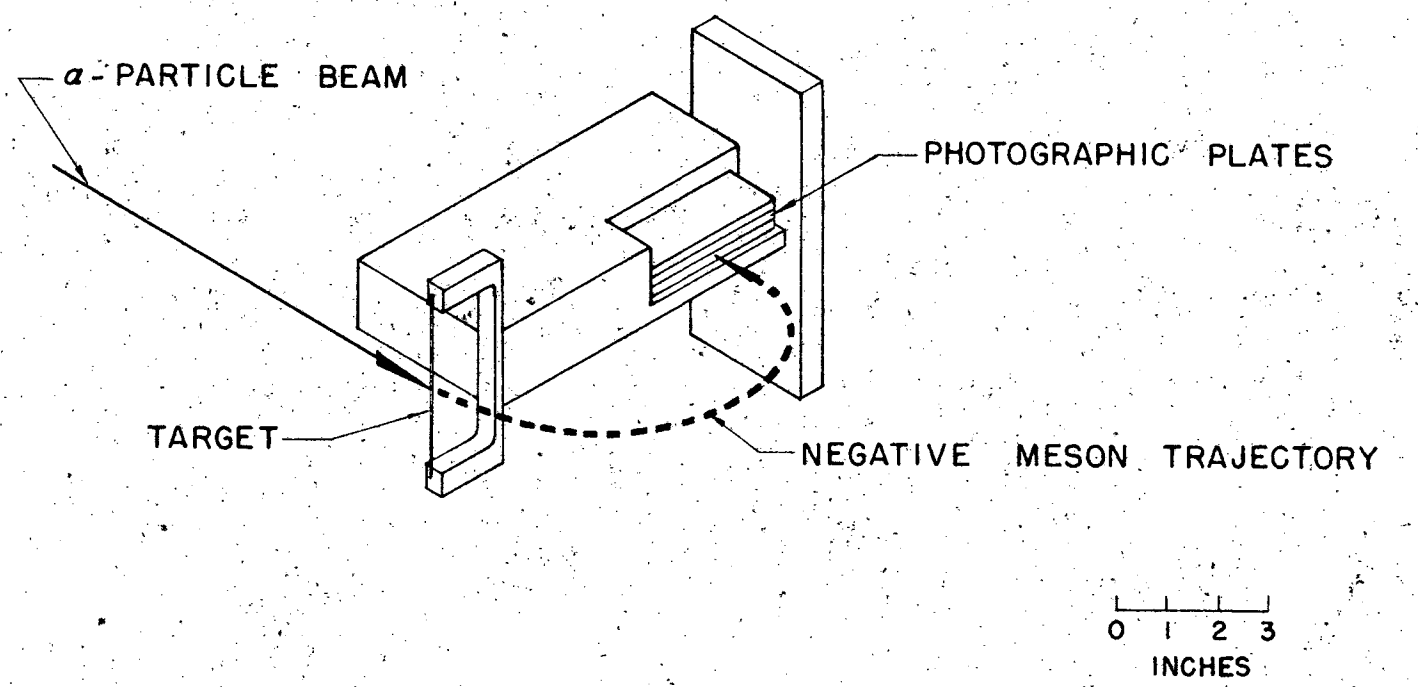
α-PARTICLE BEAM
PHOTOGRAPHIC PLATES
TARGET
NEGATIVE MESON TRAJECTORY
0 1 2 3
INCHES

FIG 3

13094

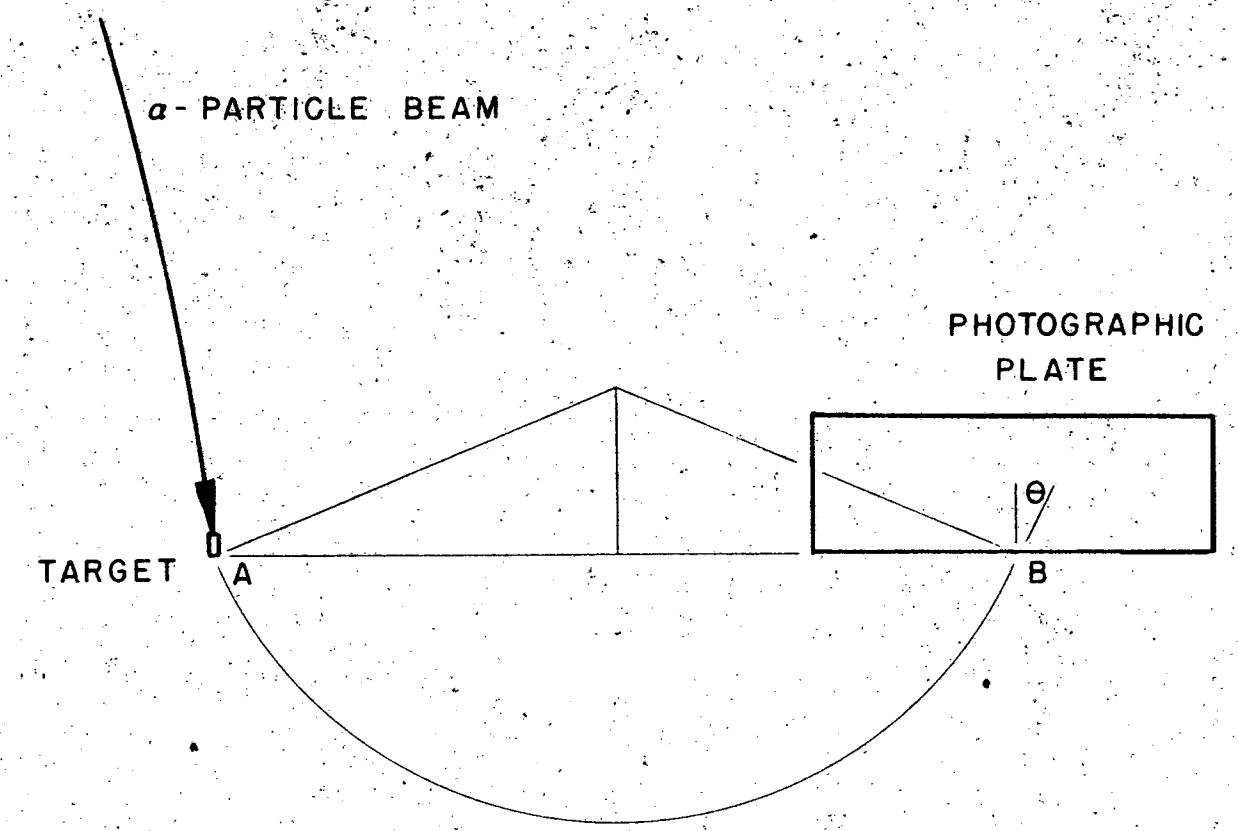

FIG 4

13123-1

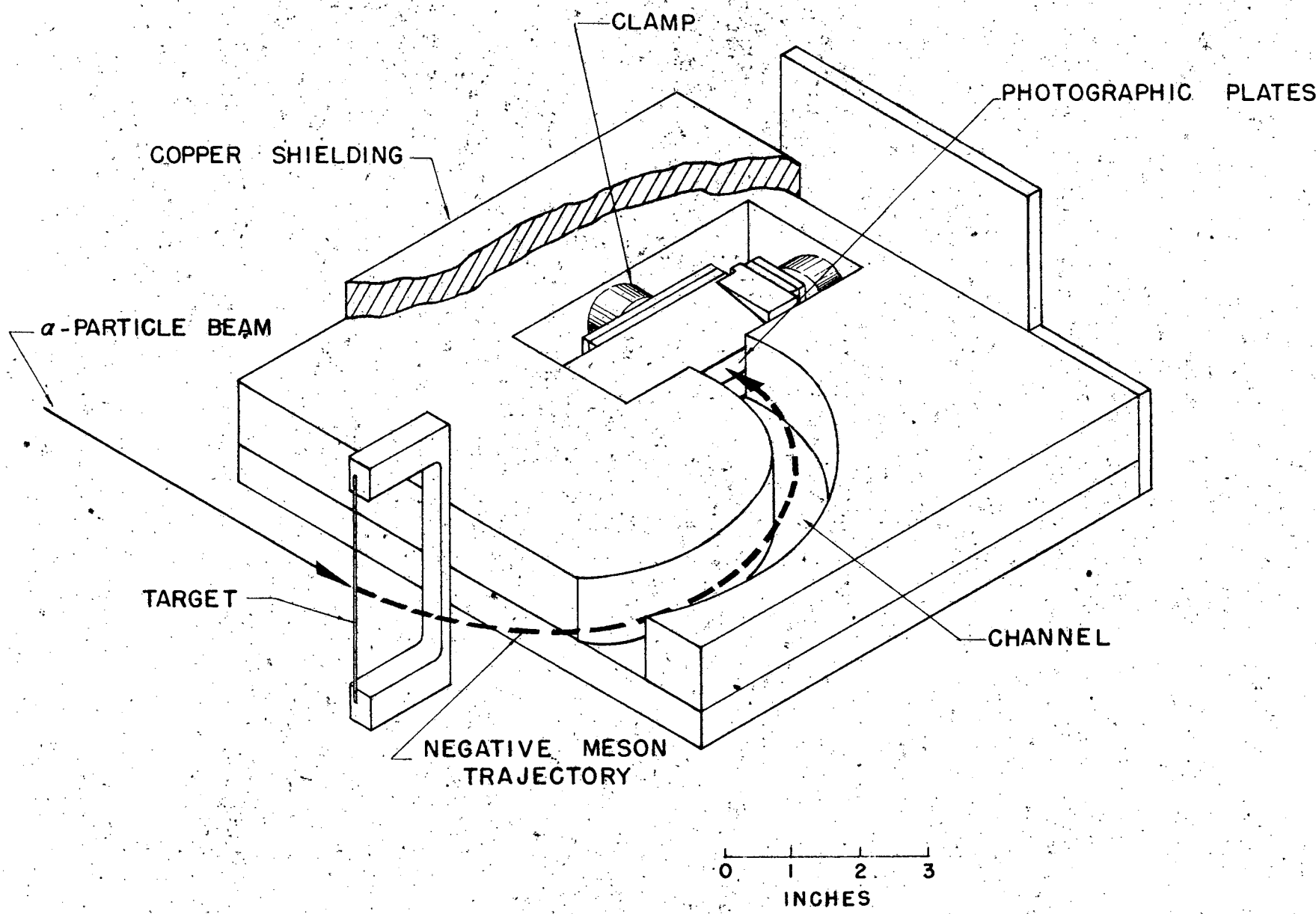
CLAMP
PHOTOGRAPHIC PLATES
COPPER SHIELDING
α-PARTICLE BEAM
TARGET
CHANNEL
NEGATIVE MESON TRAJECTORY
0 1 2 3
INCHES

FIG 5

13095-1

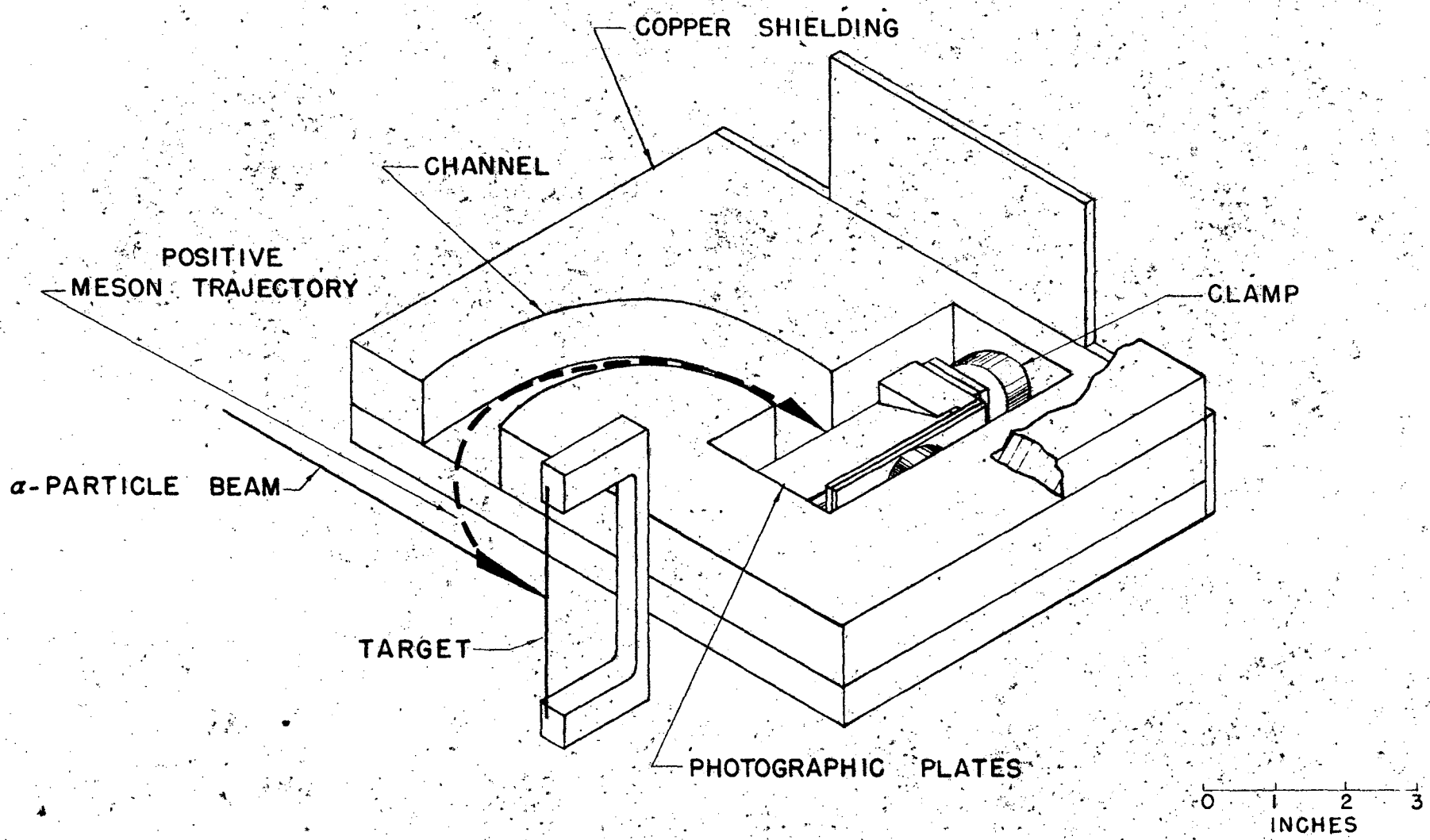
COPPER SHIELDING
CHANNEL
POSITIVE
MESON TRAJECTORY
CLAMP
α-PARTICLE BEAM
TARGET
PHOTOGRAPHIC PLATES
0 1 2 3
INCHES

FIG 6

13099-4

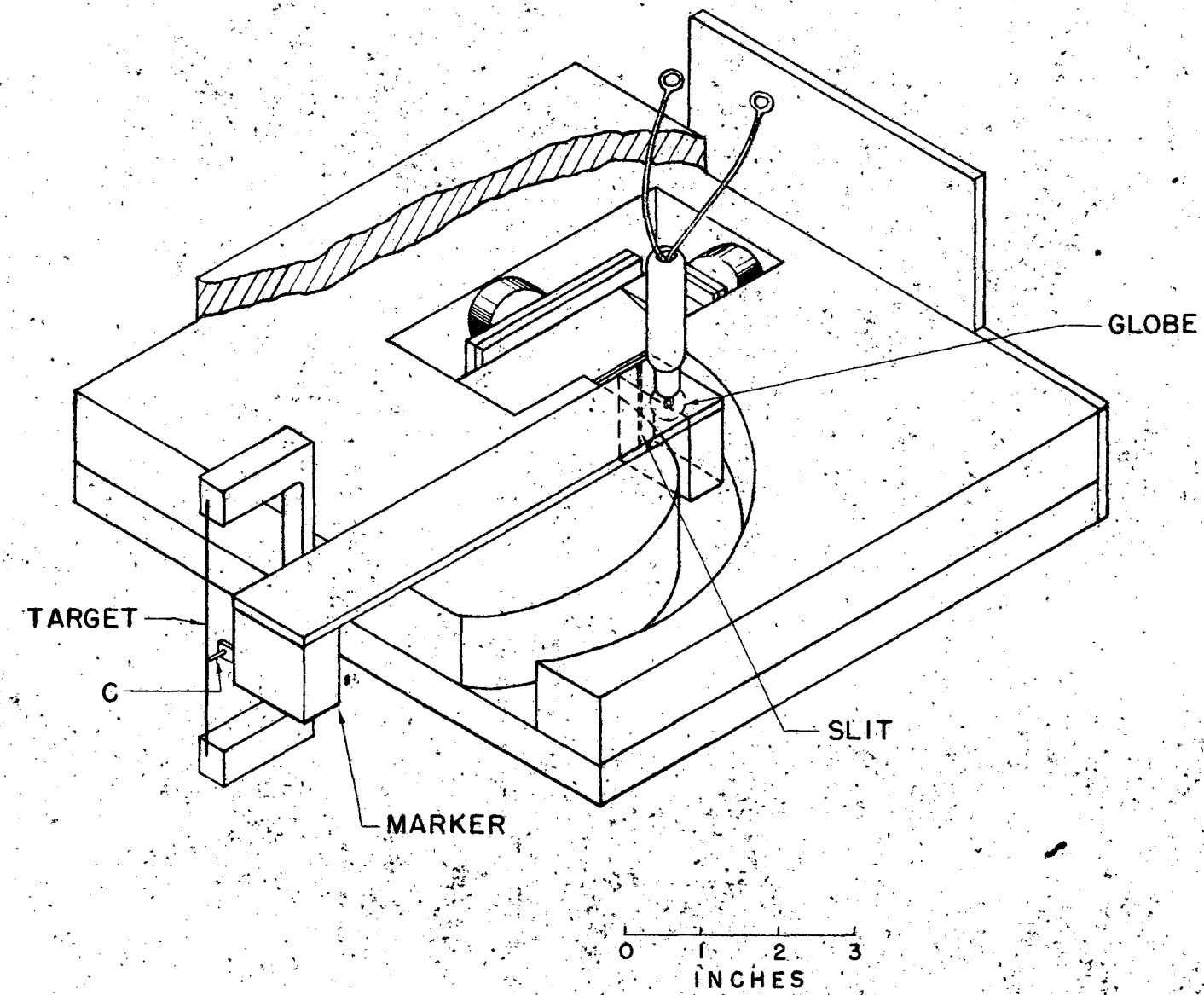

FIG 7

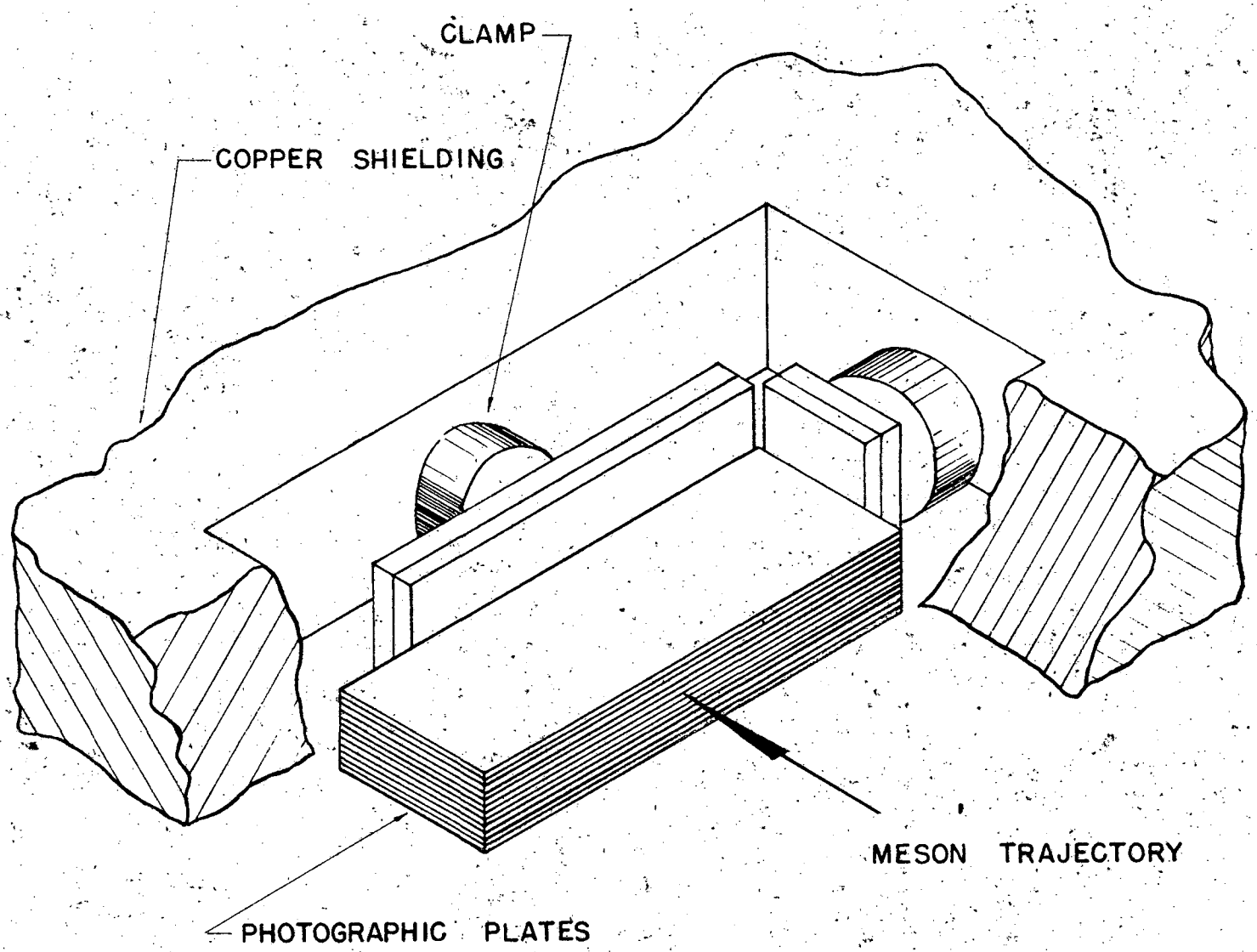

FIG 8

13097-IV

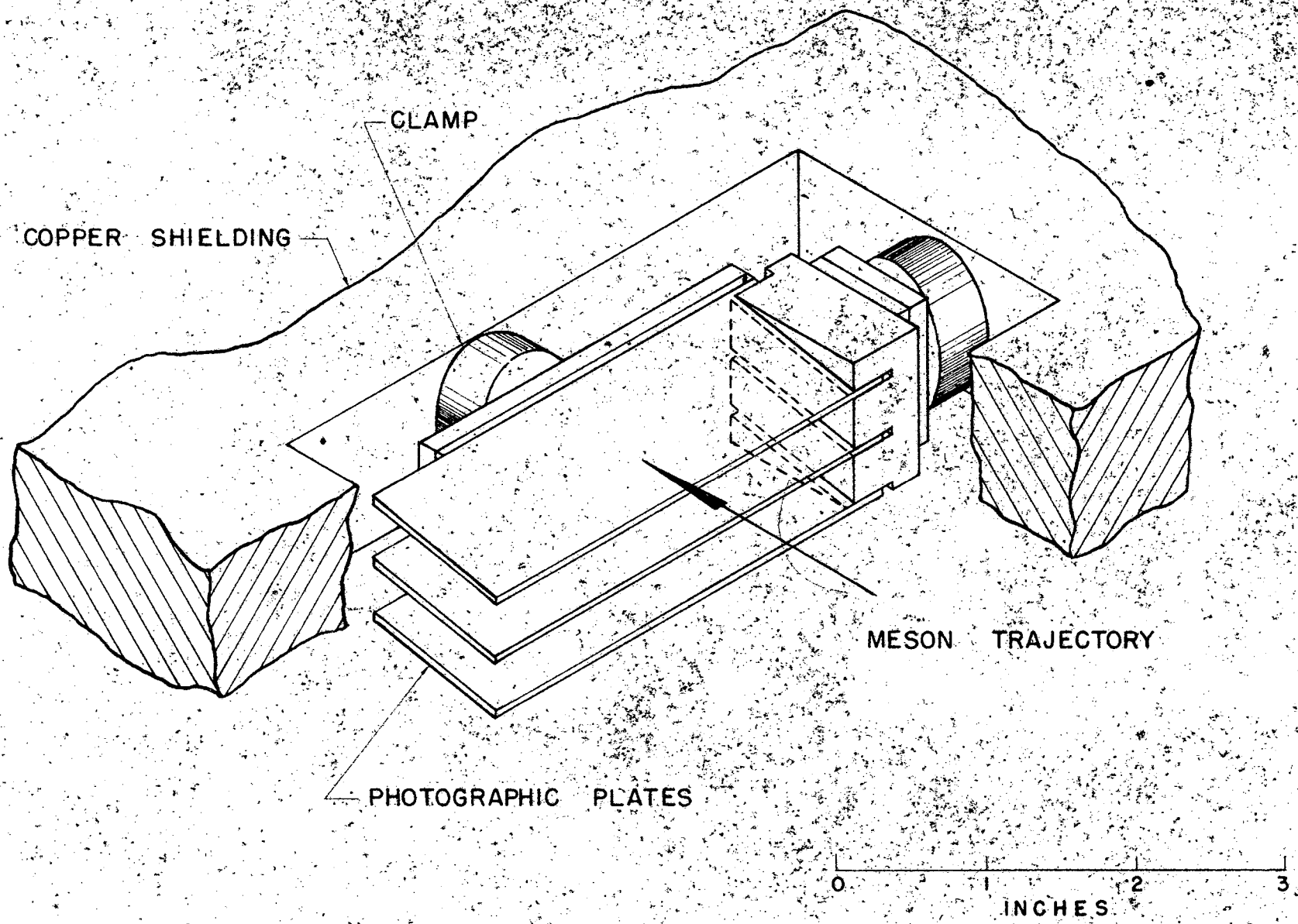
CLAMP
COPPER SHIELDING
MESON TRAJECTORY
PHOTOGRAPHIC PLATES
0
1
2
3
INCHES

FIG 9

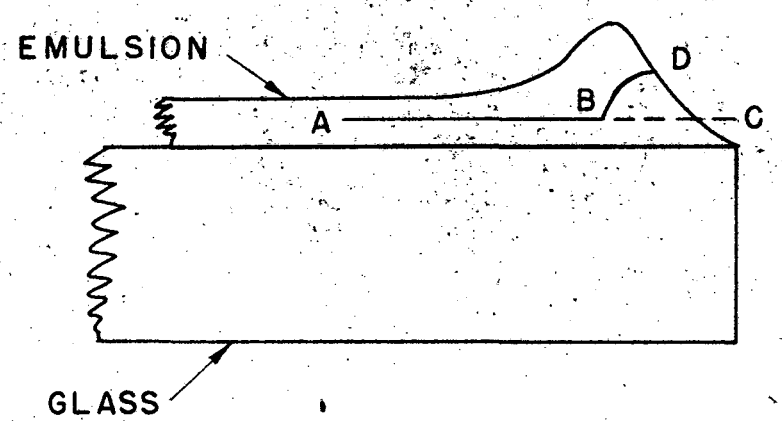

FIG 10

3. Theoretical Physics

Robert Serber

The measurements of meson masses have led to the conclusion that the third particle involved in π-μ decay has zero mass. This leads us to try to understand the phenomena without introducing any new particles. It is then possible, on the basis of what is now known, to determine the spins of the mesons. The capture of π^- and μ^- mesons can be written

(1) $$P + \pi^- \longrightarrow N$$

(2) $$P + \mu^- \longrightarrow N + \nu \qquad (\nu = \text{neutrino})$$

In order to understand the lack of stars in μ^- capture it is necessary to suppose a particle is emitted which carries off the energy. Since it is known that neither electrons nor γ-rays are emitted, this particle must be a neutrino. Since π^- capture does produce stars, it must be concluded that an additional particle is not involved in (1). It follows that the π has spin zero or one, while the μ has spin 1/2. The π-μ decay must then be

(3) $$\pi \rightarrow \mu + \nu \quad .$$

The reactions (1), (2), and (3) are not independent, since (2) is obtained from the inverse of (3), and (1).

The μ decay then takes the form

(4) $$\mu \rightarrow e + 2\nu,$$

and one would therefore expect a continuous electron spectrum. Calculation shows that this spectrum is considerably concentrated towards the upper limit, which helps explain the conflicting experiments on this subject. The lifetime of the μ agrees with β lifetimes if the same coupling constant is used.

On the basis of better experimental results, a revaluation of the cross section for meson production is in progress. Calculations on the production by 350 Mev protons are also being worked on.

The latest conclusions on the n-p scattering is that tensor forces can be included without seriously disturbing the agreement with experiment, though they are certainly no help. Accurate methods of calculating p-p scattering have been developed.

A model in which the nucleus is described as a sphere having an absorption coefficient and an index of refraction has been used to interpret the experiments on scattering and absorption of 90 Mev neutrons by nuclei. Using an absorption mean force path of between 4 and 5 x 10^{-13} cm, and an index of refraction corresponding to a potential of 25 Mev, one calculates the nuclear radii from the data on total cross sections. The results fit very well the relation $R = 1.37\ A^{1/3} \times 10^{-13}$ cm. The diffraction scattering is fairly well reproduced, although the calculated scattering in the forward direction is about 15% low.

Bevatron calculations have led to the conclusion that a reasonable fraction of the injected beam may be expected to miss the injector without any special improvements. The dynamics of the beam near resonances is being investigated, and does not look alarming. No reason to change the n value has been uncovered.

Estimates of the production of deuterons by bombardment of nuclei with high energy n rons indicate that perhaps 10% as many high energy deuterons as high energy protons might be expected. The angular distribution of the deuterons should be narrower than that of the protons, so that at small angles the numbers could be comparable.

Nuclear Cross Sections For High Energy Neutrons As Measured With Bismuth Fission Chambers

N. Knable, J. DeJuren, B. J. Moyer

A summary of the measurements of total cross sections was given in the last quarterly report, UCRL-167.

During the period of the present report efforts were directed toward evaluating the ratio of σ_i to σ_t for carbon, copper, and lead; where σ_i is the cross section for inelastic collision, and σ_t is the total cross section.

The measurements consisted of simultaneous good geometry and poor geometry attenuation studies, with the poor geometry set-up so arranged that neutrons scattered at angles up to 45° could be received by the detecting fission chamber. Figure 1 shows the experimental arrangement.

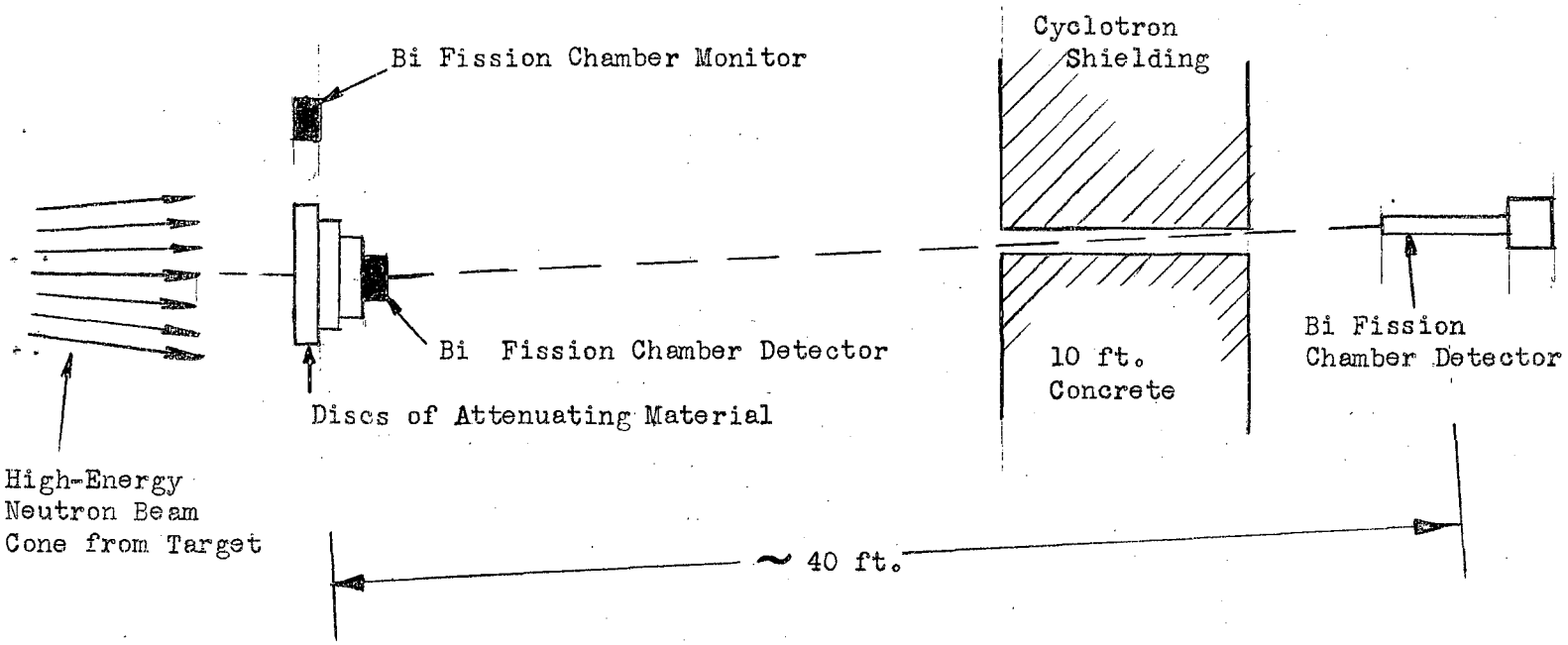

Figure 1
Plan View of Attenuation Experiments with Good and Poor Geometry

The 45° angle was chosen because studies of differential elastic scattering cross sections have shown that essentially all the neutrons elastically scattered by any thickness of attenuator here employed (up to 6") will lie well within a cone of 45° half-angle. A Bi fission chamber with proportions as indicated in Fig. 1 (4 1/2" Plate Diam., 3 plates, 3/4" plate separation) served as the first detector; and a similar one monitored the neutron beam intensity as indicated. The good geometry detector was of the same type as used in the earlier σ_t measurements.

By reducing the argon-CO_2 pressure in these chambers down to about 0.5 atm (from a previous 1.4 atm) it was possible to suppress the pulse sizes of protons, and alphas, and of pile-ups of these, with respect to the pulse sizes of fission fragments. This has greatly

lieved the problem of discrimination between the types of events counted and allowed operation considerably greater beam intensities than were here-to-fore possible. Beam intensities yielding as much as 80 counts/sec could be employed with good bias plateaus. (Because of the pulsed nature of the beam the instantaneous counting rates are much higher, by a factor of 100-300).

In interpreting the data it is assumed that: (1) any elastically scattered neutrons will still be detected by the poor geometry counter, and (2) any elastically scattered neutrons will be sufficiently low in energy as to be below the threshold for Bi fission (~50 Mev).

The tentative values for various measurements of the σ_i/σ_t ratio, subject to possible corrections related to the validity of the assumptions involved are given in the following table.

Element	σ_i/σ_t	σ_i (using previously measured σ_t)
Carbon	.460 ± .016	
	.457 ± .026	
	.434 ± .023	.225 ± .008 barns
	.454 ± .022	
	.431 ± .024	
Aluminum	.421 ± .014	.418 ± .015 barns
Copper	.392 ± .005	.783 ± .013 barns
	.39 ± .04	
Lead	.40 ± .01	1.77 ± .05 barns
	.40 ± .013	
	.38 ± .01	

An experiment is about to be performed to measure the differential elastic scattering cross section for carbon. This, when integrated, will provide a test of consistency of the three measured values, σ_t, σ_i, and σ_{el}.

5. High Energy Particles Emitted During Neutron Bombardment of Various Nuclei

Herbert York

Experiments have been started to measure the angular and energy distribution of the high energy charged particles emitted by nuclei during 90 Mev neutron bombardment.

To determine both the energy and type of a secondary particle, its $H\rho$ and range in carbon are simultaneously measured. The $H\rho$ is measured in the usual way by using a magnet with a variable field. The particle is detected by a counter telescope, consisting of four proportional counters, placed at the point where the particle leaves the magnetic field. Its range is determined by either one of two methods.

The first involves placing an absorber A_1 in front of the first counter, and an additional absorber A_2 in front of the last counter. The first three counters are operated in coincidence and the last in anti-coincidence. Hence only particles with ranges between A_1 and A_2 are detected.

The second method involves placing the absorber A_1 before the last counter, and then desensitizing this counter so that it only counts particles which just penetrate A_1, and thus delivering large pulses in the last counter.

Results so far are very tentative, but some qualitative features may be mentioned at this time.

Both deuterons and protons have been found with energies from 25 Mev up to about 100 Mev. Other particles have not been found, but are not excluded. The ratio of deuterons to protons is greatest for a carbon target (compared to copper and lead, the only other targets investigated) and larger at 10° than at 25°, these being the angles between the neutron beam and the emitted particles. The maximum ratio (for a carbon target and 10°) is very roughly two deuterons to three protons. For copper this ratio is between 1:2 1/2 and 1:4, and for lead between 1:5 and 1:10.

6. 90 Mev Neutron Differential Scattering Cross Sections

A. Bratenahl, R. Hildebrand, C. Leith, B. J. Moyer

The measurement of the angular distribution of elastically scattered neutrons from Be, C, Al, Cu, Ag, Pb, using as a detector proportional counters in coincidence detecting recoil protons of energy greater than 60 Mev from 2 inches of paraffin has been completed. In the angular range (6° and greater) we used a 3 inch diameter beam and spherical scatterers 2 inches or less in diameter. To extend the measurements to smaller angles a beam defining system was developed which provided a beam 1 inch wide and 2 inches high, and scatterers were used which were larger in cross section than the beam.

We have yet to measure the attenuation of the neutron flux by these scatterers in order that the self attenuation correction can be applied to the measurements of scattered flux. This experiment is not completed.

An absolute differential cross section measurement is planned. Relative differential cross sections for the six elements already measured will thus be provided with an absolute scale. The presentation of the data gathered will be withheld until the next report, by which time both relative and absolute differential scattering cross sections, and total elastic scattering cross sections, should be determined.

Considerable effort was given to establishing accurate and convenient methods of aligning the target-collimator-scatterer-detector system. A photographic system has proved to be rapid and sufficiently accurate.

7. High Energy Gamma Rays From Cyclotron Target

B. J. Moyer, H. F. York, R. Bjorklund

There are three processes which may yield photons of energy above usual nuclear transition energies from targets bombarded by the high-energy cyclotron beam. These are (1) brehmstrahlung (2) excitation of high-energy nuclear levels such as the dipole oscillation described by Teller and Goldhaber (3) decay of charged or neutral mesons, if they are formed, and if they yield photons upon decay. If high energy gammas are found in sufficient number, their origin might be inferred from a study of their energy distribution.

In order to investigate this problem an electron pair counter was set up outside the shielding in line with the neutron beam hole. The deuteron beam was run backward, i.e., in the direction which sends the high energy neutron beam away from the hole. A small fraction of the gamma photons originating at the target may then come through the neutron beam hole and be detected.

The pair counter consists of a magnet (pole area 12" x 30", gap 1 3/4"), a radiator to originate the pairs, and four counter tubes operated in four-fold coincidence. This is shown in plan view in Fig. 1. The energy resolution of this first arrangement is not high because of the large breadth of the counters, but by operating the magnetic field at chosen values up to 14,000 gauss, the mean detection energy can be adapted to photons up to 100 Mev. At a given value of magnetic field the detection efficiency vs. energy of photon has a maximum value at this mean detection energy, and decreases uniformly to zero at the extreme energies detectable by virtue of counter size. The extreme range of energies detected is approximately $E_m \pm .3\ E_m$, where E_m is the mean detection energy.

The following statements may be made about the early results thus far obtained:

(1) Photons are observed from any cyclotron target employed (Be, Cu, Pb) extending up to mean detection energies of ~100 Mev.

(2) Between 30 Mev and 100 Mev the yield of photons falls regularly with increasing energy. Below 30 Mev the data are not at present clear.

(3) Pb gives a larger proportion of counts at low energies (i.e., below 30 or 40 Mev) than does Be.

(4) The cross section for production of photons detected with a mean detection energy of 70 Mev is of the order of 10^{-30} cm^2 per nucleus.

The counting rates are only of the order of one count per 100 seconds, and consequently the amount of data thus far accumulated is not large.

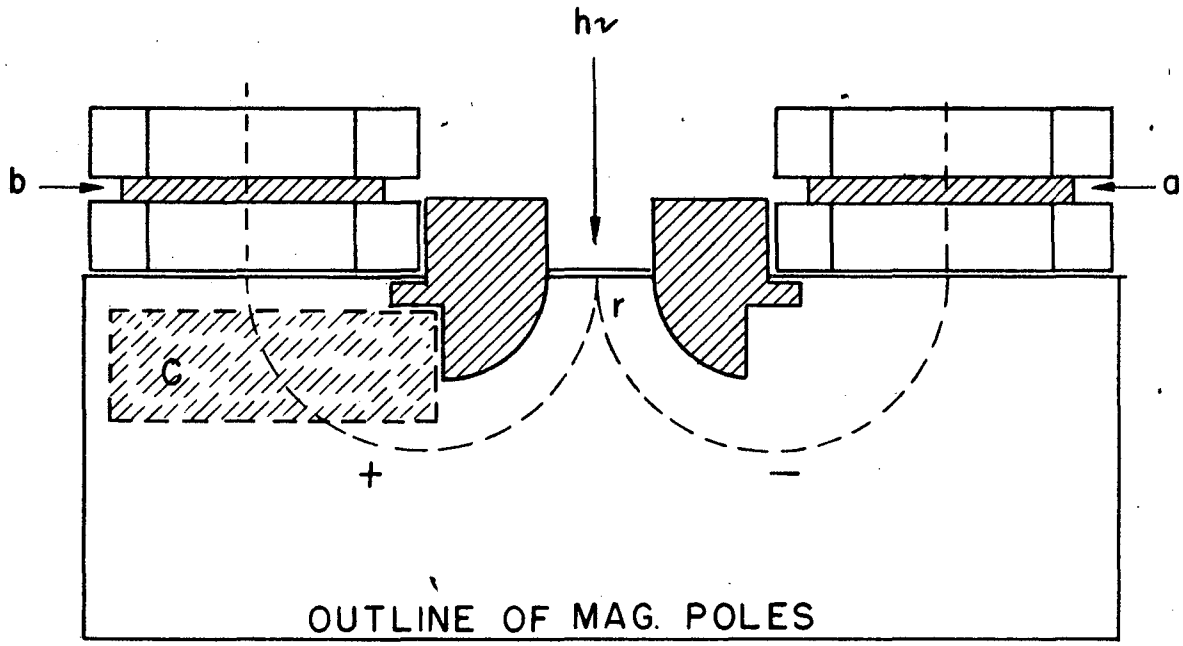

PLAN VIEW OF PAIR COUNTER

Fig. 1

a, b: Aluminum absorbers to suppress background counts due to low energy electrons.

c: Thick Pb block for absorbing out the pair counts.

r: Radiator (usually this is a .010" Ta sheet).

8. Isotope Analysis

L. Tolman, W. Crandall, W. Siri, B. J. Moyer

This quarterly period has seen the Nier Spectrometer brought into a convenient form in which chart recorders trace simultaneous plots of ion beam current and magnetic flux density.

Certain of the components, and a discussion of some recent analyses are presented in the following paragraphs and pictures.

The pictures in Figs. 1, 2 and 3 show the following features:

Fig. 1

Diffusion pump and trap in foreground.
Upper and lower background show spectrometer tube.
In center b.g. is seen the germanium crystal fluxmeter inserted between pole tips.

Fig. 2

Preamplifier vacuum housing and magnetic shield in lower foreground. Pole tips with germanium fluxmeter in upper portion.

Fig. 3.

Control panels. Chart recorders for ion beam and magnetic field at near end. Precision vernier voltmeter and ammeter for accelerating voltage and magnet current built into table.

Ion Beam Current Amplifiers

Two 100% feedback direct current amplifiers have been installed, using type "32" tube preamplifier stages to measure the ion current collected on the adjustable slit and the collector plate. Zero to ten millivolt Leeds and Northrup Speedomax recorders connected through a divider to the output of the amplifiers allow a permanent record of ion current covering a range from 10^{-15} to 3×10^{-11} amperes to be recorded.

The current amplification depends directly on the magnitude of the grid resistor in the preamplifier stage and, since it is desired to measure an ion current of 10^{-15} amperes, a resistance of 10^{11} ohms has been used. The preamplifier must be operated in a vacuum to insure stable operation. To reduce disturbances from stray magnetic fields a heavy iron housing has been installed.

To obtain satisfactory operation of the D.C. amplifier, it was found necessary to carefully select the input tube and grid resistor. Background fluctuation could be reduced by a factor of 100 or more through such a careful selection. Also polarization of certain of the grid resistors introduced objectionable decay in the amplifier output. Using an R.C.A. "32" tube and a 100,000 Megohm Victoreen resistor the background fluctuations were reduced to 10^{-15} amperes. These fluctuations appear to come primarily from the tube and further improvement in this direction may be anticipated.

The collector end of the mass spectrograph tube has been completely re-wrapped with copper shielding bonded to the preamplifier housing to insure good electrostatic shielding.

Germanium Fluxmeter

A magnetic field measuring device, utilizing the Hall Effect in a germanium crystal has been installed and tested for sensitivity and stability. Figure 4 shows the mounting of the germanium.

Currents up to 40 milliamperes were passed through the germanium crystal and the e.m.f. developed across the crystal was measured with a D.C. amplifier similar to that used for measuring ion currents in the mass spectrograph (Figure 5). A sensitivity of .1 mv./gauss was easily obtained with some instability in the output noted. It is believed that most of the instability arises from poor contact of the e.m.f. collector knife edges on the germanium and ultimately a technique for soldering leads to the germanium crystal may have to be developed.

The e.m.f. developed across the crystal was found to be linear with the magnetic field applied (Figure 6). Further tests will be needed to determine its applicability to alternating fields.

Ion Gauge

A new ion gauge supply was installed which, when set for maximum sensitivity, indicates nominal pressures of 2×10^{-9} mm. of mercury for the smallest scale division. By this criterion, nominal pressures of 5×10^{-8} mm. of mercury have been attained, with recorded ion currents of the order of 10^{-14} amperes. The ion gauge is located on the pumping line between the diffusion pump and the spectrometer tube, so the pressures recorded are not to be taken at face value as the conditions in the tube.

Summary of Recent Mass Spectrographic Analysis

Carbon Samples. Samples of CO_2 collected from some specially grown algae were analyzed to ascertain whether any isotope enrichment could be observed. Expected relative abundances of $(CO_2)_{44, 45, 46}$ were calculated from published isotope ratios for carbon and oxygen. These were then corrected for capillary flow differences due to the method of introducing the sample into the mass spectrograph from the sample system (Figure 7). A comparison of these calculated percentages with those determined from normal CO_2 samples and algae sample showed no significant differences.

Argon Samples. Samples of Argon used in the local manufacture of Geiger counter tubes were analyzed to determine impurities present. Less than .002% of oxygen, nitrogen and carbon dioxide were present.

Tin Samples. Samples of tin enriched by the calutron were analyzed and a summary of the results obtained are as follows:

Mass Number	Normal Sn	Percent Abundances of Isotopes	
		Sn_{116} Sample	Sn_{120} Sample
115	.4	.1	-
116	15.5	77.8	3.5
117	9.1	7.6	1.6
118	22.5	4.3	5.4
119	9.8	4.3	4.0
120	28.5	4.8	84.9
122	5.5	.5	.44
124	6.8	.6	.35

These results indicate an enrichment factor of 19.1 for Sn^{116}, and 14.1 for Sn^{120}; the enrichment factor is defined as the ratio:

$$\frac{\frac{P'}{100-P'}}{\frac{P}{100-P}}$$

; in which P, P' = percent abundance of isotope in question before and after processing.

No evidence of hydride ions was seen, but there was a background of residual ion beams in this region which may render the values of the less abundant isotope percentages somewhat inaccurate. For the purposes in hand it is not necessary to obtain more valid analyses.

Figures 8 and 9 show traces of background ion beams, and of beams used in the tin analyses, respectively. The latter was made in a test run with normal $SnCl_4$.

Mercury Samples. Two samples of mercury from the Bureau of Mines, reputedly enriched respectively in light and heavy isotope components were analyzed. No significant deviations from the normal mercury spectrum were observed.

Deuterium Mass Spectrograph. The stainless steel spectrometer tube has been completed and tested for leaks. An oven has been wrapped about the tube and the tube has been mounted on the collector and all water cooling lines installed. A 10 liter D.P.I. diffusion pump with a 150 cm^2 trap installed and work is now in progress on feedback amplifiers similar to those in use on the 6 inch radius mass spectrograph.

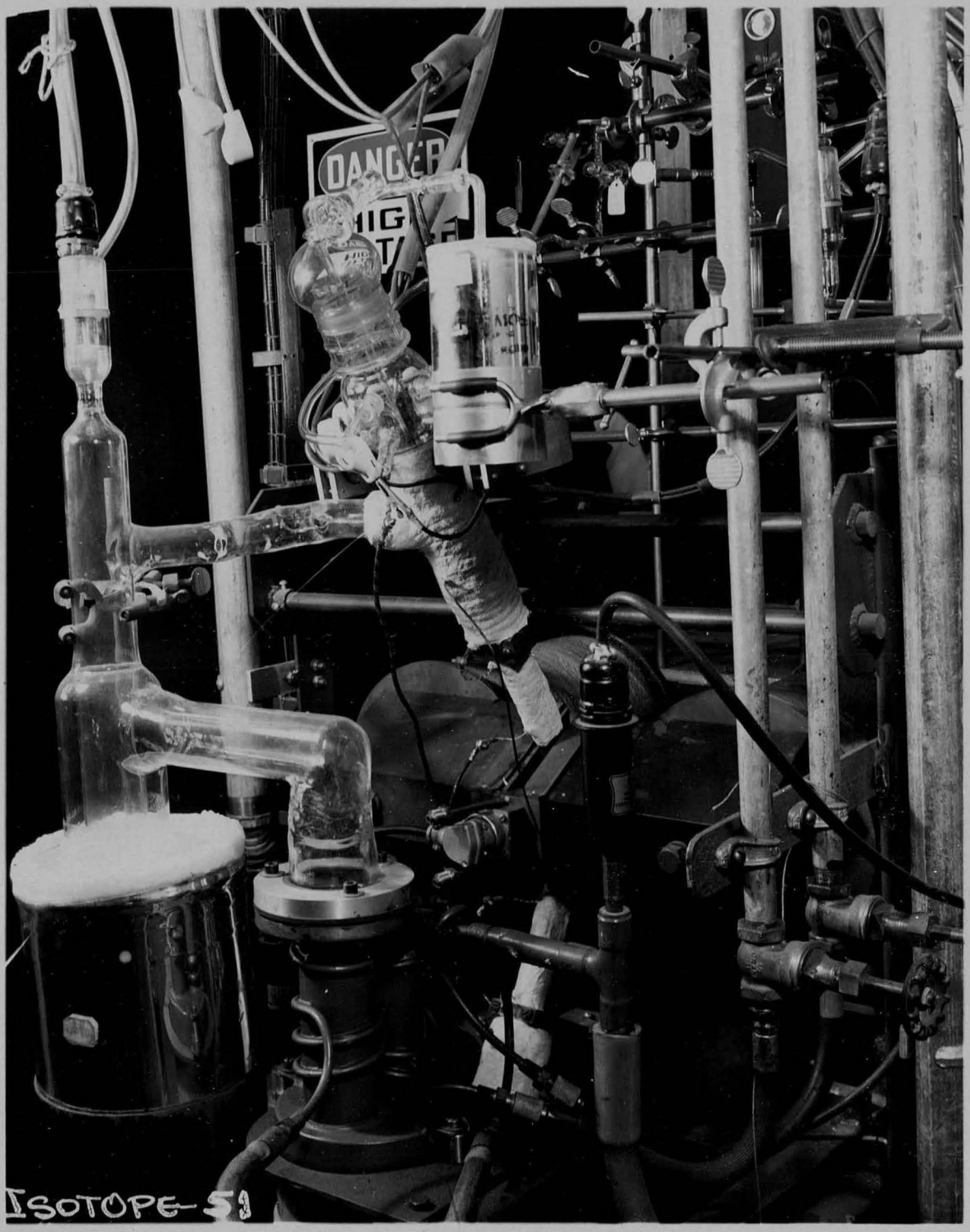

FIG. 1

KODAK—SAFETY
OZ-270

FIG. 2

OZ-271

FIG. 3

OZ-272

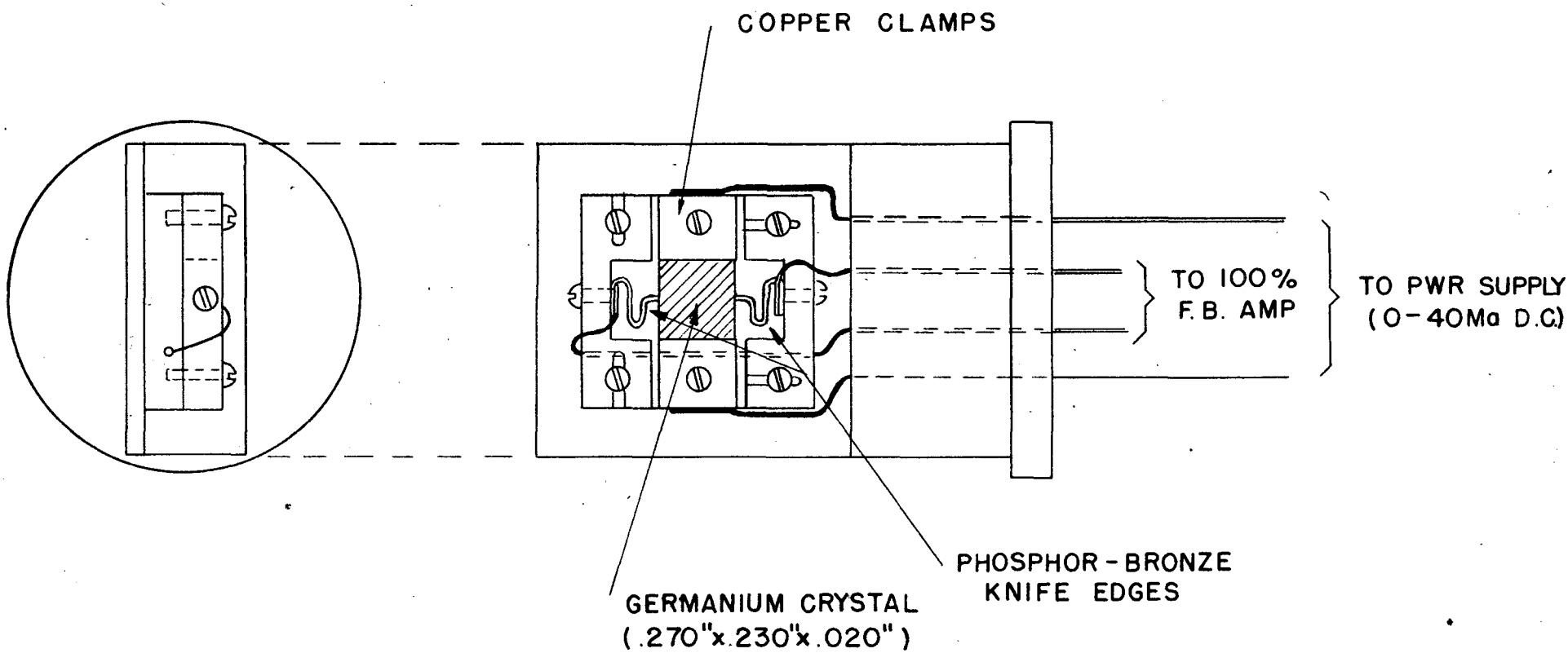
COPPER CLAMPS
TO 100%
F.B. AMP
TO PWR SUPPLY
(0-40Ma D.C.)
PHOSPHOR-BRONZE
KNIFE EDGES
GERMANIUM CRYSTAL
(.270"x.230"x.020")

FIG 4

13136-1

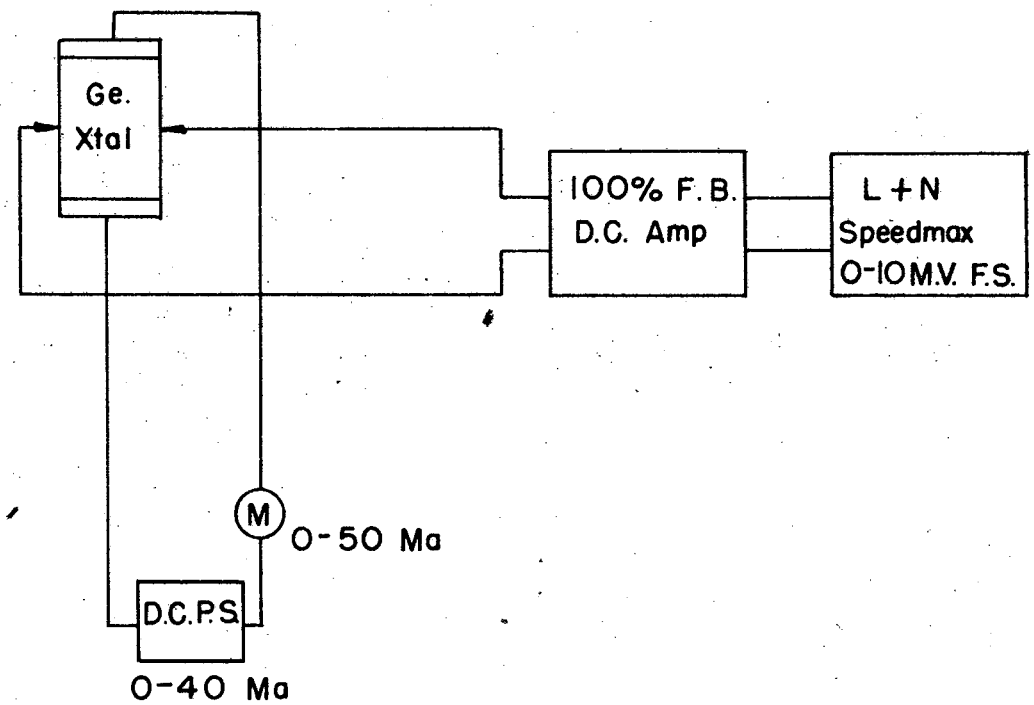

FIG 5

13137-1

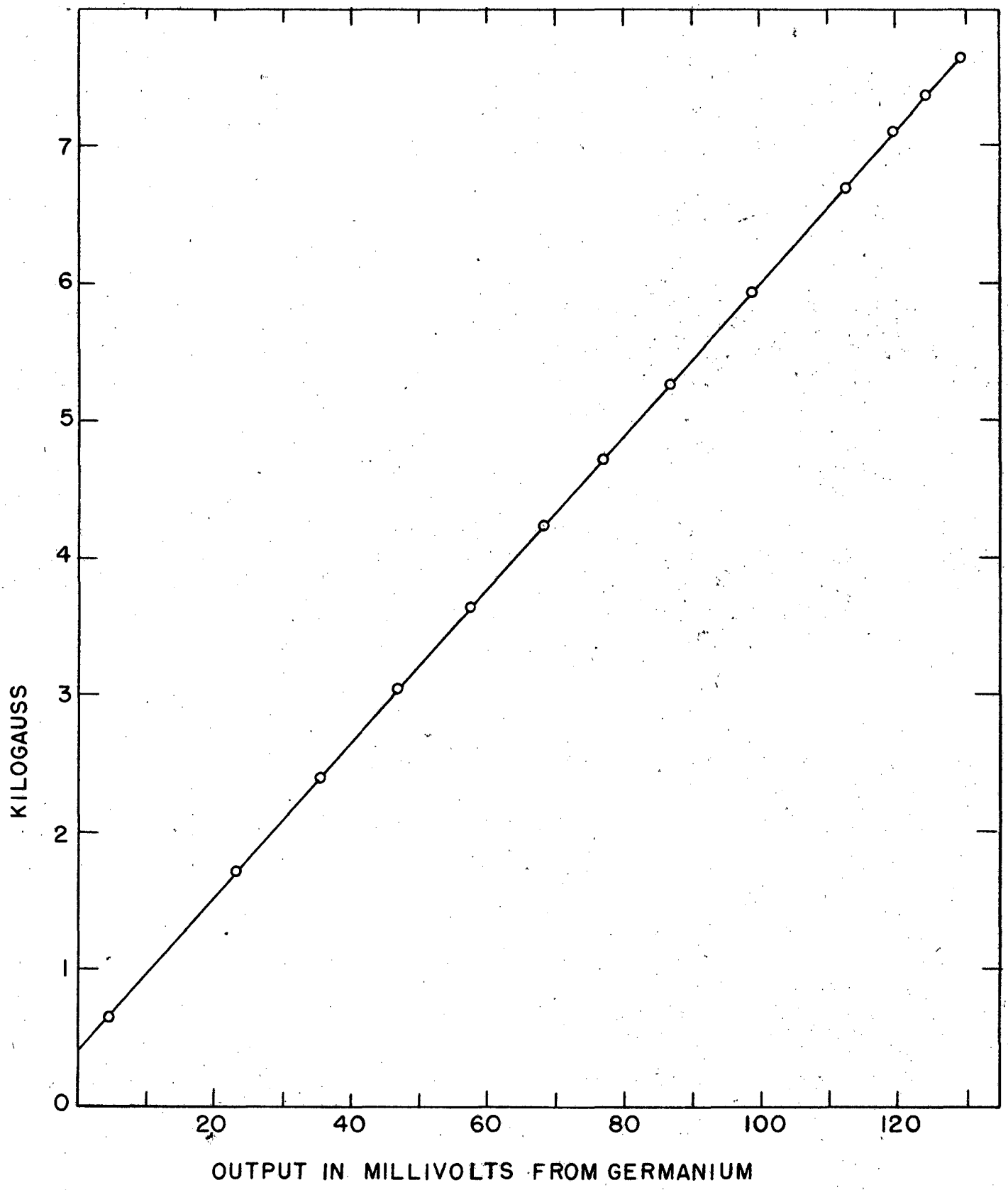
KILOGAUSS
0
1
2
3
4
5
6
7
20
40
60
80
100
120
OUTPUT IN MILLIVOLTS FROM GERMANIUM

FIG 6

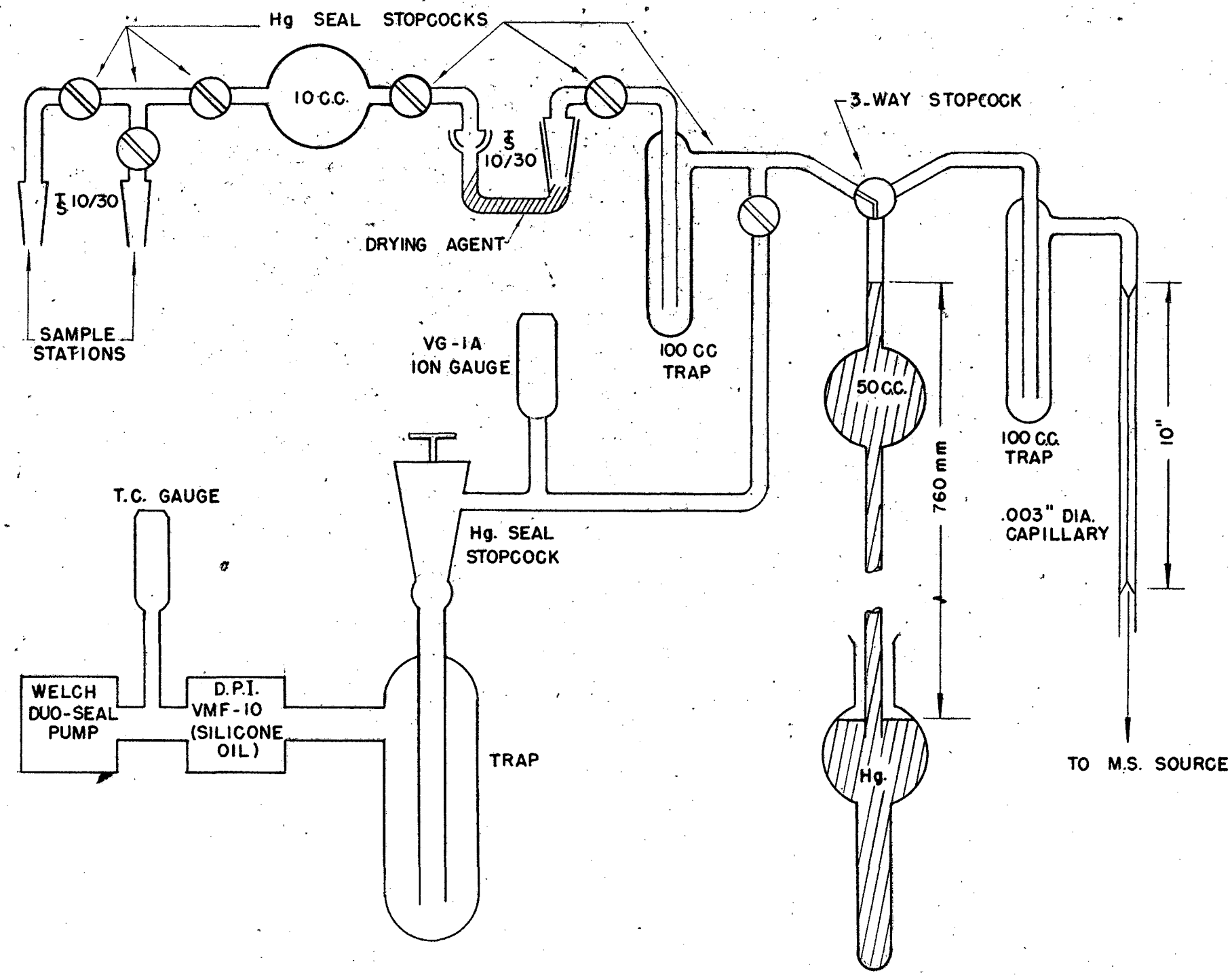
Hg SEAL STOPCOCKS
10 C.C.
3-WAY STOPCOCK
10/30
10/30
DRYING AGENT
SAMPLE STATIONS
VG-1A ION GAUGE
100 CC TRAP
50 C.C.
760 mm
100 C.C. TRAP
10"
.003" DIA. CAPILLARY
T.C. GAUGE
Hg. SEAL STOPCOCK
WELCH DUO-SEAL PUMP
D.P.I. VMF-10 (SILICONE OIL)
TRAP
Hg.
TO M.S. SOURCE

FIG. 7

Figure 8

This is a background run obtained from the mass spectrograph with the amplifier operating at maximum sensitivity. A slight amount of the cadmium spectrum is present, due to silver solder used in the construction of the spectrometer tube. The rapid fluctuations are due to the preamplifier stage, and the sudden displacement at the right side of the page is due to the automatic calibration of the Speedomax recorder.

Figure 9

This is a run made with normal tin tetrachloride in the sample system. The sensitivity of the amplifier circuit is one hundredth that of the background run of Figure 8. The tin spectrum, as well as the tin monochloride spectrum, can be easily identified. For a more accurate determination of the heights of the peaks the magnetic field would be swept at a slower rate to be sure the recorder follows the input signal precisely.

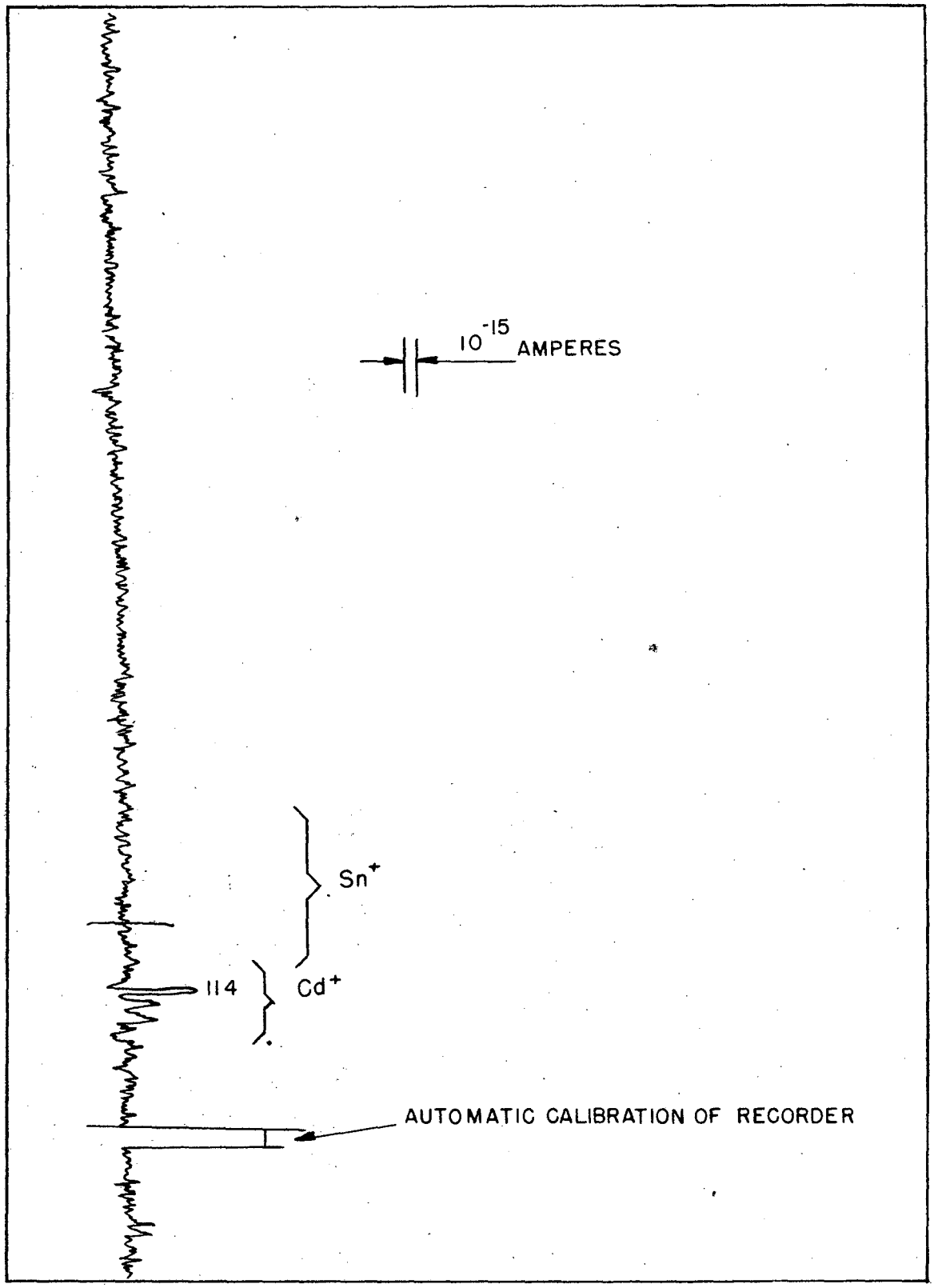

FIG 8

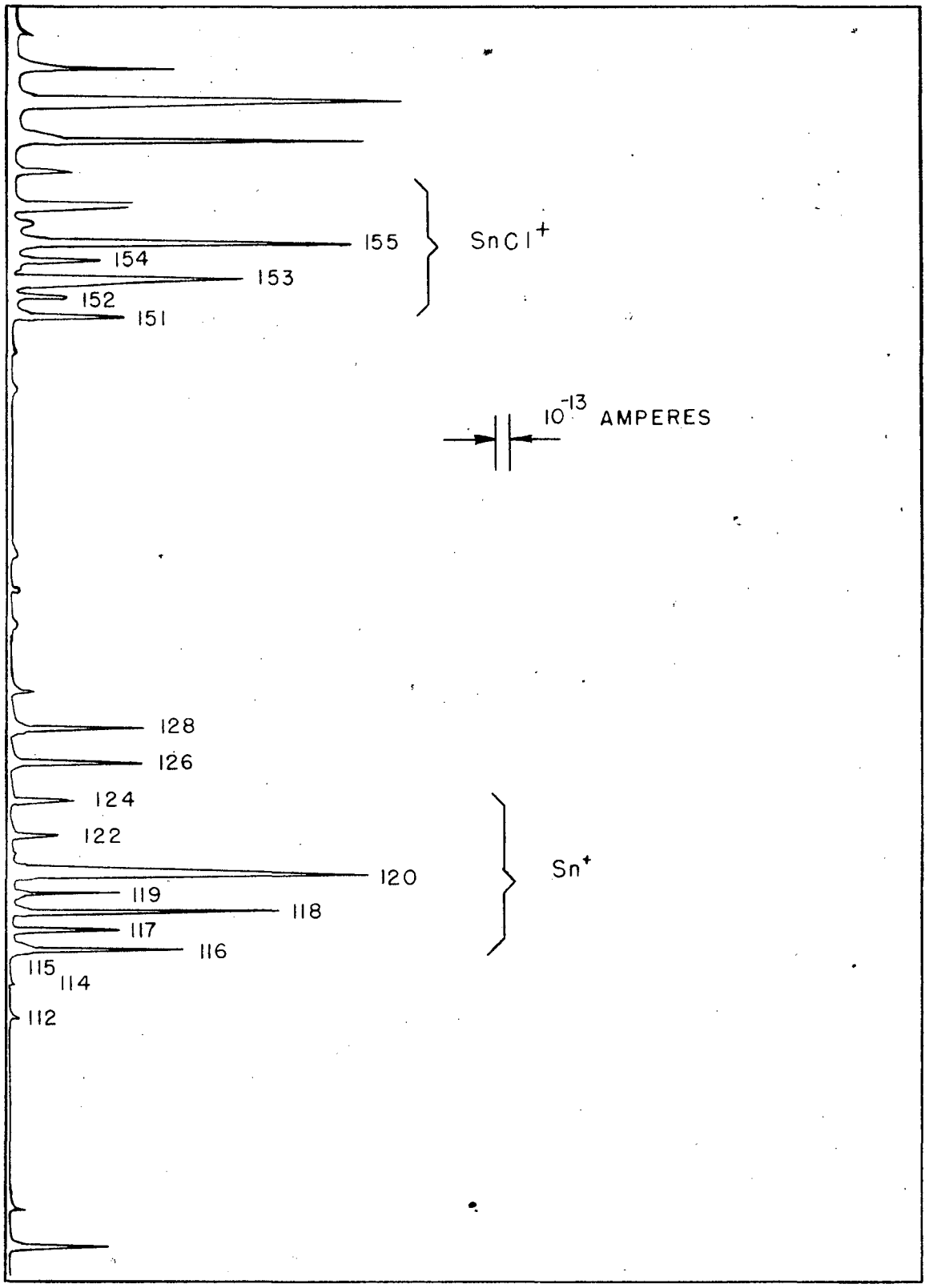
155
154
153
152
151
SnCl+
10-13 AMPERES
128
126
124
122
120
119
118
117
116
115
114
112
Sn+

FIG 9

9. Scattering and Other Studies

Emilio Segrè

Scattering of Elementary Particles

The neutron neutron scattering can not be attacked directly and as was pointed out in the last quarterly report the study of dp scattering is a promising way to collect information on this subject. An apparatus for measuring the scattering cross section elastically scattered deuterons on an absolute scale as a function of the scattering angle has been perfected and satisfactorily tested. No definite results from this apparatus are available as yet, but it seems likely that the elastic scattering cross section in dp scattering is lower than predicted in a theory by Goldberger and Chew, Phys. Rev., 74, 809 (1948). This point has a direct bearing on the additivity of the n and p cross section in scattering experiments of protons or neutrons on deuterons. The technique so far developed is versatile and will allow the study of elastic and inelastic scattering of deuterons or other charged particles by all kinds of targets.

Decay Constant of Be^7

The experiment on the variation of the decay constant of Be^7 in different chemical compounds (UCRL-137) has been renewed by comparing BeO with BeF_2. The data show an effect

$$\frac{\lambda_{\text{oxide}} - \lambda_{\text{fluoride}}}{\lambda} = 0.003$$

More observation time is needed however to obtain a reliable result.

Fission Studies

The work on the energy distribution of the fragments of U^{238} and U^{235}, Th and Bi under 90 and 40 Mev neutron bombardment has been partially completed and a separate report is being written. The main results are as follows: The distributions of number versus energy show only one maximum instead of two as occurs with low energy fission. The energy of this maximum is very close to the average energy obtained in low energy fission. It is 75 Mev for U^{238}; 83 Mev for U^{235}; and 80 Mev for Th, respectively. For Bi it is slightly lower - 71 Mev. The energies correspond approximately to the Coulomb energy of the two fragments when in contact. These results and the chemical evidence favor a mechanism of fission according to which practically all the energy of the impinging particle is dissipated in evaporating neutrons, and the final nucleus undergoing fission is only slightly excited.

We have also measured the fission cross section 90 Mev neutrons with the following results: natural $U\ \sigma_f = 1.4 \pm 0.25 \times 10^{-24}$ cm^2; Th $1.0 \pm 0.2 \times 10^{-24}$ cm^2; and Bi $\sigma_f = 0.05 \pm 0.01 \times 10^{-24}$ cm^2. For 40 Mev nuetrons we obtained the following results: natural $U\sigma_f = 1.75 \pm 0.3 \times 10^{-24}$ cm^2; Th $\sigma_f = 1.05 \times 0.2 \times 10^{-24}$ cm^2.

In order to measure fission cross sections using charged particles as projectiles we have tried to use a differential chamber. The primary beam crosses the two sections of chamber which are connected in opposition. In this way the ionization produced by the beam cancels and it is possible to detect the fission fragments. Preliminary experiments with this method seem quite promising.

10. P-P Scattering Experiments in the Linear Accelerator

H. Bradner

Photographic Plate Method

One thousand tracks have been tabulated in the first attempt to obtain the angular distribution of scattered protons. It is apparent that the background to be subtracted out was not chosen correctly, and we are awaiting more runs.

Ionization Chamber Method

Data has been obtained for a preliminary differential scattering cross section curve. Spurious counts due to neutron background recoils have been reduced to 10 per cent of the total counts by gating the scalers to be operative only during the "on" time of the R.F.

11. Short Half Life Investigations in Linear Accelerator

H. Bradner

Study of the half-lives of Al^{25} and Al^{26} via separated Mg isotopes has been completed, with the following results:

Half life of Al^{25} = 7.3 ± 0.2 sec.

Half life of Al^{26} = 6.3 ± 0.2 sec.

Proton energy was varied by means of aluminum absorbers in order to obtain the rough activation curves of Al^{25} and Al^{26} shown in Figures 1 and 2. Feather analysis of the positron energies yielded end points of approximately 3 Mev in agreement with allowed transitions.

The 20-second half life of C^{10} reported by Sherr et al[1] has been confirmed by bombardment of separated B^{10} in the form of boron metal. A 2 Mev positron was found, as reported by Sherr.

A new 3-second half life appearing from proton bombardment of Ni^{58} has been tentatively assigned to Cu^{58}.

A very high energy positron activity of approximately .01-second half life and 20.7 Mev threshold has been obtained by bombarding carbon with protons. It is tentatively assigned to N^{12}. The half life is compatible with the assumption that the transition is allowed. The experimentally determined threshold is 400 kilovolts higher than would be permitted by the proton-emission stability of N^{12} (using 11.015 for C^{11} mass) but there is reason to question the accuracy of the threshold measurement.

---

[1] R. Sherr, H. R. Muether, M. G. White; Phys. Rev., 74, 1239 (1948).

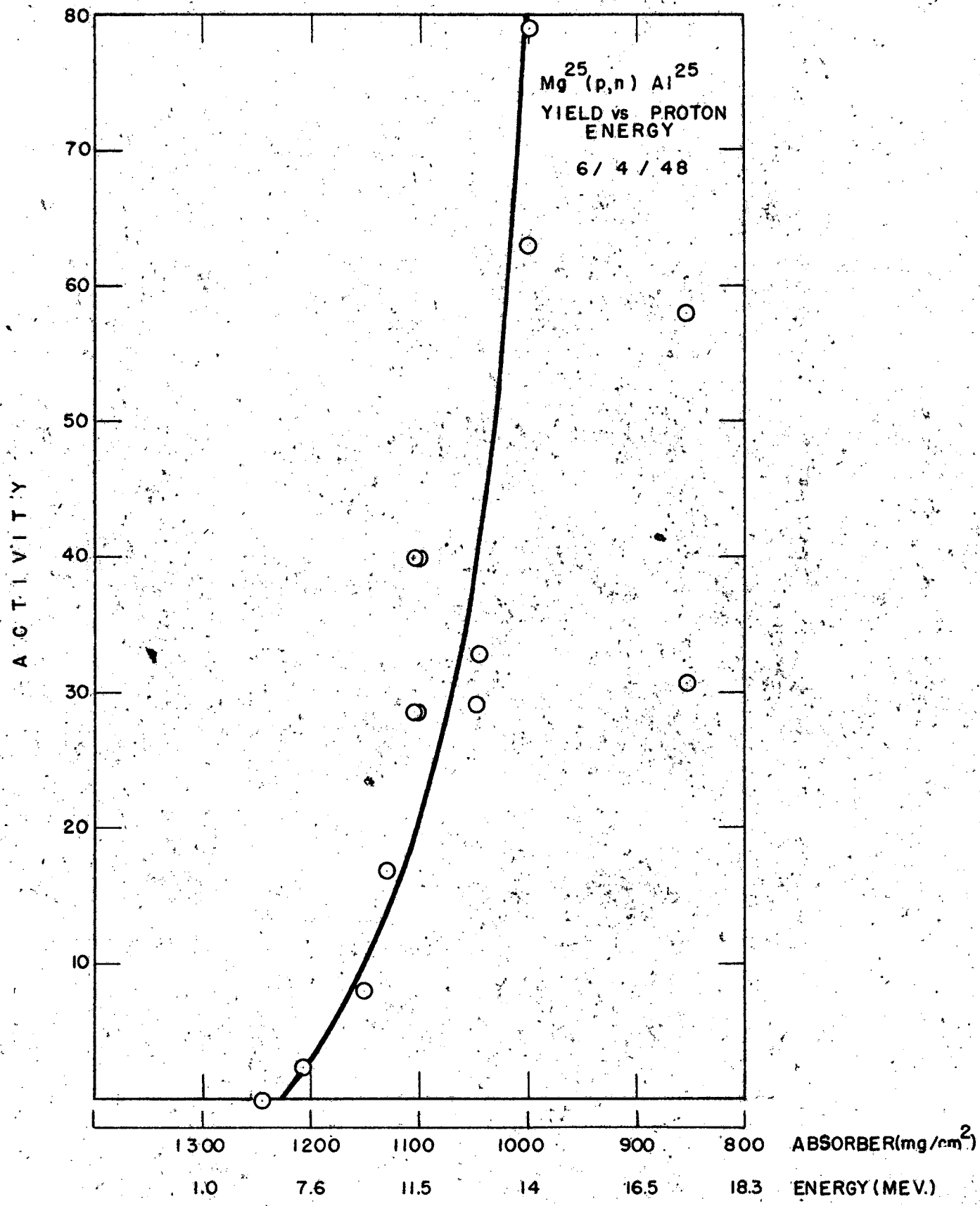
$Mg^{25}(p,n)\ Al^{25}$
YIELD vs PROTON ENERGY
6/ 4 / 48
ACTIVITY
80
70
60
50
40
30
20
10
1300
1200
1100
1000
900
800
ABSORBER(mg/cm^2)
1.0
7.6
11.5
14
16.5
18.3
ENERGY (MEV.)

Fig. 11

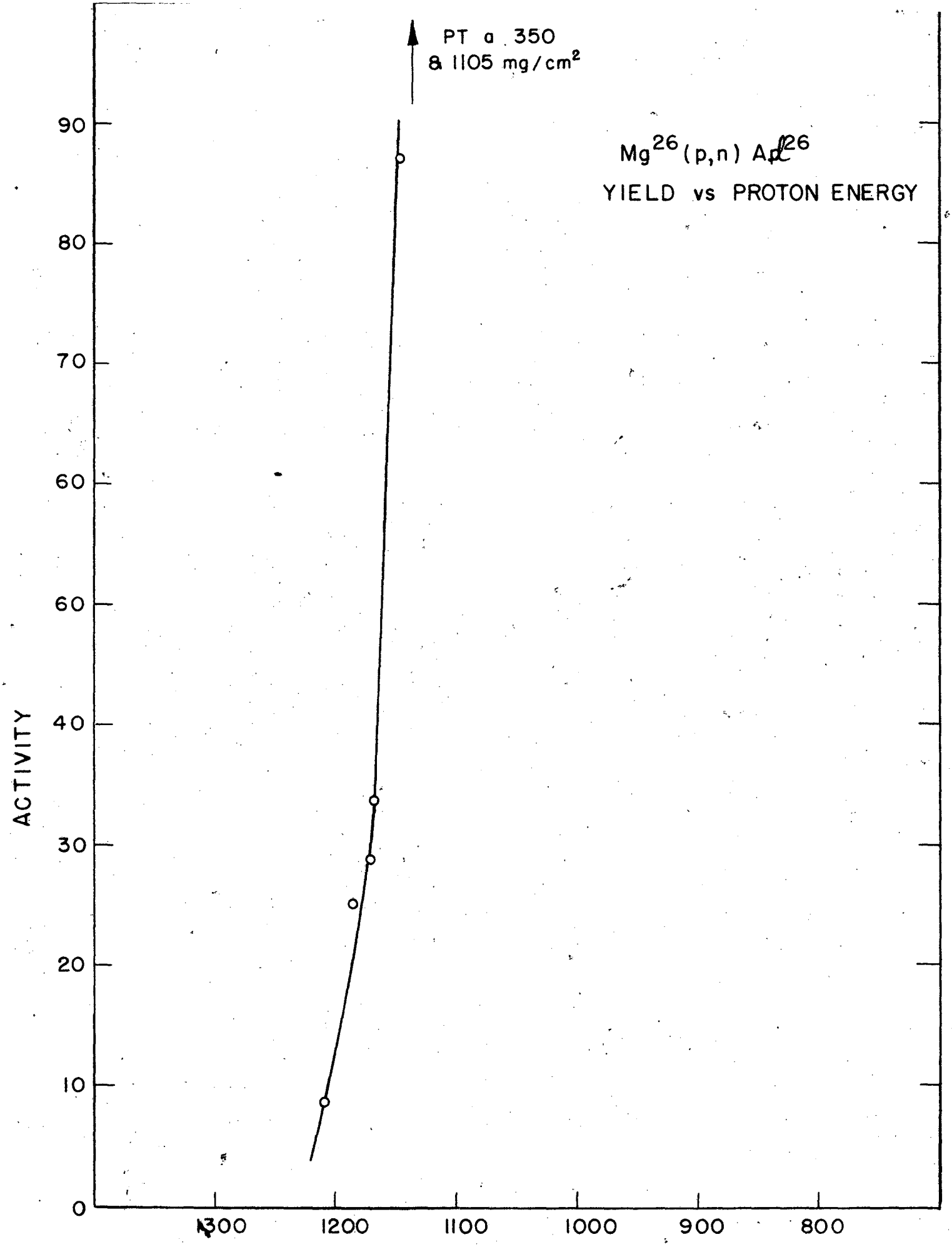
PT a 350
& 1105 mg/cm²
Mg26 (p,n) Al26
YIELD vs PROTON ENERGY
ACTIVITY
90
80
70
60
60
40
30
20
10
0
1300
1200
1100
1000
900
800
ABSORBER (mg/cm²)

Fig. 2

12. Inelastic Scattering of Protons

E. Martinelli

A photographic method is used to measure the energy distribution of inelastically scattered protons. The 32 Mev linear accelerator is used as a source of protons. Eight plates are exposed simultaneously at fixed polar angle, and the track lengths from 0-200 microns are measured on each plate. With appropriate aluminum absorbers between the target and each plate, the energy distribution from 0-16 Mev or 16-28 Mev can be determined in one run.

To determine the energy resolution of the camera, an exposure was made with 16 Mev protons on carbon. The following energy levels of C^{12} were observed - 0; 4.8 ± .2; 10.0 ± .4 Mev. This confirms results obtained by Fulbright (private communication) at Princeton. The width of the levels at half maximum were of the order of 1.0 Mev. The calculated width at half maximum with the beam stopped down to 16 Mev is 0.7 Mev considering only straggling in the various absorbers, and the initial spread of the beam. Experiments are being continued with carbon and aluminum.

13. The Detection of Light and Heavy Mesotrons Outside the Tank of the 184-inch Cyclotron

W. Panofsky

It is of general interest to make the mesons artificially produced in the 184-inch cyclotron available for general experiments outside the tank. Thus far only photographic techniques have been used in conjunction with the Berkeley meson work. By bringing the beam outside the tank it is hoped that cloud chamber, and possibly counter methods, may become accessible to meson work. In addition the measurement of the lifetime of the π meson appears possible if long meson trajectories are obtained.

The method discussed here accomplishes the removal of the mesons from the cyclotron tank by having the mesons produced in a thin target struck by the 380 Mev. alpha particle beam enter a region of very weak magnetic field which permits them to leave the tank along a path of weak curvature. The technical problem involved here is therefore to produce a magnetic shield which reduces the field of the cyclotron from about 14,000 gauss, to the neighborhood of 1,000 gauss, and then introduce this shield within a very short distance from the circulating beam without disturbing the dynamics of the beam itself.

The main problem in the design of a magnetic shield of this type to operate in a magnetic field of 14,000 gauss is a problem of saturation of the iron. This problem can be met only if the flux density in the iron only slightly exceeds the flux density in the surrounding field. This condition can be met by using a shield whose major extent is perpendicular to the direction of the field. If we approximate such a shield by an oblate spheroid, the mathematical analysis of the saturation and shielding behavior of such a body in an external field can be made. As a result of this analysis, it can be shown that a shielding ratio of only 1.3 is obtainable for a shield of spherical geometry, while for a spheroidal shield of axial ratio two to one, the shielding ratio of three to one is obtainable; while for an axial ratio of four to one, the shielding ratio of 30 to one is feasible, in an external field of 14,000 gauss. The above calculations are based on cold rolled steel. On the basis of these calculations a shield was designed in accordance with an axial ratio of four to one, bent in the shape of the trajectory computed from a set of magnetic measurements. The resultant overall geometry is shown in Figure No. 1. It is seen that the curvature of the mesons entering is greatly decreased in the shield, permitting the mesons to enter the reentrant chamber in the side of the cyclotron. Figure No. 2 shows the magnetic field along the meson trajectory with the magnetic shield. The disturbance produced by this shield is only 5 per cent at beam radius. This disturbance is compensated by a set of magnetic shims fastened to the pole of the cyclotron. Unfortunately it is not possible to calculate the focusing properties of the meson shield theoretically, owing to the very variable saturation conditions near the channel through which the mesons are passing. An intensity of mesons expected from the channel is therefore difficult to predict. However, a counting rate of 1,000 mesons per minute for a beam current of 10^{-7} amperes of alpha particles is the best figure which can be calculated from the data known thus far.

Until now only four mesons have been detected inside the reentrant chamber in the cyclotron wall. Two of these are light mesons and two are heavy mesons. The fact that the light mesons are also obtained through this channel lends additional support to the belief that the light mesons are actually formed in the cyclotron target and are not produced by disintegration in flight. The total time of flight in the chamber is 10^{-8} second, and an additional 10^{-8} second is obtainable in the reentrant chamber without any additional magnetic changes. If the π meson lifetime is therefore not in excess of 5×10^{-8} second, the measurement of the lifetime should be possible in this geometry by a comparison of the numbers of π

μ mesons as a function of distance along the meson trajectory. It is also planned to check the focusing properties of the magnetic channel by means of one million volt alpha particles produced by a thick radioactive alpha sample mounted on the regular cyclotron target position.

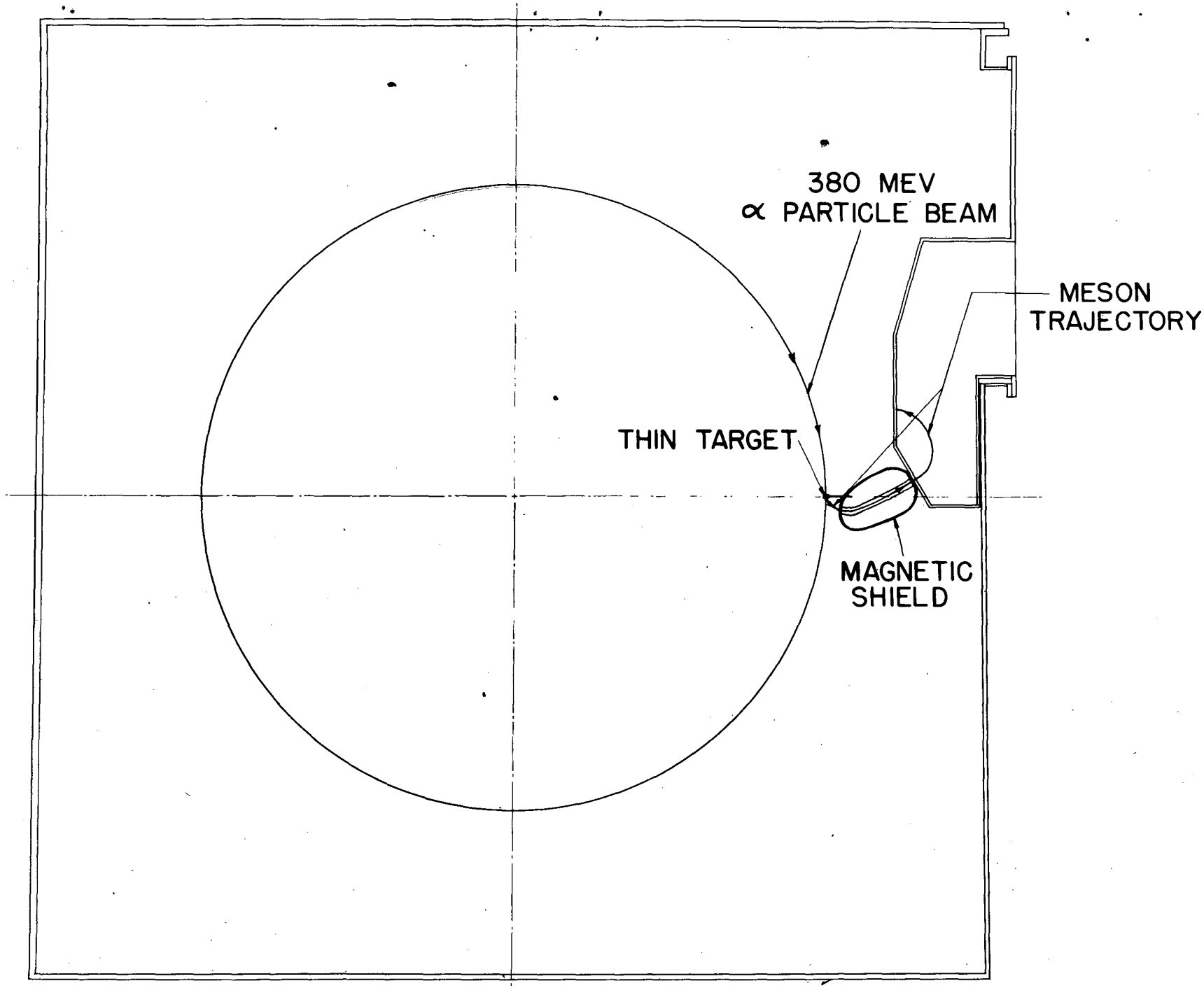
380 MEV
α PARTICLE BEAM
MESON
TRAJECTORY
THIN TARGET
MAGNETIC
SHIELD

Fig. 1

02 - 91

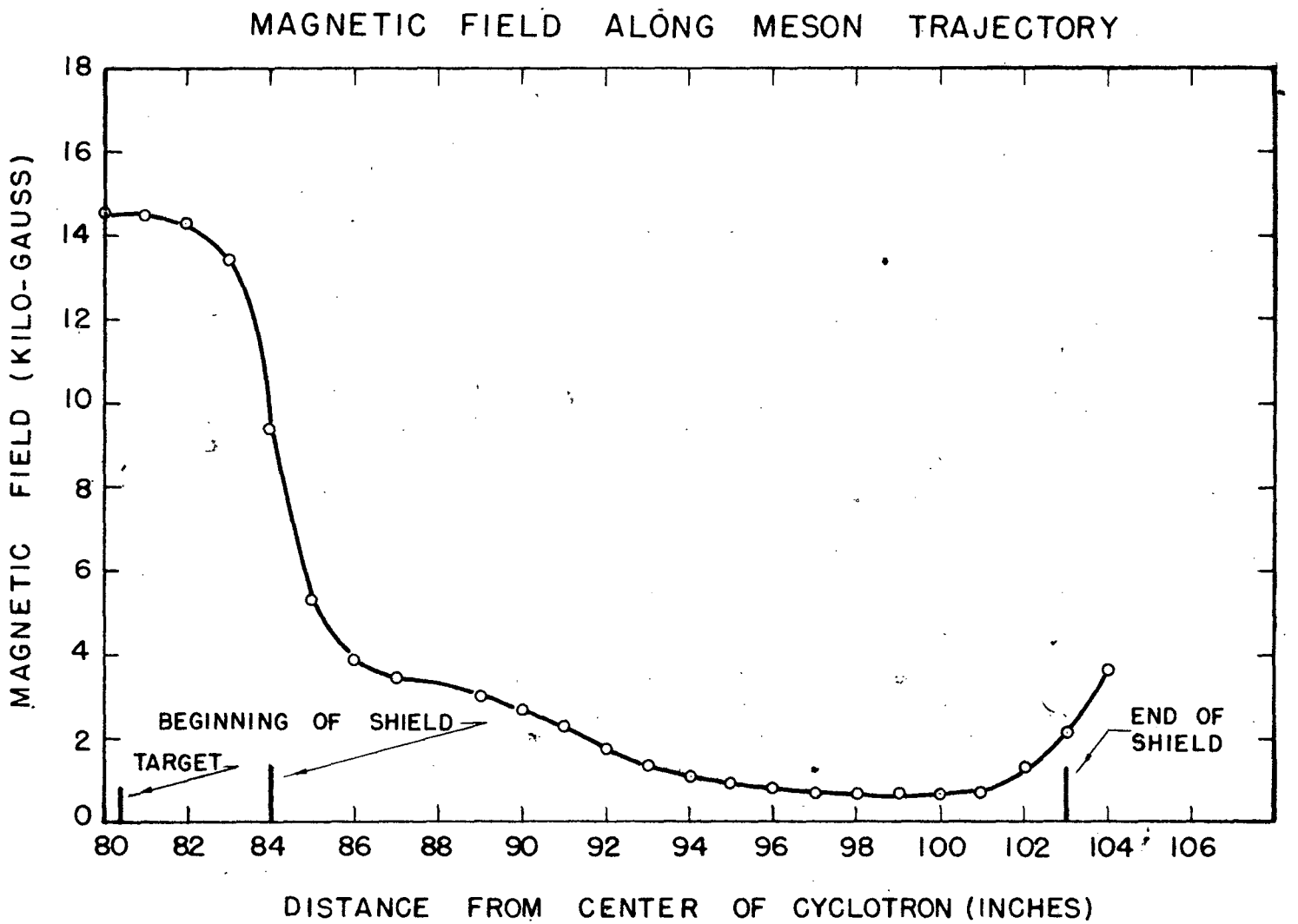
MAGNETIC FIELD ALONG MESON TRAJECTORY
MAGNETIC FIELD (KILO-GAUSS)
18
16
14
12
10
8
6
4
2
0
80
82
84
86
88
90
92
94
96
98
100
102
104
106
DISTANCE FROM CENTER OF CYCLOTRON (INCHES)
BEGINNING OF SHIELD
TARGET
END OF SHIELD

FIG. 2

II. ACCELERATOR AND CALUTRON OPERATION AND DEVELOPMENT

1. 184-Inch Cyclotron Operation

James Vale

Proton Conversion

Modifications to the proton conversion unit have been made as a result of the radio-frequency tests. One of the major changes was a multiple contact switch mounted inside the vacuum system and manually operated through a chevron vacuum seal. This switch was found necessary for rapid change-over in operation from accelerating protons to accelerating deuterons, or vice versa. In addition the width of the transmission line stub was made smaller so that it would be the same as the dee stem. Change-over in operation from protons to deuterons or alpha particles is expected to be a matter of minutes.

Rotary Condenser

The major trouble with the rotary condenser has been the opening of water leaks in the vacuum system. These leaks have been the result of two difficulties: first, the zircon insulators, which support the rotor, have developed cracks allowing water to pass into the vacuum system, and second, rubber gaskets have deformed enough to open leaks. Both of these difficulties have a common cause, which is the high temperature reached in the rotor during operation.

An attempt to prevent breakage of the insulators has consisted of increasing clearances between the insulators and the metal parts so that expansion of the parts will not strain the insulators. A solution to the gasket problem seems to lie in the use of "O" ring gaskets. These gaskets seal a vacuum joint by virtue of the pressure on the other side of the vacuum.

Magnet Pole Piece Oil Band

During the early stages of operation of the cyclotron, it was found that the vacuum tank pressure increased when the magnet was turned on. The cause of the vacuum difficulty seemed evident, when oil, presumably from the magnet coil cooling system, was found seeping out from the cracks between the pole piece slabs in the vacuum system.

In an attempt to determine whether this oil was the cause of the vacuum trouble, a stainless steel band with rubber gaskets was installed allaround the pole piece and covering the space between two slabs. Provision was made to pump on this volume by an auxiliary pump. Results of this test indicated that a band of this type was not satisfactory, therefore a program was gotten under way to weld a steel band all around the top pole piece in the vacuum system during the installation of the proton unit.

Magnetic Cones.

It has been known for some time that magnetic focusing of the ions in the center of the cyclotron is necessary for optimum beam output. Since there was some question whether there was enough magnetic focusing in the 184-inch cyclotron, new steel cones were made and

installed. The cones in use for the past year, were six inches in diameter at the base and two inches high. The new cones tried were two types: one had a base diameter of nine inches and was three inches in height, and the second a double cone having a base of six inches in diameter, and reaching a height of four inches.

Neither of the two types of cones seemed to give any improvement over the cones that had been in use.

Telescoping Probe Extension

The present probe system in the 184-inch cyclotron does not allow the probe to reach any closer to the center of the cyclotron than about the 20 in. radius point. However, it was felt that certain experiments involving current reading probes that could reach the center were necessary. Therefore a telescoping probe tube was added to one of the present tubes so that an extension of about 24 in. beyond the present limit was possible. This extension can be controlled after insertion of the probe into the tank.

A further use for this probe was found in the meson research program. The length of material that can be inserted in the cyclotron tank is limited by the probe air lock. With this probe extension it was found possible to get a much larger effective length by mounting part of the equipment on the fixed tube and part on the extension and inserting into the tank when the telescoping system was collapsed.

Beam Experiments

One of the attempts to increase the amount of beam obtainable with the cyclotron consisted of increasing the dee voltage during injection time. This rise in dee voltage was obtained by pulsing the oscillator plate voltage to about fifty percent above the normal operating point. This pulse was about 100 microseconds in length. In addition, this voltage pulse could be moved in time so that it could be placed anywhere in the frequency modulated cycle.

No increase in beam was observed, but in addition no decrease in beam could be seen even though the voltage pulse was moved over the whole frequency modulated cycle.

This point is of interest theoretically because in the past it was felt that loss of beam would result if voltage spikes were present on the dee.

2. 60-inch Cyclotron

J. G. Hamilton, G. Bernard Rossi, James F. Miller, William P. Ball, Kenneth D. Jenkins, Kenneth Relf, Thomas M. Putnam Jr., Leland K. Neher

Operation

There were available 3,672 hours of possible operating time from May to October, 1948, inclusively. This time was consumed as follows:

Bombardment Time:

Deuterons	697.4 hrs.	
Alphas	636.9 hrs.	
Protons	988.4 hrs.	
TOTAL	2322.7 hrs.	2322.7 hrs.

Experimental Time:

Ion sources (1) open	7.7 hrs.	
(2) Water cooled hood	31.9 hrs.	
C^{16}_{12} & B^{5}_{10} Acceleration	19.0 hrs. (See below)	
D. C. Filament heater	8.4 hrs.	
Microinterceptor target	33.9 hrs.	
Beam development (1) alpha	106.2 hrs.	
(2) deuteron	5.2 hrs.	
(3) proton	17.8 hrs.	
Dee tuning	17.7 hrs. (See below)	
Gas analyzer	2.0 hrs.	
Magnet shims	5.2 hrs.	
North oscillator tube characteristics	1.0 hrs. (See below)	
Beam pattern	.8 hrs.	
Vacuum tank alignment	10.4 hrs.	
Ion source gas line	1.0 hrs.	
Dee frequency measurements	16.0 hrs. (See below)	
	284.2 hrs.	284.2 hrs.

Outage:

Maintenance, check up, etc.	694.2 hrs.	
Enforced shutdown	370.9 hrs.	
	3672.0 hrs.	3672.0 hrs.

Bombardment efficiency: 63.25%
Operational efficiency: 70.99% See Figure 1

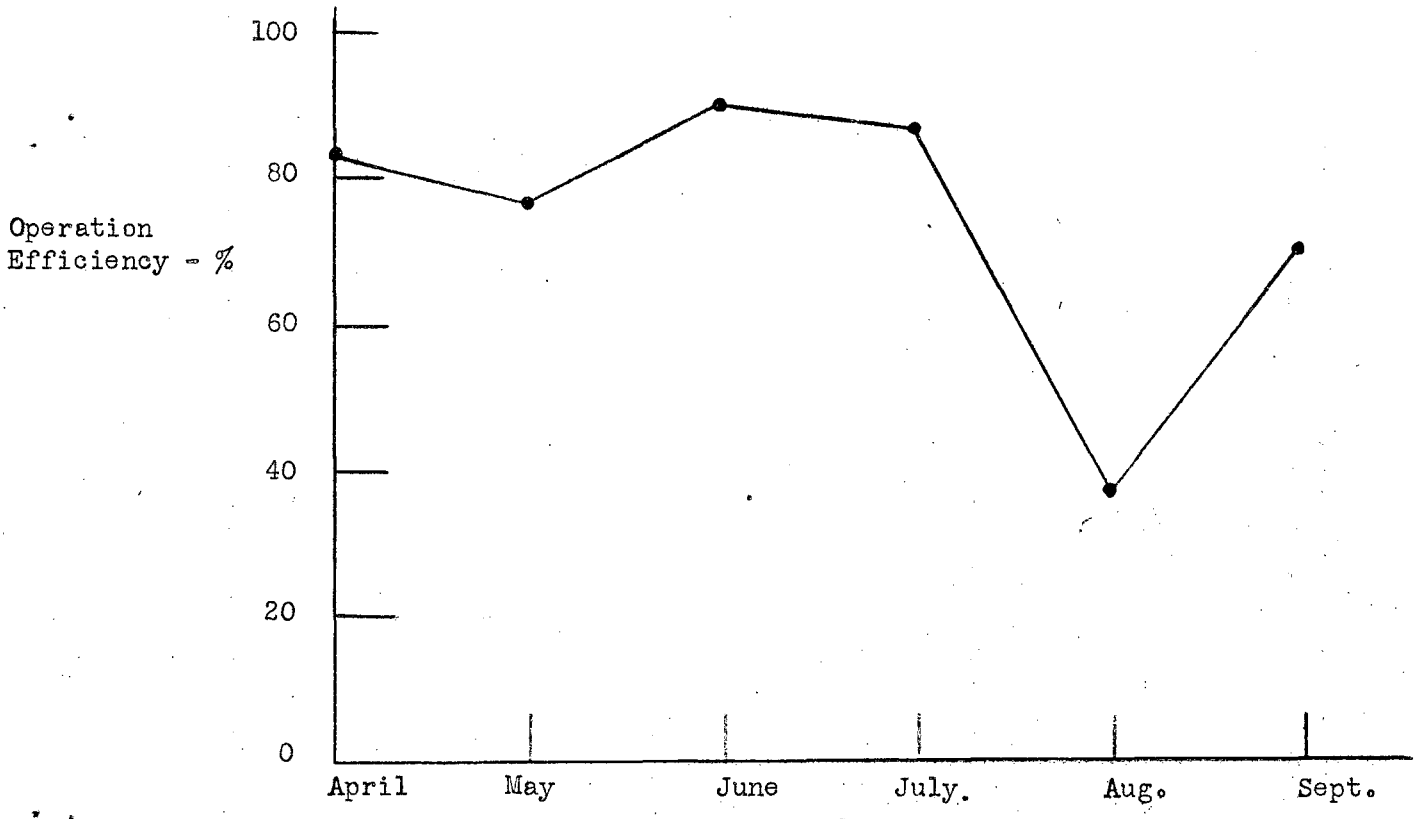

Fig. 1

Bombardments. During the period from May through September, 1948, there were 141 targets bombarded on the 60" cyclotron. Of these, 67 were with deuterons, 52 with alphas and 22 with protons. The bulk of bombardments were made for groups connected with the University of California Radiation Laboratory. Outside groups were represented by Argonne National Laboratories, University of Rochester, U. S. Navy (Hunters Point) and the University of Wyoming.

Outage Time. The most time-consuming outage item in the period was a forced shutdown occurring in the early part of August. This was occasioned by a rupture in the west R.F. stem throat about 6" from the R.F. connection to the dee. Due to the fact that the rupture was associated with the water cooling line, the decision was made to remove the stem and replace with heavy gauge copper. This occurred on August 2, 1948. The machine was completely dismantled and the west stem lines removed.

Work completed during the shutdown included the replacement of the throat section in the west dee stem liners, both top and bottom. During the assembly of the new sections, the main W. R.F. clamp warped out of alignment, necessitating hard soldering the west U-house in place at the time of installation, to minimize radiation. Also installed at this time were new thick-walled cooling lines in the new sections.

Other work carried on during the repair included the installation of the new probe assembly, despite the fact that the probe has not been tested. This can be tested separately the drydock and installed at a later date. Effort was made to flatten the lower tank lining beneath the ion source. The area was heated to anneal and pounded into shape as well as possible. The upper ion catcher was replaced because of the condition of the tungsten tip and the appearance of impending water leaks in the cooling line.

Anticipated bombardments requiring higher energy particles dictated an increase operating frequency. This required shortening the dee stems by movement of the shorting spiders. In this manner, the frequency was changed from 11.395 m.c. to 11.62 m.c. This repair was completed in 370 hours. A breakdown of time showed the following:

Disassembly	32.0 hrs
Repairing stem	137.0 hrs
Assembly	49.3 hrs
Frequency measurements	7.0 hrs
Leak hunting	89.6 hrs
Bake in	55.1 hrs
	370.0 hrs

Considerable time was spent (after the system had been baked in) adjusting the various parameters. The deuteron beam was located without much difficulty but was peaked at 8-10 μa with a power input of about 120 KW. This was very poor from an overall efficiency point of view. Repeated adjustments of source, magnet shims and dee yielded very little response, with the exception of those made on the west dee horizontal. This dee carries the ion exit channel. Repeatedly, it was found that when the exit dee was moved 7 divisions (1/4") toward the tank center, beam increases of a factor of approximately 2 were realized. However, centering the beam on the target through deflector adjustments was impossible. Also, excessive sparking and heating was noted in the narrow throat between the dees and the main section of the dee stems.

Efforts at adjustments to increase the beam at a fixed dee setting 1/4" out from the position of natural maximum yielded little results. The central pyramidal shims were moved, and the deflector, east dee and ion source were adjusted without appreciable increase in beam.

A survey of magnetic field plots indicated that at the exit radius, the field drop off slope had increased from 5.3% to about 6% because of the higher field associated with the increased frequency. Thus, it was decided that the frequency should be returned to the former level of 11.350 m.c. until such time that peripheral field shims can be designed and constructed to decrease the drop-off at the exit radius and until more dee voltage is made available.

Evidence that the beam was not approaching the exit channel at a desirable angle was shown when the deflector was removed during the frequency lowering. Figure 2 shows the section of the deflector adjacent to the exit strip. The dark pointed mark is an area of deep erosion which occurred down the channel about 1/4" beyond the exit strip. In other words, the beam was striking the deflector at an angle instead of being tangent to it. Because of this, the position of the source and dee center was checked. It was found that the center of the East (feeler) dee was 1/4" off center along the line between the dees and the source was about 1/2" off in the same direction. It had been found previously that the beam was better when the source was off center and it had been lined up with the dee as a reference. However, the dee was apparently not assembled on center during the above mentioned overhaul and, hence, induced an erroneous position for the ion source.

With the operating frequency lowered to 11.35 m.c. and the corresponding reduction of 12 amps in magnet field current, the beam output has been doubled. Average operating beam intensities are now as follows:

Alpha particles	5-6 μa
Deuterons	30-40 μa
Molecular hydrogen (for protons)	15-20 μa

FIG. 2

DEEP EROSION ON SECTION OF DEFLECTOR ADJACENT TO EXIT STRIP

OZ-280

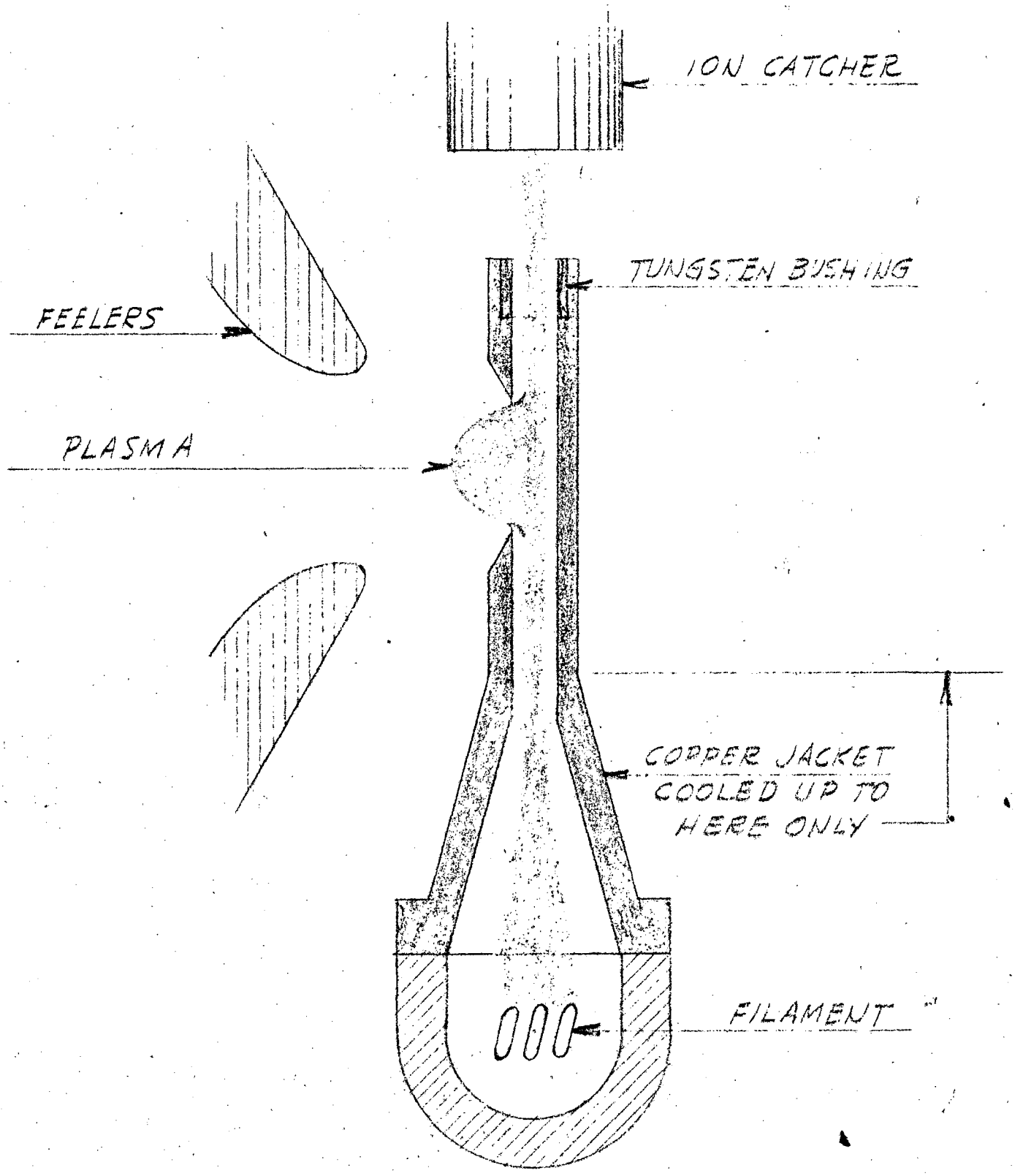

HOODED SOURCE

FIG. 3

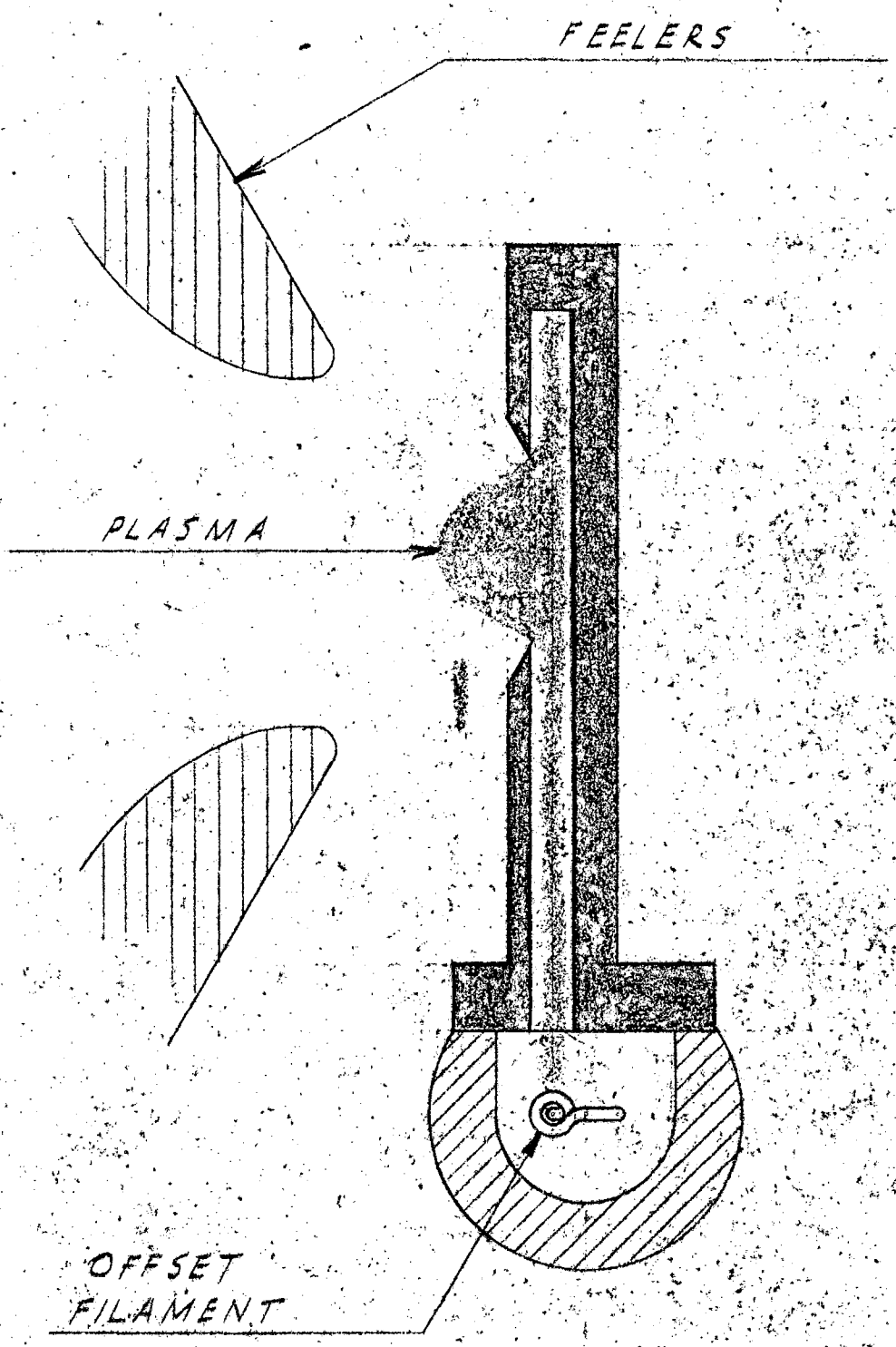

HOODED CONE

FIG. 4.

ı Source Development

Ion Sources. Water cooled completely hooded source. This source was designed to provide the following features:

1. Complete ion hood - this eliminates the need for a water cooled ion catcher above the arc, thus providing for more freedom in adjusting.
2. Water cooled hood - to provide for dissipation of heat generated internally by the arc and externally by off-center high energy ion bombardment.
3. Arc shield - complete shielding of the ion arc with the exception of a 1" x 1/8" opening facing the dee feelers. This feature lowers the ion loading of the oscillator to a comparatively small amount.
4. Collimated electron beam - a 1/4" collimating hole placed above the heated tungsten filament provides electron collimation, increasing the ion arc density.
5. General cone shape - this has been changed from the bulky copper section (Fig. 3) to a cylindrical section 17/32" in diameter and 4-1/2" long (Fig. 4). This permits a closer approach to the electric field forming feelers without danger of arcing of the R.F. voltage from them. The use of this source has been very satisfactory. Performance with deuterons and alpha particles has been as good as with any other type cone used. However, with protons the erosion of the cone has been less and the life of the source has been considerably longer.
6. Filament - in order to allow the close approach to the feelers mentioned above, it was necessary to place the collimating chamber off-center in the direction of the feelers. This required the use of a different type of filament than has been previously used. A 70 mil three-turn coil filament was previously used (Fig. 5). This was modified as per Fig. 6.

Fig. 5

Fig. 6

With this new filament, adjustments appear to be less sensitive than before. Other types of filaments were tried to stabilize the arcs jumping from turn to turn and to further define the area exposed to the arc (Fig. 7).

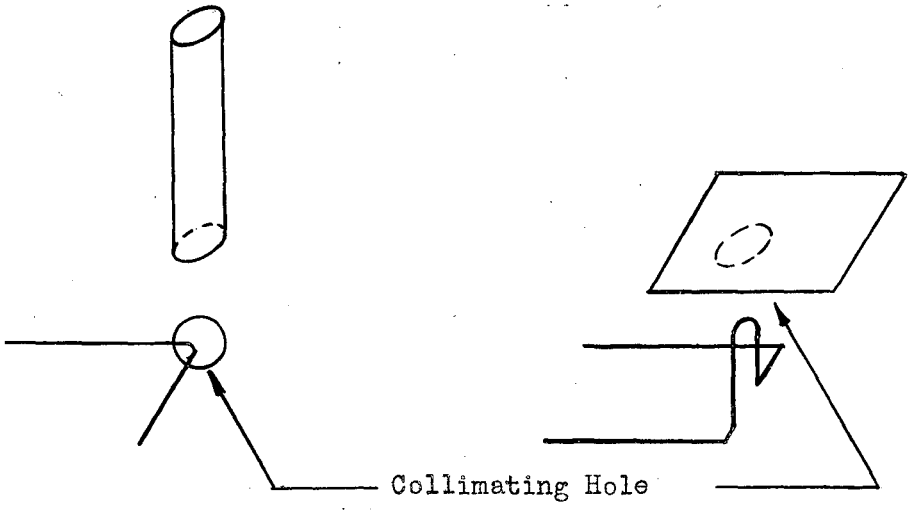

Fig. 7

s System. From time to time, drastic differences in beam output have been noted with no parent change in operating conditions. On these occasions, inspection revealed small air or water leaks contaminating the gas supply. In the case of the use of both deuterium and hydrogen, the gas was produced by electrolysis. This system was under question with respect to proton acceleration and lead to the use of commercially bottled hydrogen. Before the use of this commercial gas, 4-5 μa of protons was peak performance. Since this bottled gas has been used, proton beams up to 20 μa have been realized. This same effect was noted with bottled deuterium gas on one occasion.

The gas system in use to transport gas from the generators in the control room to the vacuum tank consisted of a run of about 100 feet of 1/2" copper tubing. The pressure in this system had been estimated at 300 μa (3×10^{-2} mm). This long tube did not lend itself to fast outgassing or decontamination when changes in gas were made. During the above tests, this line was by-passed and the gas was injected through a 6 foot section of 1/2" copper. Since bottled hydrogen is available commercially, it is now being used instead of the self-generated gas. A new gas system has also been installed eliminating the long vacuum run to the tank. The present short vacuum run is adequately exposed for leak checking since small leaks have been found to have a marked effect on beam intensities.

Identification Experiments with Heavy Ions

In the program to accelerate carbon or boron ions, there have been three runs with the 60" cyclotron during the past quarter. The main attention has been paid to getting a means of detecting particles without ambiguity. Further, instrumentation was sought which would give quantitative data as a basis for adjustments and for the design of new ion sources to produce the complete ionization required.

An optical detection system was tried, using anthracene crystals in which the emerging particles produced scintillations. These were picked up by a photomultiplier tube outside the magnetic field and gave pips on a synchroscope screen. While this method provides a very fast counter, the pulses varied so much in height that carbon ions could not be distinguished from alpha particles. The latter come from helium contamination in the tank and resonate so closely above the carbon ions that it is difficult to separate them. Even though we inserted increasing thicknesses of absorbing aluminum foils in the beam, no visual effect could be detected in the pips (such as intensification of the heights of carbon pips at the end of the Bragg curve and the cutting out of the carbon particles before the alphas were extinguished). All pips were cleared by absorption path length equivalent to about 148 mg/cm^2 Al, which corresponds closely to 36.8 Mev alphas.

A run was made next using an ionization chamber hooked up to an oscilloscope. This was checked by substituting a photographic chamber containing Ilford nuclear emulsions for the ionization chamber when optimum beams were obtained. The ionization chamber gave visual results more satisfactory than those from the anthracene counter. Three components could be found to the beam near C^{12} resonance:

1. a low-resonant portion, not affected by the deflector voltage, even when turned to zero. It was cut out by about 30 mg/cm^2;
2. a component which, with the particular conditions of the day, could be quite distinctly separated from the alphas, both by pip heights and magnet resonance, though the resonance curves overlap, the alphas being higher. This component was absorbed by about 40 mg/cm^2 Al;
3. Alphas, of normal absorption length.

The nuclear emulsions served to confirm the oscilloscope. Emulsions D-1 and E-1 were used, which should show only alphas or heavier particles. On one plate, exposed for five

seconds to the full beam when the oscilloscope indicated carbons well resolved from alphas, ere are two distinct types of tracks. The heavy track being about 65 microns long (which corresponds well with expected length of about 165 microns for 110 Mev carbons, when account is taken of the fact that the absorption path length before entering into the photographic chamber is about 28 mg/cm^2 Al and the initial range of the carbons at 110 Mev should be about 49 mg/cm^2 Al). The lighter tracks are about 330 microns long (approximately correct for alphas, which should have an expected length of about 510 microns at 36.8 Mev. An energy of 36.8 Mev corresponds to an aluminum absorption length of 146 mg/cm^2, but it must be recalled that this was diminished by an equivalent path of 28 mg/cm^2 Al before entering the chamber). The ratio of carbons to alphas was about ten to one, and a count of tracks along grid lines gives a minimum estimate of the order of 70,000 carbons per second. See sketch in Fig. 8.

Another plate exposed to a 1/8" slit beam (Fig. 9) with the photographic plate placed well back in the hope that the alphas and carbon beams would be separated by the magnetic field after their energy was degraded by the 28 mg/cm^2 Al leading to the chamber, gave no evident separation. Here we tuned visually for an approximately equal ratio of alphas and carbons, but the normal alphas were about fifty times as numerous as carbons. This slit beam showed a third component (apparently that observed on the oscilloscope) besides the normal alphas (emulsion length of about 380 microns) and the carbons (65 microns path length). Note that the path length of the alphas here appears to be a little longer than in the other plate described. This may be a real effect since Fig. 8 was at slightly lower magnet resonance, but more probably is not real and is due to the fact that alpha tracks were too sparse at entering the emulsion to be followed, since, in general, they could not be traced up in the emulsion as far as the surface grains. Although the two plates were of the same emulsion, the tracks are noticeably less dense in Fig. 8.

The third component had been bent by the magnet to fall over all the portion of the film lying on the inside of the path cut out by the normal beam from the slit. The tracks were light, of apparent density that of alphas, but were shorter (varying widely, but averaging around 120-160 microns). They had many more bends from collisions, and their angle of track in the emulsion was much more sharply bent in by the magnet. This third component was even more numerous than the normal alphas. See Fig. 9 for typical view at point A.

A supplementary motor-generator set was installed in the building previously housing the 37" cyclotron, to permit going up to magnet resonance for $C^{13(6+)}$ ions. Such ions were detected by the ionization chamber and by tracks taken in Ilford nuclear emulsions. The range of these ions was about 7 mg/cm^2 Al longer than that of $C^{12(6+)}$ ions. Counts made along grid lines of a plate exposed for 1 minute gave an estimate of only about 50 particles per second. Compare this with the C^{12} beam in light of the fact that we used CO_2 gas having the natural distribution of carbon isotopes - 1.1% C^{13} - and that the magnetic field shape at this high resonance is theoretically very poor.

A run was made with BF_3 gas in an attempt to accelerate $B^{10(5+)}$ ions. There was fair visual evidence of a small boron beam on the upper side of alpha resonance, but cyclotron operating conditions were poor, due to sparking of the deflector, which became progressively worse. This sparking may have been caused by the nature of the gas used, since BF_3 with hydrogen gives HF. Indeed, operation did not return to normal until a couple of days later. A try was made for $B^{11(5+)}$ ions, but no beam was observed at this high resonance.

The next run to be made will be an attempt to get quantitative data with a Richardson scaler with discriminator to cut out alphas and count only carbons. It is hoped a long snout will serve to cut out other than carbon and normal alphas.

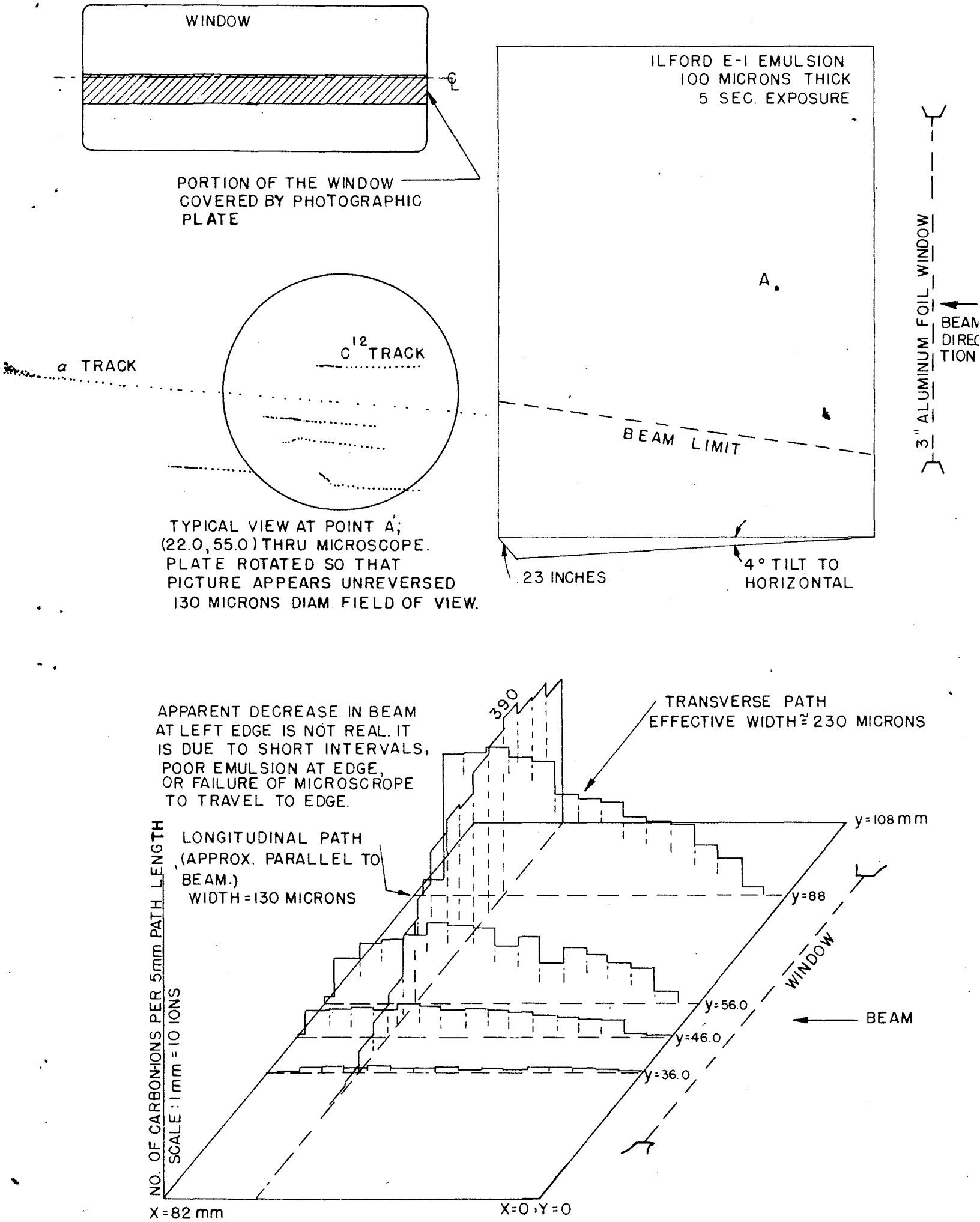
WINDOW
℄
PORTION OF THE WINDOW COVERED BY PHOTOGRAPHIC PLATE
ILFORD E-1 EMULSION
100 MICRONS THICK
5 SEC. EXPOSURE
A
3" ALUMINUM FOIL WINDOW
BEAM DIRECTION
α TRACK
C12 TRACK
BEAM LIMIT
TYPICAL VIEW AT POINT A; (22.0, 55.0) THRU MICROSCOPE. PLATE ROTATED SO THAT PICTURE APPEARS UNREVERSED 130 MICRONS DIAM. FIELD OF VIEW.
23 INCHES
4° TILT TO HORIZONTAL
APPARENT DECREASE IN BEAM AT LEFT EDGE IS NOT REAL. IT IS DUE TO SHORT INTERVALS, POOR EMULSION AT EDGE, OR FAILURE OF MICROSCROPE TO TRAVEL TO EDGE.
390
TRANSVERSE PATH EFFECTIVE WIDTH ≅ 230 MICRONS
LONGITUDINAL PATH (APPROX. PARALLEL TO BEAM.) WIDTH = 130 MICRONS
NO. OF CARBON-IONS PER 5mm PATH LENGTH
SCALE: 1mm = 10 IONS
y = 108 mm
y = 88
y = 56.0
y = 46.0
y = 36.0
WINDOW
BEAM
X = 82 mm
X=0, Y=0

FIG. 8

13166-1

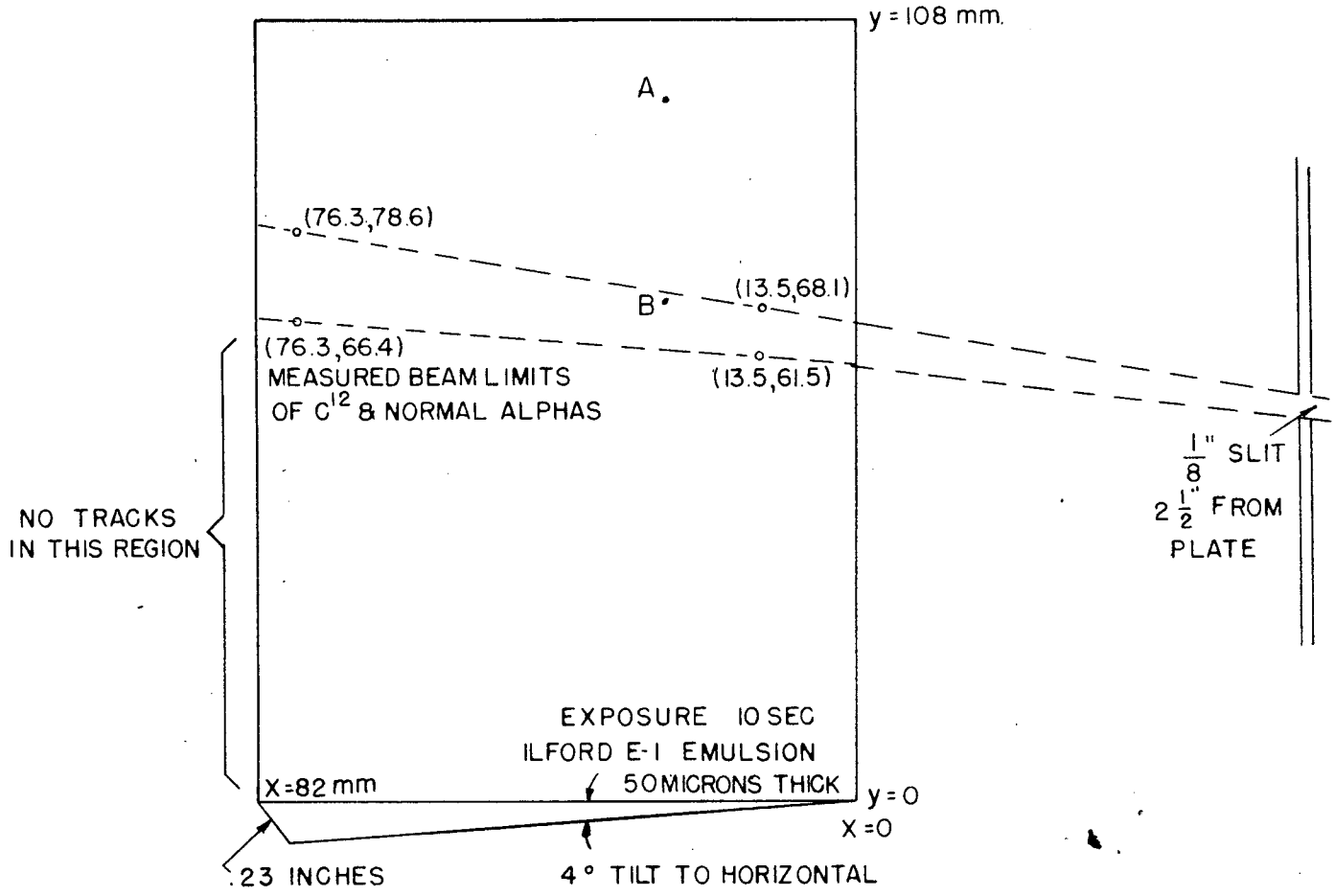

VIEWS AT RIGHT TAKEN THROUGH OIL-IMMERSION MICROSCOPE, 1000 ×. PLATE ROTATED THRU 180° SO THAT PICTURES APPEAR UNREVERSED.

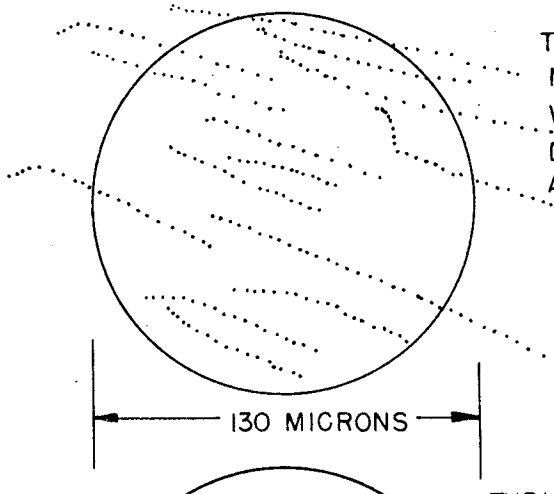

TYPICAL VIEW, POINT A. NOTE ANGLE OF TRACKS, WIDELY VARIABLE LENGTH DENSITY OF GRAINS ALONG TRACK ABOUT THAT FOR ALPHAS.

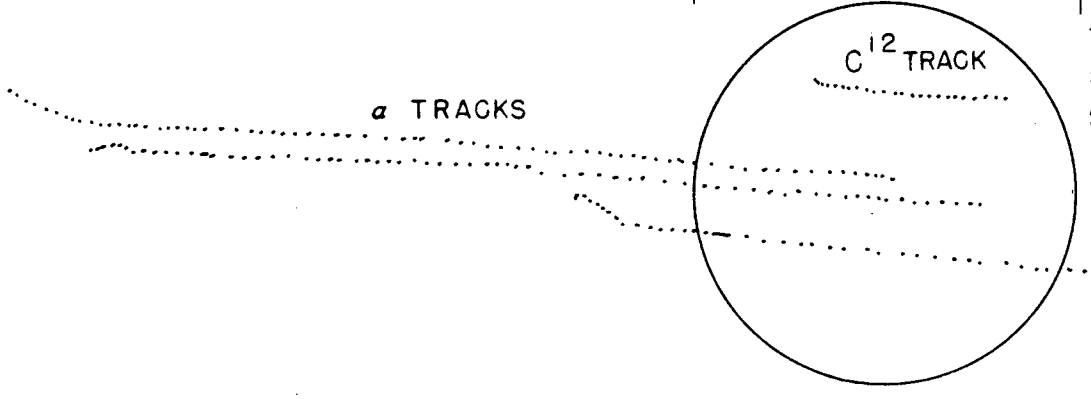

TYPICAL VIEW, POINT B. NOTE UNIFORM SLOPE, SMALLER THAN AT A. TRACKS ARE OF UNIFORM LENGTH: ABOUT 370 MICRONS FOR α'S: 65 MICRONS FOR C^{12}

FIG. 9

13167-1

e Effects of Peripheral Magnetic Shims on the Magnetic Field

Purpose. It is expected that the operation of the 60" cyclotron can be improved in several ways by the proper shimming of the magnetic field. Three possible improvements may be as follows:

1. More energetic particles in the beam due to less dropping off of the field near the periphery, giving a greater value of B to the particles as they enter the deflector channel.

2. Larger beam currents due to more uniform magnetic field throughout the trajectory. This should make it possible for more of the particles to stay in phase throughout their trajectories and require less dee voltage to obtain the same beam.

3. Smoother operation of the deflector - it is suspected that the smoothness of deflector operation and the life of the deflector insulators is closely related to the uniformity of the magnetic field in the deflector region. Thus, if a more uniform magnetic field can be obtained by shimming, deflector operation may be improved.

Description of the Shims. The shims used in this test consisted of annular rings made of mild steel. They were 7/8" thick and had an outside diameter of 57 inches. They were built in sections, which could be linked easily for rapid installation. Fig. 10 shows the general assembly diagram of these shims. They were constructed so that extra sections could be added to the inside of the rings, thus varying their widths. Two widths were tried and measured in this determination. They were 3 1/2 inches and 5 1/2 inches. For comparison, the field was also measured without any of the peripheral shims present.

The shims were tried in pairs. One ring was installed between the upper tank cover and the upper pole face, while a second one was placed between the lower pole face and lower tank cover, as shown in Fig. 11. They were centered so that their axes coincided with the axis of the pole faces.

In all determinations, the usual operation set of pyramidal magnetic shims, consisting of a stack of four 1/16" circular plates of rapidly decreasing diameters, was left in the center between the tank walls and the pole faces.

Procedure. The method of making the magnetic measurements was as follows: The absolute magnitude of the magnetic field was determined by putting a flip coil of known area in the center of the tank in the median plane and lining it up with its axis parallel to the magnetic field. The coil was then rotated through 180° about an axis perpendicular to the axis of the coil. The electrical impulse generated was measured with a General Electric Fluxmeter. The fluxmeter deflection was then compared with a deflection from a calibrated Hibbert Magnetic Standard, and the magnitude of the magnetic field in the center of the tank was thereby determined.

The uniformity of the magnetic field along the median plane was determined in a somewhat similar manner. However, instead of the flip coil, a search coil of known area was substituted. The coil was mounted on a car, which moved along six-foot tracks. This "box car" was provided with stops, so that this car (on which the coil was mounted) could be moved in 1 inch jumps. The search coil was mounted solidly on the car, so that its axis remained parallel to the field during the determination. The schematic of the circuit used is shown in Fig. 12.

FIG. 10

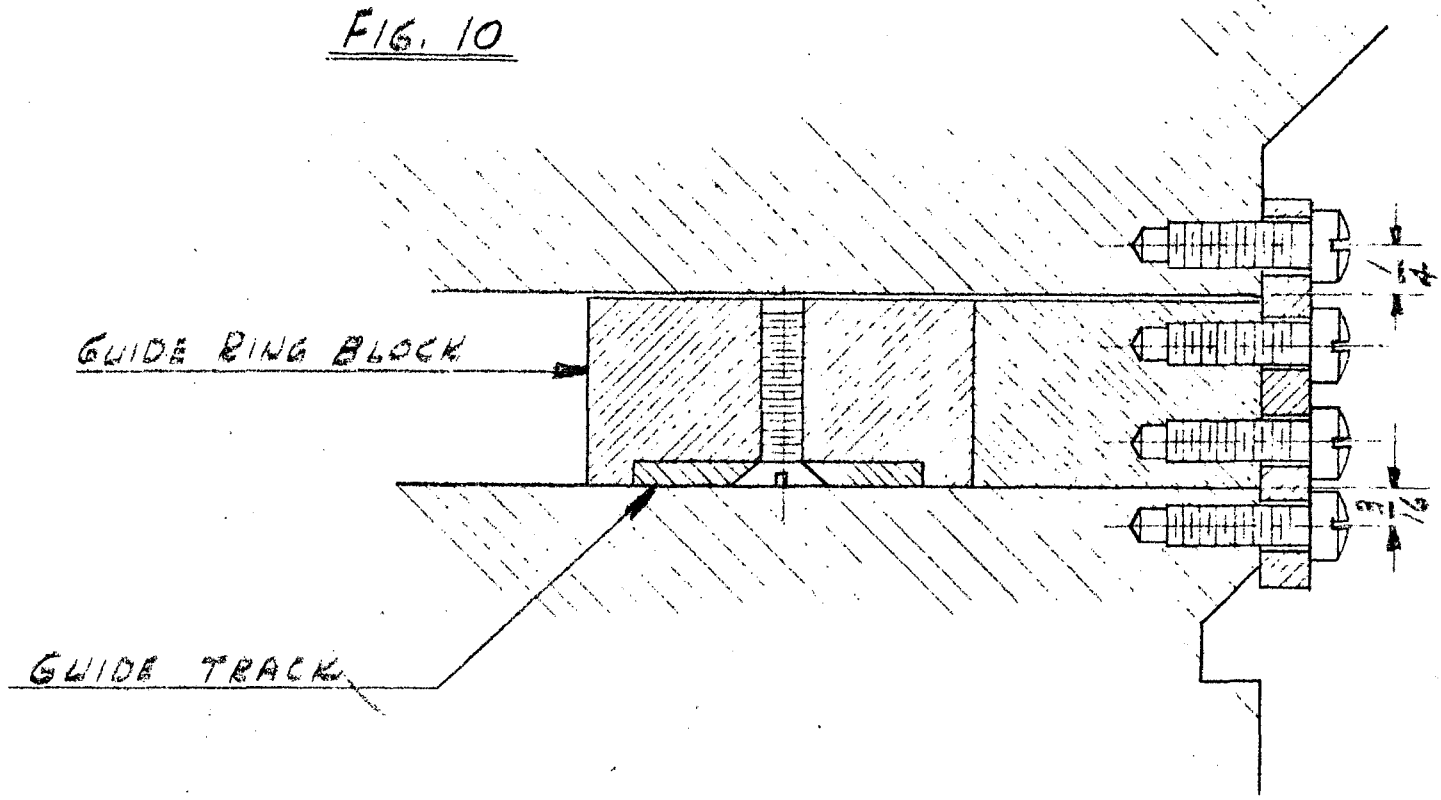

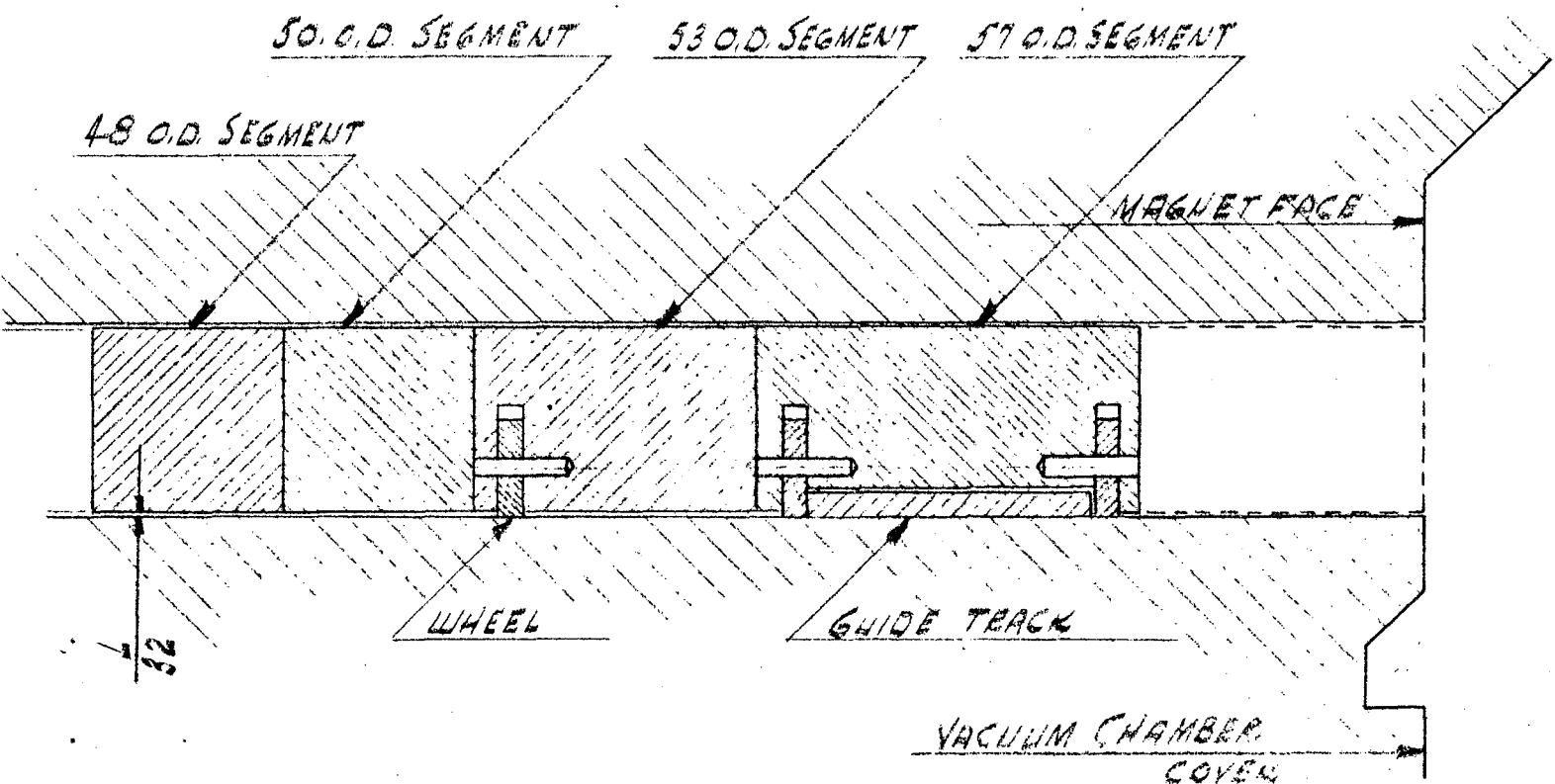

SECTION THRU WHEELS

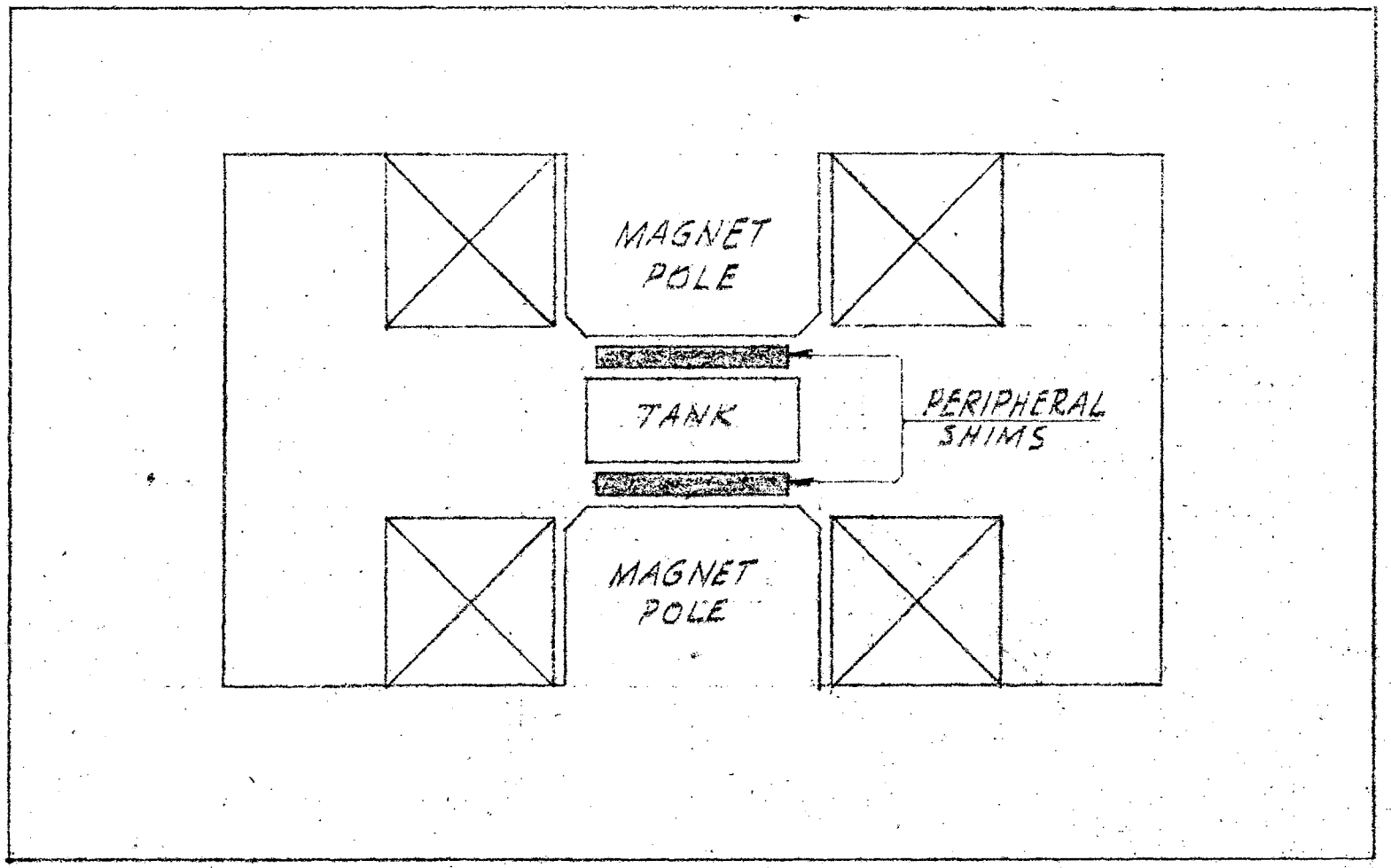

Peripheral Shim Position Diagram

FIGURE 11

60-13

13206-1

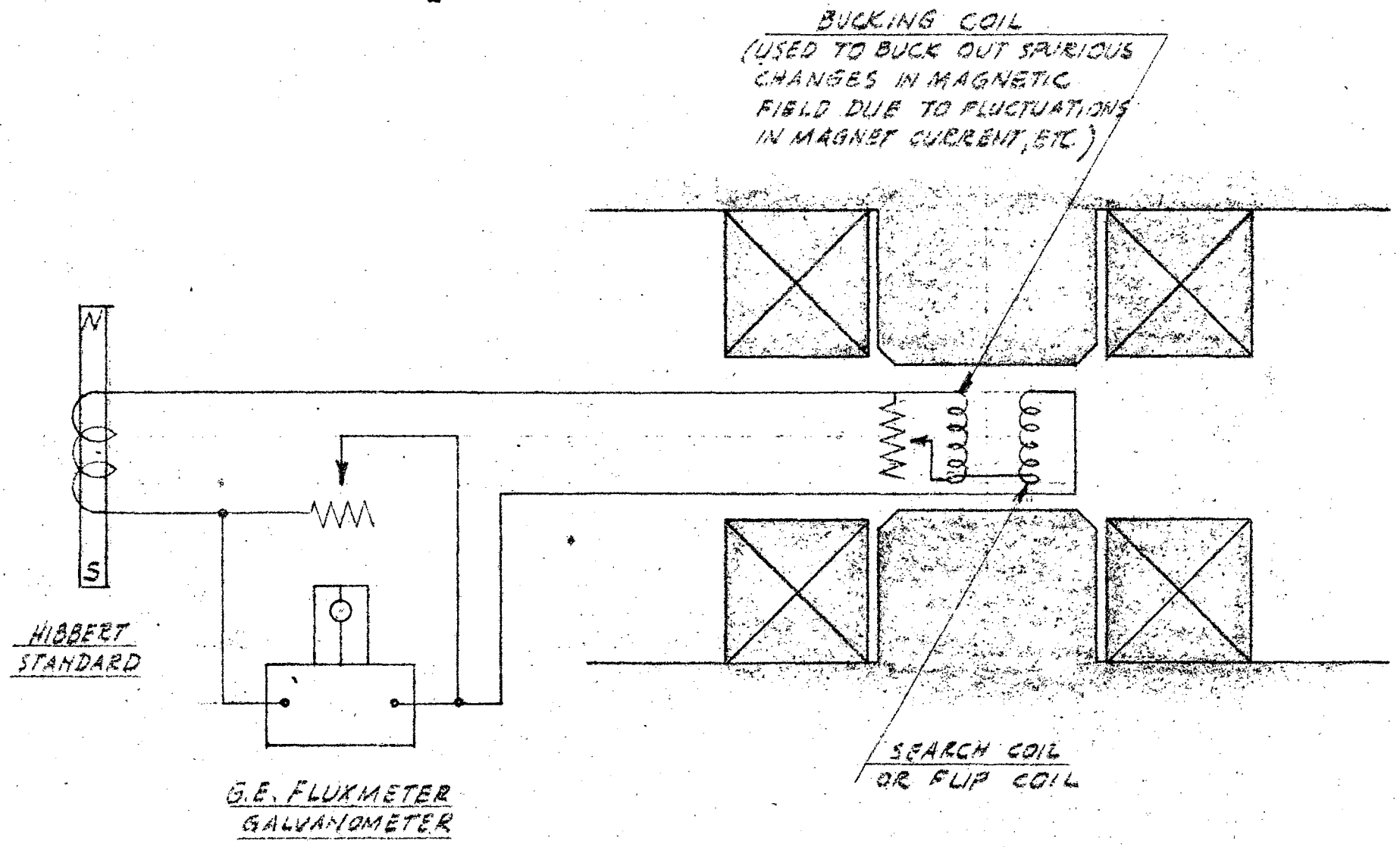

Schematic of Magnet Measurement Circuit

FIGURE 12

60-19

13207-1

The runs were made with the coil located in the median plane of the gap. It was ved in the north-south direction across the diameter of the pole face . The runs extended om 26" south of the center to 44" north of the center.

Results. The results are found in Figures 13 - 18 and are plotted graphically in Figures 19 and 20. It is seen from these graphs that there is approximately a 0.5% less drop in field at the 25 inch radius with the shims present than without them. Since the energy of the particles is proportional to the square of the field, this means a 1% gain in energy of the particles. This lower drop in field also means that more of the particles should stay in phase. It is expected that this will increase the beam current. Since the slope of the graph is steeper with the shims than without them, a greater curvature of the magnetic field in the deflector region is indicated with the shims than without them. It is expected that this may be more detrimental than beneficial to the operation of the deflector.

In the presence of the shims, since the drop in field is very slow as one goes away from the center, the magnetic focusing is reduced over most of the trajectory. This would tend to reduce the beam current. In the case of the full peripheral shims, 5 1/2 inches x 7/8 inch, there is actually a rise in the field, as one goes away from the center in a southerly direction. This would indicate an actual magnetic defocusing of the beam, since the curvature is inward instead of outward in this region.

The expected decrease in beam due to lack of focusing out to 18 inches was noted when actual beam tests were made. The beam was reduced by a factor of about 10. A further attempt to decrease the fall off in field at the exit strip will be made in the form of internal shims. It will be possible to insert copper plated rings inside the vacuum, the shape and size of which is to be determined by model testing. With this kind of shim, it should be possible to decrease the percentage fall off of the field at the exit strip to 2 1/2-3 percent and, hence, to obtain a considerable increase in beam.

Figure 13

Shim Arrangement: Pyramid

Magnet Current: 290 amps

Sensitivity: 35.461 gauss/cm.

Median Plane

Field in Center: 15,395 gauss

Inches from Center South	Average Deflection	Percent Change	Total Percent Change
1	.01	.002	.002
2	.04	.009	.011
3	.07	.016	.027
4	.11	.025	.052
5	.17	.039	.091
6	.19	.044	.135
7	.21	.048	.183
8	.24	.055	.238
9	.25	.058	.296
10	.28	.064	.360
11	.28	.064	.424
12	.26	.060	.484
13	.26	.060	.544
14	.25	.058	.602
15	.26	.060	.662
16	.28	.064	.726
17	.30	.069	.795
18	.39	.090	.885
19	.51	.117	1.002
20	.73	.168	1.170
21	1.12	.258	1.428
22	1.74	.401	1.829
23	2.84	.654	2.483
24	4.54	1.046	3.529
25	7.19	1.656	5.185
26	11.04	2.543	7.728

Figure 14

Shim Arrangement: Pyramid
Sensitivity: 35.407 gauss/cm (A)
70.718 gauss/cm (B)
Field in Center: 15.371 gauss

Magnet Current: 290 amps

Median Plane

Inches from Center North		Average Deflection	Percent Change	Total Percent Change
(A)	1	.00	.000	.000
	2	.03	.007	.007
	3	.08	.018	.025
	4	.11	.025	.051
	5	.16	0.37	.088
	6	.19	.044	.131
	7	.20	.046	.177
	8	.23	.053	.230
	9	.25	.058	.288
	10	.25	.058	.346
	11	.28	.064	.410
	12	.30	.069	.479
	13	.30	.069	.548
	14	.29	.067	.615
	15	.24	.055	.670
	16	.31	.071	.742
	17	.36	.083	.825
	18	.44	.101	.926
	19	.58	.134	1.060
	20	.84	.193	1.253
	21	1.23	.283	1.536
	22	1.90	.438	1.974
	23	3.07	.707	2.681
	24	4.86	1.119	3.801
	25	7.69	1.771	5.572
	26	11.45	2.638	8.210
	27	16.36	3.769	11.978
(B)	28	10.81	4.973	16.951
	29	12.83	6.903	22.854
	30	13.81	6.354	29.208
	31	13.81	6.354	35.562
	32	12.78	5.880	41.442
	33	11.45	5.268	46.710
	34	9.99	4.596	51.306
	35	8.78	4.039	55.345
	36	7.77	3.575	58.920
	37	6.93	3.188	62.108
	38	6.22	2.862	64.970
	39	5.73	2.636	67.606
	40	5.25	2.415	70.021
	41	4.86	2.236	72.257
	42	4.60	2.116	74.373
	43	4.32	1.988	76.361
	44	4.02	1.849	78.210

Figure 15

Shim Arrangement: Pyramid + (3 1/2" x 7/8") Peripheral

Sensitivity: 35.524 gauss/cm. Magnet Current: 290 amps

Field in Center: 15,217 gauss Median Plane

Inches from Center South	Average Deflection	Percent Change	Total Percent Change
1	.00	.000	.000
2	.00	.000	.000
3	.00	.000	.000
4	.02	.005	.005
5	.04	.009	.014
6	.04	.009	.023
7	.04	.009	.032
8	.03	.007	.039
9	.05	.012	.051
10	.02	.005	.056
11	.02	.005	.061
12	.01	.002	.063
13	.02	.005	.068
14	.08	.019	.087
15	.05	.012	.099
16	.08	.019	.118
17	.14	.033	.151
18	.21	.049	.200
19	.37	.086	.286
20	.63	.147	.433
21	1.06	.247	.680
22	1.72	.402	1.082
23	2.84	.663	1.745
24	4.61	1.076	2.821
25	7.25	1.693	4.514
26	11.10	2.591	7.105

Figure 16

Shim Arrangement: Pyramid + (3 1/2" x 7/8") Peripheral
Sensitivity: 35.524 gauss/cm (A)
84.305 gauss/cm (B)
Field in Center: 15,217 gauss

Magnet Current 290 amps
Median Plane

Inches from Center North		Average Deflection	Percent Change	Total Percent Change
(A)	1	.00	.000	.000
	2	.01	.002	.002
	3	.01	.002	.004
	4	.03	.007	.011
	5	.06	.014	.025
	6	.07	.016	.041
	7	.05	.012	.053
	8	.07	.016	.069
	9	.06	.015	.083
	10	.07	.016	.099
	11	.07	.016	.115
	12	.05	.012	.127
	13	.09	.021	.148
	14	.10	.023	.171
	15	.06	.014	.185
	16	.12	.028	.213
	17	.22	.051	.264
	18	.27	.063	.327
	19	.43	.100	.427
	20	.74	.173	.600
	21	1.20	.280	.880
	22	1.85	.432	1.312
	23	3.07	.717	2.029
	24	4.90	1.144	3.173
	25	7.79	1.819	4.992
	26	11.59	2.706	7.698
	27	16.57	3.868	11.566
(B)	28	9.22	5.108	16.674
	29	10.92	6.050	22.724
	30	11.79	6.532	29.256
	31	11.79	6.532	35.788
	32	10.92	6.050	41.838
	33	9.77	5.413	47.251
	34	8.56	4.742	51.993
	35	7.51	4.161	56.154
	36	6.62	3.668	59.822
	37	5.90	3.269	63.091
	38	5.23	2.898	65.989
	39	4.82	2.670	68.659
	40	4.40	2.438	71.097
	41	4.12	2.283	73.380
	42	3.82	2.116	75.496
	43	3.53	1.956	77.452
	44	3.34	1.850	79.302

Figure 17

Shim Arrangement: Pyramidal + (5 1/2" x 7/8") Peripheral

Sensitivity: 35.409 gauss/cm. Magnet Current: 290 amps

Field in Center: 15.545 gauss Median Plane

Inches from Center South	Average Deflection	Percent Change	Total Percent Change
1	-.011	-.011	-.05
2	-.014	-.025	-.06
3	-.007	-.032	-.03
4	.000	-.032	.00
5	.000	-.032	.00
6	.000	-.032	.00
7	.000	-.032	.00
8	-.002	-.034	-.01
9	-.007	-.041	-.03
10	-.002	-.043	-.01
11	-.005	-.048	-.02
12	-.005	-.053	-.02
13	-.002	-.055	-.01
14	.002	-.053	.01
15	.007	-.046	.03
16	.018	-.028	.08
17	.032	.004	.14
18	.055	.059	.24
19	.093	.152	.41
20	.162	.314	.71
21	.269	.583	1.18
22	.435	1.018	1.91
23	.715	1.733	3.14
24	1.132	2.865	4.97
25	1.765	4.630	7.75
26	2.665	7.295	11.70

Figure 18

Shim Arrangement: Pyramidal + (5 1/2" x 7/8") Peripheral
Sensitivity: 35.345 gauss/cm (A) Magnet Current: 290 amps
70.699 gauss/cm (B) Median Plane
Field in Center: 15,478 gauss

Inches from Center North		Average Deflection	Percent Change	Total Percent Change
(A)	1	.04	.009	.009
	2	.03	.007	.016
	3	.04	.009	.025
	4	.05	.011	.036
	5	.04	.009	.045
	6	.02	.005	.050
	7	.01	.002	.051
	8	.01	.000	.051
	9	.00	.000	.052
	10	.01	.002	.054
	11	.01	.002	.056
	12	.04	.009	.065
	13	.00	.000	.065
	14	.00	.000	.065
	15	.09	.021	.086
	16	.11	.025	.111
	17	.16	.037	.148
	18	.29	.066	.214
	19	.47	.107	.321
	20	.79	.180	.501
	21	1.26	.288	.789
	22	2.00	.456	1.245
	23	3.29	.751	1.996
	24	5.23	1.194	3.190
	25	8.11	1.852	5.042
	26	12.02	2.745	7.787
	27	17.07	3.898	11.685
(B)	28	11.29	5.144	16.829
	29	13.27	6.046	22.875
	30	14.31	6.520	29.395
	31	14.31	6.520	35.915
	32	13.24	6.032	41.947
	33	11.83	5.390	47.337
	34	10.38	4.729	52.066
	35	9.08	4.137	56.203
	36	8.04	3.663	59.866
	37	7.13	3.249	63.115
	38	6.39	2.911	66.026
	39	5.83	2.656	68.682
	40	5.35	2.438	71.120
	41	4.96	2.260	73.380
	42	4.63	2.110	75.490
	43	4.30	1.959	77.449
	44	4.05	1.845	79.294

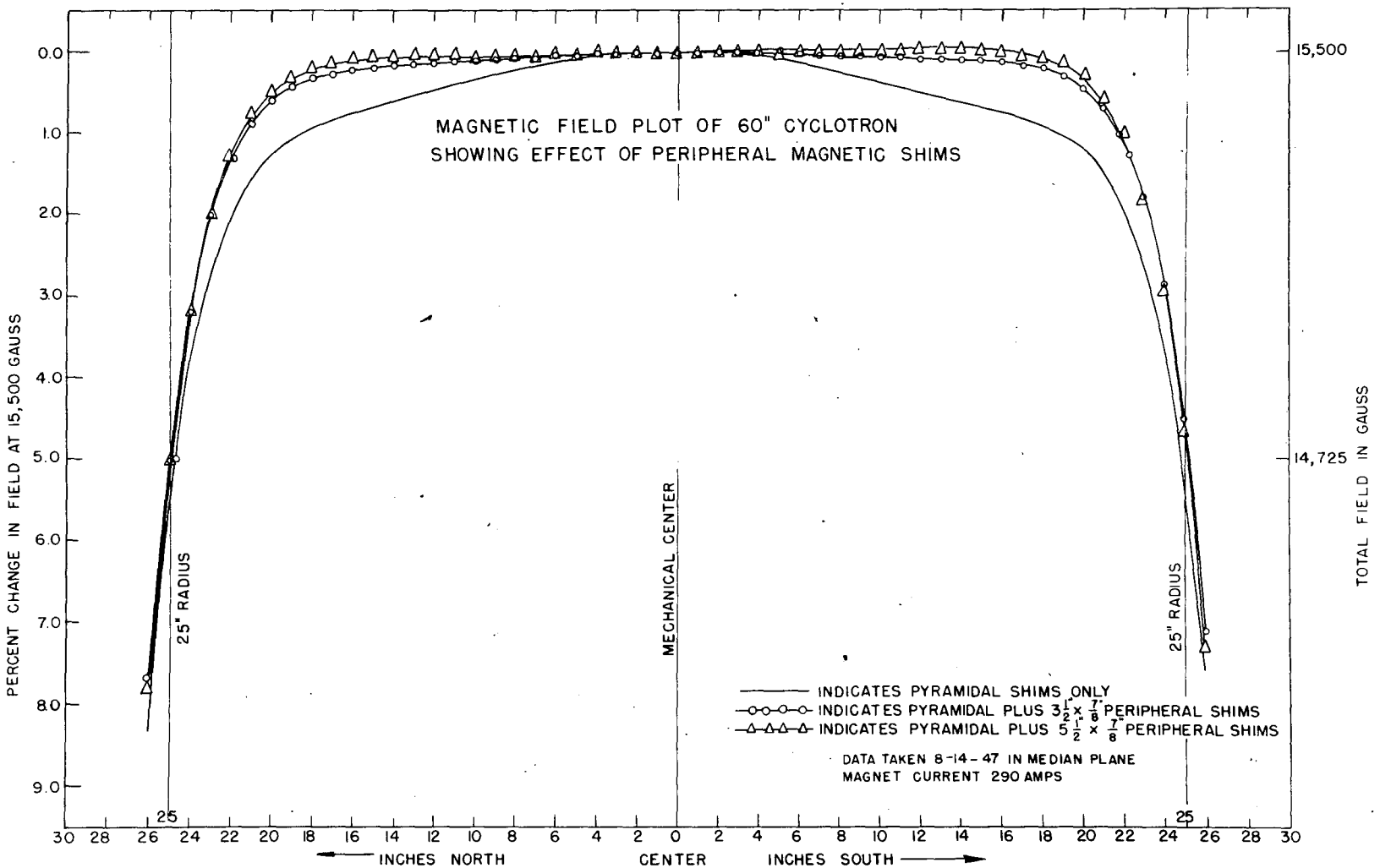
MAGNETIC FIELD PLOT OF 60" CYCLOTRON
SHOWING EFFECT OF PERIPHERAL MAGNETIC SHIMS
PERCENT CHANGE IN FIELD AT 15,500 GAUSS
TOTAL FIELD IN GAUSS
15,500
14,725
25" RADIUS
MECHANICAL CENTER
INDICATES PYRAMIDAL SHIMS ONLY
INDICATES PYRAMIDAL PLUS 3½" x 7/8" PERIPHERAL SHIMS
INDICATES PYRAMIDAL PLUS 5½" x 7/8" PERIPHERAL SHIMS
DATA TAKEN 8-14-47 IN MEDIAN PLANE
MAGNET CURRENT 290 AMPS
INCHES NORTH
CENTER
INCHES SOUTH

FIG. 19

OZ-285

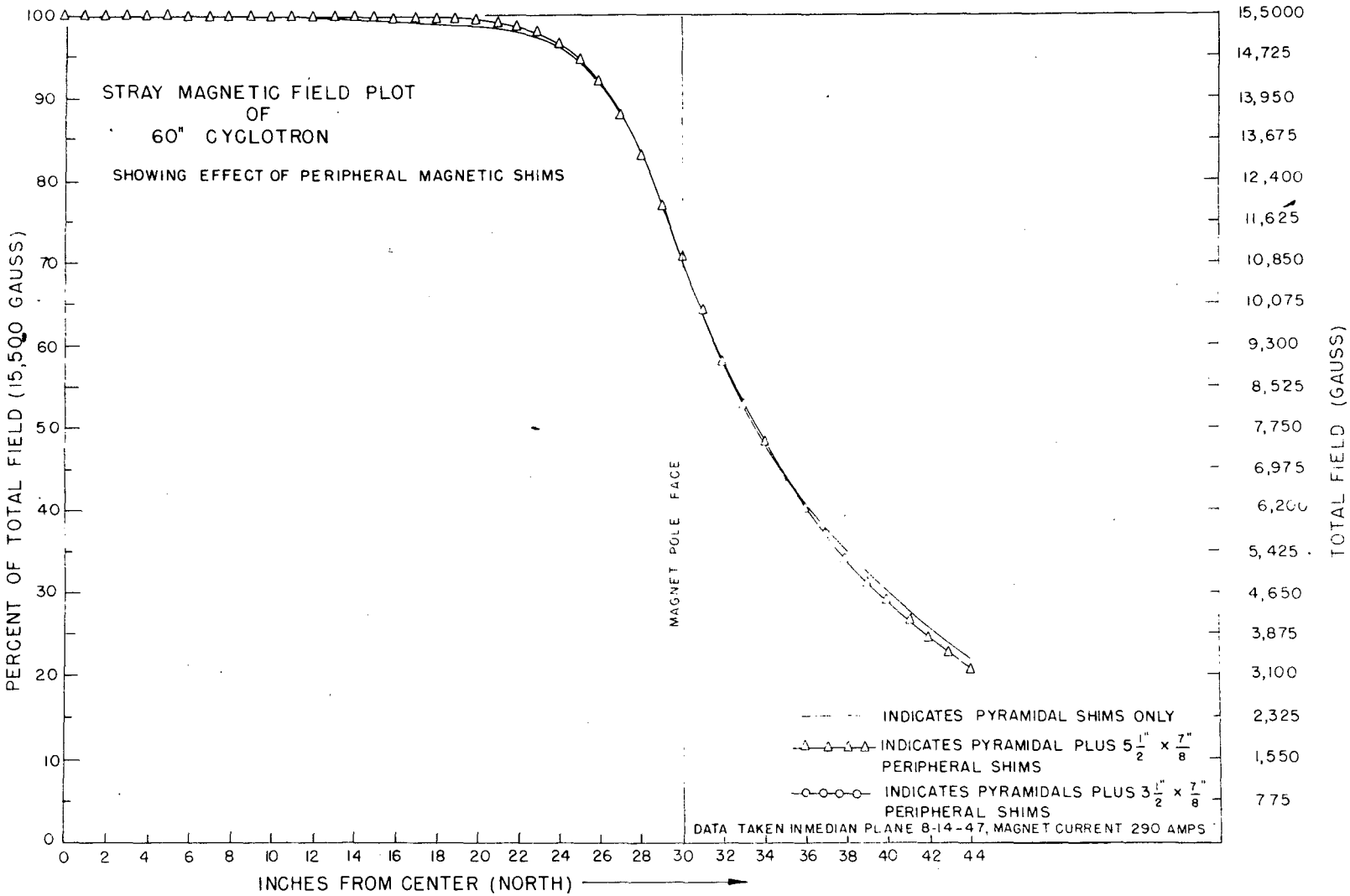
STRAY MAGNETIC FIELD PLOT
OF
60" CYCLOTRON
SHOWING EFFECT OF PERIPHERAL MAGNETIC SHIMS
PERCENT OF TOTAL FIELD (15,500 GAUSS)
TOTAL FIELD (GAUSS)
INCHES FROM CENTER (NORTH)
MAGNET POLE FACE
INDICATES PYRAMIDAL SHIMS ONLY
INDICATES PYRAMIDAL PLUS 5 1/2" x 7/8" PERIPHERAL SHIMS
INDICATES PYRAMIDALS PLUS 3 1/2" x 7/8" PERIPHERAL SHIMS
DATA TAKEN IN MEDIAN PLANE 8-14-47, MAGNET CURRENT 290 AMPS
100
90
80
70
60
50
40
30
20
10
0
0 2 4 6 8 10 12 14 16 18 20 22 24 26 28 30 32 34 36 38 40 42 44
15,5000
14,725
13,950
13,675
12,400
11,625
10,850
10,075
9,300
8,525
7,750
6,975
6,200
5,425
4,650
3,875
3,100
2,325
1,550
775

FIG. 20

OZ-286

Oscillator "Tube Characteristics" and "Operating Efficiencies".

There are many reasons for taking the tube characteristics, although the primary interest is the oscillator efficiency. By having a continuous check upon the oscillator efficiency, the variations in beam current can be made independent of the oscillator. The oscillator was built to withstand powers many times our present power. So, when making adjustments on the cyclotron which cause the oscillator efficiency to change, it is necessary to change only the oscillator input until the R.F. power is the same as it was before. The R.F. power output would be fixed by the heat dissipation of the dees. This paper will cover primarily a simple and rapid method of calculating the R.F. power output with an absolute accuracy of 3 percent and a comparison accuracy of less than 1 percent.

Tube Characteristics. The tube characteristics are obtained by placing a variable D.C. power supply on the plate of the oscillator tube and biasing the grid to cut-off. The grid is pulsed into the conducting region for 10 to 100 microseconds, at a rate of 60 cycles per second. By varying the plate supply and the amplitude of the grid pulse, any grid and plate voltage can be supplied during the pulse. A syncroscope is used to measure the instantaneous voltage or currents on the tube . The signals to the scope were taken from the dropping resistors (Fig.21); R_1 grid current; R_2 plate current; R_5-R_6 plate voltage; R_3-R_4 grid voltage ; and applied to one of the vertical deflection plates of the scope. As each signal is applied, a second D.C. voltage is applied to the other vertical deflection plate. At the time that the trace goes through zero, the voltage of the signal and the D.C. measuring voltage have the same value. A voltmeter is used to measure the D.C. voltage which in turn gives the instantaneous voltage of the signal at the time the trace went through zero. From knowing the value of the voltage dividers and the resistance of the current resistors, all the instantaneous values of voltages and current in the tube at the time can be calculated.

The equipment consists of a 0-20 KV, 500 μa supply for the plate of the tube. A bank of high voltage condensors (20 μf.) are used to hold the plate voltage constant even though 200 amperes are drawn momentarily. The resistor, R_2, is variable to 1, 2, or 4 ohms depending on the current being read. The voltage divider R_5-R_6 is 100:1 and is frequency compensated.

The pulsing equipment uses two WL677 Thyratrons to obtain a square pulse. This square pulse is applied to the grids of eight 304's in parallel, which operates as a gating tube to apply the variable 0-2500 volt, 500 μa grid supply to the grid of the main oscillator tube. The grid supply also has a bank of condensors (20 μf.) to maintain its voltage during the pulse. All the grid current from the main oscillator tube passes through the 304's which sometimes totals 60 amperes. The grid current resistor R_1 is 4 ohms and the voltage divider R_3-R_4 is 10:1 frequency compensated. The pulse width was made variable so that a sufficient time could elapse for all transients to disappear, so that all readings could be taken at a quiescent condition.

The synchroscope is triggered by the grid voltage pulse such that any given point on the trace corresponds to the same time on each of the four pulses. The signal selector switch applies the bucking voltage to the scope in the correct direction and connects the voltmeter to each voltage as selected so that only one meter need be used.

To obtain any constant current curve (e.g., plate current 10 amps.), R_1 is set to ms and plate current measuring potentiometer to 40 volts. Starting at a low plate voltage (approximately 500 volts) and observing the plate current pulse, the grid pulse is increased until the trace passes through zero at the center. The grid voltage is then selected and the grid voltage measuring potentiometer adjusted until the trace passes through zero at the center. Then the plate voltage is selected and the plate voltage measuring potentiometer adjusted until

4 MEGAWATT TUBE TESTER

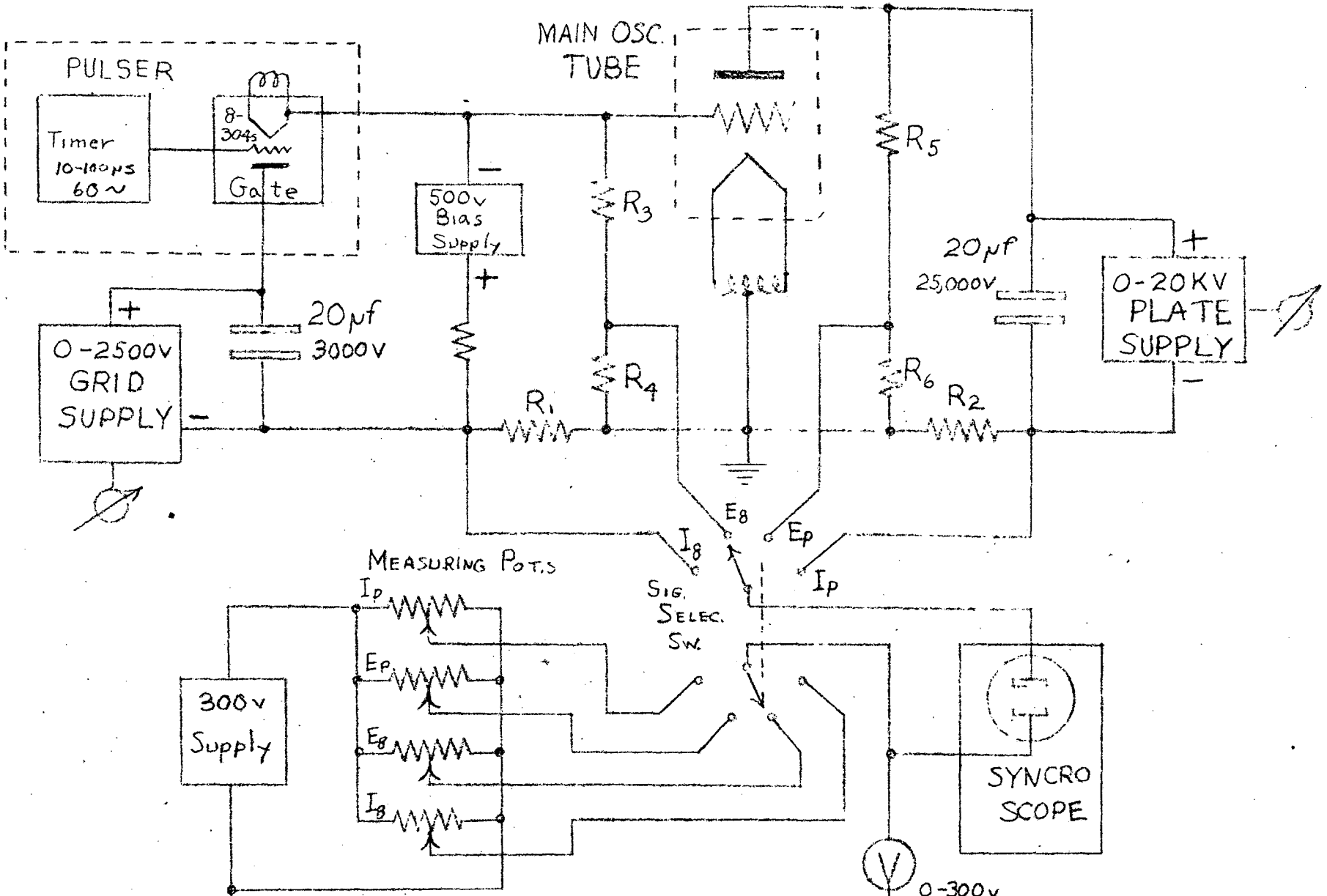

FIG. #21

trace passes through zero at the center. The grid and plate voltages are recorded. The procedure is repeated for increased plate voltages, for example, as every 500 volts at low voltages and every 1000 volts at high voltages.

Oscillator Efficiency. In calculating the operation of an oscillator, the following values must be known:

1. E_{bb} plate supply voltage
2. E_c bias voltage
3. $E_{p(1)}$ peak R.F. plate voltage
4. $E_{k(1)}$ peak R.F. cathode voltage
5. I_b average plate current
6. I_c average grid current
7. $I_{p(1)}$ fundamental peak R.F. plate current
8. $I_{g(1)}$ fundamental peak R.F. grid current

When the above values are known, all powers and efficiencies can be calculated, such as:

P_{bb}	input power	$E_{bb} \times I_b$	(1)
P_c	bias power	$E_c \times I_c$	(2)
P_b	plate power	$E_{p(1)} \times I_{p(1)} \times 0.5$	(3)
P_d	driving power	$E_{k(1)} \times (I_{p(1)} + I_{g(1)})\ 0.5$	(4)
P_p	plate dissipation	$P_{bb} - P_b - P_d$	(5)
P_g	grid dissipation	$P_d - P_c - \hat{E}_k \times \hat{I}_{p(1)} \times 0.5$	(6)
P_L	output power	$P_b - P_d$	(7)
η	plate efficiency	P_{bb} / P_b	(8)
η_L	oscillator efficiency	P_{bb} / P_L	(9)

Of the eight fundamental quantities, only the first six are readily measured. The fundamental peak R.F. plate and grid current cannot be measured directly. In some applications, it would be possible to measure these two currents by placing a wattmeter in the plate and grid circuit. However, this is hardly possible at 11 M.C. and 100 K.W. When the plate and grid current follow any geometric law, it is possible to establish a ratio between the average and fundamental R.F. currents. The plate current of a vacuum tube follows a "three halves power curve" and the grid follows a square power curve, which makes it possible to calculate the R.F. currents. The peak R.F. grid current does not vary more than 5% from 1.8 times the D.C. grid current. When calculating the output of a self excited oscillator, such a large error in the R.F. grid current will not affect the output power by more than 0.3 percent. Thus, it is safe to assume a ratio in the grid circuit to be 1.8. Such an assumption is not permissible in the plate, as any error in the ratio of the D.C. to R.F. currents will be passed on to the answer unchanged. A more elaborate system must be employed if the total accuracy is to be less than 1.0 percent. Either a graphical or analytical method can be used. The graphical method has the edge on simplicity and speed, is as accurate as the analytical and it will take into account any irregularities that exist. The ratio of the R.F. to D.C. plate current approximates the following equation within 0.2 percent.

$$\frac{\hat{I}_{p(1)}}{I_b} = 1.67 + 0.36 \quad \frac{uE_c - E_{bb}}{u\hat{E}_{g(1)} - \hat{E}_{p(1)}} \tag{10}$$

The graphical method (shown in Figure 22) is the same as the above equation except that it takes one more thing into account. Since the plate current only follows a 3/2 curve as long as a space charge exists, as soon as saturation sets in the curve begins to slope off. In Fig. 22, the curves of alpha show a correction to the value of K, which is half the ratio of the D.C. to R.F. plate current. Two ordinates are shown on Fig. 22 that have not been discussed: The minimum plate voltage $e_{p(min.)}$ and the maximum positive grid voltage $e_{g(max.)}$. These two voltages are easier and more accurate to measure than the R.F. plate and grid voltages and they also have the property of having ground as a reference level which the R.F. voltages do not. To use the graph, the plate and bias voltages are used to find the point "Q" and the minimum plate and grid voltages are used to find the point "P". Using the straight edge of a piece of paper, let the edge intersect the points "P" and "Q". Mark the points "P" and "Q" and the point "R" where the edge of the paper intersects the line "C-C". Move the paper until the point "Q" lies on "A" and move point "P" until it lies on the line "B-B". Read from the K lines at point "R" one-half the ratio of the D.C. to R.F. plate currents. If the point "P" lies to the left of any α line, that value must be subtracted to get the ratio.

Power output

$$\begin{aligned} P_L &= \hat{E}_{p(1)} \times \hat{I}_{p(1)} - \hat{E}_{g(1)} \times \hat{I}_{g(1)} \\ &= (E_{bb} - e_{p(min.)} - e_{g(max.)}) \times (K - \alpha)\, I_b \\ &= (E_c + e_{g(max.)}) \times 0.91_c \end{aligned} \tag{11}$$

From the tube characteristics, two items must be known, i.e., the amplification of the tube and the point (where a correction must be made to K) that the plate current deviates from the 3/2 power curve. The oscillator filament power affects the current at which saturation occurs. It would be necessary to have a chart for each value of filament voltage unless the filament voltage is set high enough so that the plate current never reaches saturation. In this case, there need be no correction of the value of K.

Several claims have been made as to the accuracy of such a system. Each measurement can be made to a certain accuracy and has a certain weighting factor.

Measurement	Error	Weight(Eq. 11)	Effective Error
E_{bb}	1%	1.00	1.00%
E_c	1%	.10	.10%
I_b	1%	1.00	1.00%
I_c	1%	.20	.20%
$e_{p(min.)}$	3%	.10	.30%
$e_{g(max.)}$	3%	.05	.15%
K	1%	1.00	1.00%
$I_{g(1)}$	5%	.20	1.00%

By taking the effective error in equation 11 and finding the most probable error, it is close to three percent. The above errors are caused by the meters used to read the currents and voltages except for the values of K and $I_{g(1)}$. The error in the R.F. grid current has been explained. The error in the value of K can be found from equation 10. The value of μ can have a possible error of 20 percent and only affect the value of K by less than 1 percent. Even if the plate current followed directly with the grid voltage, the value of K would only be in error by 1 percent.

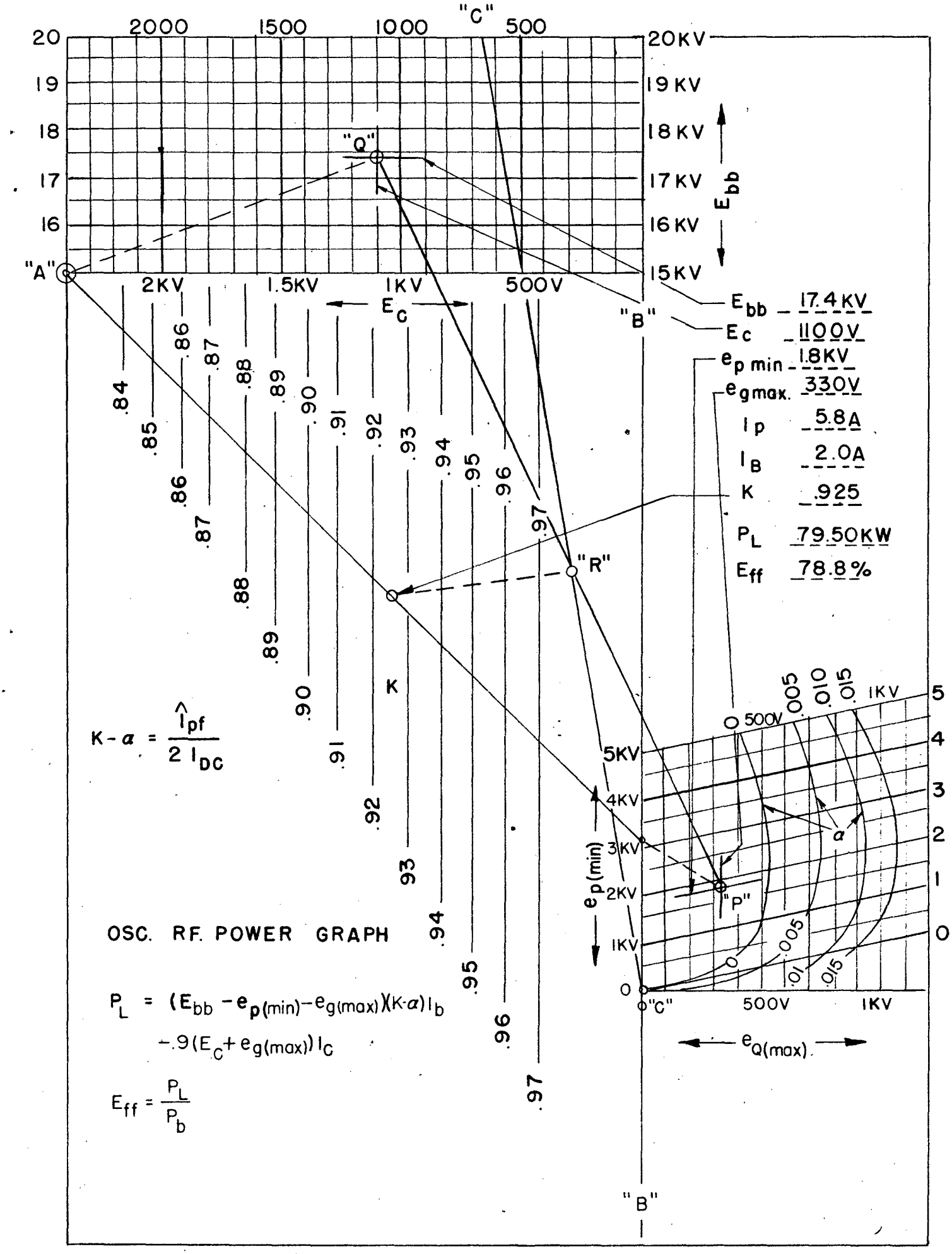
"C"
2000
1500
1000
500
20
19
18
17
16
20KV
19KV
18KV
17KV
16KV
15KV
E_{bb}
"Q"
"A"
2KV
1.5KV
1KV
500V
E_c
"B"
E_{bb} 17.4KV
E_c 1100V
$e_{p\,min}$ 1.8KV
$e_{g\,max.}$ 330V
I_p 5.8A
I_B 2.0A
K .925
P_L 79.50KW
E_{ff} 78.8%
.84
.85
.86
.87
.88
.89
.90
.91
.92
.93
.94
.95
.96
.97
"R"
K
$K-\alpha = \frac{\hat{I}_{pf}}{2\,I_{DC}}$
0
.005
.010
.015
1KV
500V
5
4
3
2
1
0
5KV
4KV
3KV
2KV
1KV
0
$e_{p(min)}$
α
"P"
"C"
500V
1KV
$e_{Q(max)}$
OSC. RF. POWER GRAPH
$P_L = (E_{bb} - e_{p(min)} - e_{g(max)})(K-\alpha)I_b$
$-.9(E_c + e_{g(max)})I_c$
$E_{ff} = \frac{P_L}{P_b}$
"B"

FIG. 22

13165

Conclusion. The absolute accuracy of the oscillator efficiencies is not the most important ing as it only affects the heating of the dee circuits through the power delivered to them. The dees are not going to fail for an inaccuracy of 3 percent. More important to the operation is the accuracy between two consecutive calculations. Two consecutive calculations are only incorrect by the error in reading the meters and in obtaining the value of K. Thus, it is safe to assume that for comparison of two calculations that they will be within 1 percent of the true ratio.

R.F. Problems

ANALYSIS OF THE CYCLOTRON DEE CIRCUITS

Introduction. The electrical circuit formed by the cyclotron dee stems and dees is shown in Fig. 23. The important factors concerned for proper operation of the radio-frequency system of the cyclotron which depend directly upon the dee circuit constants are: (a) the frequency of oscillation, (b) the relative magnitude and phase of the currents flowing in the dee stems, (c) the relative magnitude and phase of the two dee-to-ground voltages. The currents flowing in the dee stems determine the voltages induced in the coupling loops for loops of a given dimension. These determine the length of the transmission lines and their terminations, to be used in coupling the main oscillator to the dee circuits. This section is devoted to a discussion of the behavior of the electrical circuit shown in Fig. 23, the electrical circuit formed by the two dee-to-dee ground capacities, the dee-to-dee coupling capacity, and the two inductances represented by the dee stems. All circuit parameters are assumed to be lumped constants.

Determination of the Resonant Frequencies of the Cyclotron Dee Circuits. The resonant and anti-resonant frequencies of the circuit shown in Fig. 23 may be calculated (a) by setting up the simultaneous differential equations for the circuit and solving them, (b) by writing dwon the vector potential drops in accordance with Kirchoff's laws, and (c) by plotting proper reactance and susceptance curves[1].

Method of Differential Equations - Losses Neglected. Transform the circuit of Fig. 23 to the equivalent circuit of Fig. 2. The transformation equations are[2]:

$$\bar{C}_1 = \frac{\frac{1}{C_1} + \frac{1}{C_2} + \frac{1}{C_3}}{\frac{1}{C_1 C_3}}$$

$$\bar{C}_2 = \frac{\frac{1}{C_1} + \frac{1}{C_2} + \frac{1}{C_3}}{\frac{1}{C_2 C_3}} \qquad (1)$$

$$\bar{C}_3 = \frac{\frac{1}{C_1} + \frac{1}{C_2} + \frac{1}{C_3}}{\frac{1}{C_1 C_2}}$$

1. Everitt, W.L., "Communication Engineering", 2nd edition, pp. 86-87, McGraw-Hill Book Company, Inc., (1937).

2. Ibid, p. 36

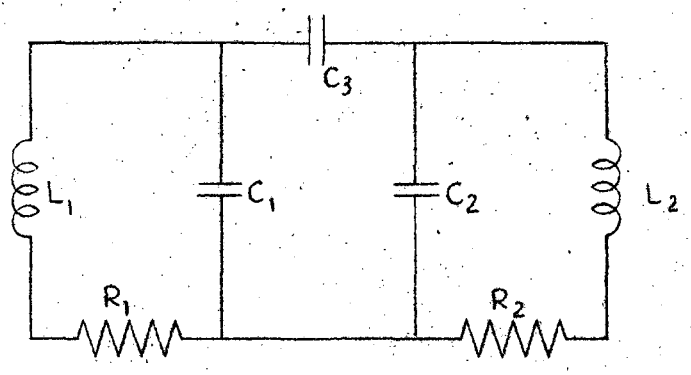

FIG. 23

ACTUAL DEE CIRCUIT ASSUMING LUMPED CONSTANTS

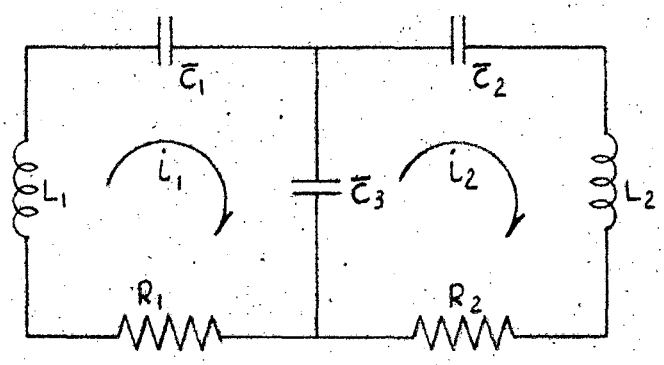

FIG. 24

EQUIVALENT DEE CIRCUIT

The currents i_1 and i_2 are the same in both cases when the transformations are rried out in accordance with equations (1).

The mesh equations are:

$$E - L_1 \frac{di_1}{dt} - \frac{q_1}{C_1} - \frac{q_3}{C_3} = 0 \tag{2}$$

$$- \frac{q_3}{C_3} - \frac{q_2}{C_2} - L_2 \frac{di_2}{dt} = 0 \tag{3}$$

Differentiating these:

$$- L_1 \frac{d^2 i_1}{dt^2} - \frac{dq_1}{dt} \frac{1}{C_1} - \frac{dq_3}{dt} \frac{1}{C_3} = 0 \tag{4}$$

$$- L_2 \frac{d^2 i_2}{dt^2} - \frac{dq_2}{dt} \frac{1}{C_2} - \frac{dq_3}{dt} \frac{1}{C_3} = 0 \tag{5}$$

Substituting the relations:

$$\frac{dq_1}{dt} = i_1$$

$$\frac{dq_2}{dt} = i_2 \tag{6}$$

$$\frac{dq_3}{dt} = i_1 - i_2$$

into (4) and (5) gives:

$$L_1 \frac{d^2 i_1}{dt^2} + \frac{i_1}{C_1} + \frac{(i_1 - i_2)}{C_3} = 0 \tag{7}$$

$$L_2 \frac{d^2 i_2}{dt^2} + \frac{i_2}{C_2} + \frac{(i_2 - i_1)}{C_3} = 0 \tag{8}$$

The solutions to equations (7) and (8) are of the form:

$$i_1 = I_1 \sin \omega t$$

$$i_2 = I_2 \sin \omega t \tag{9}$$

Differentiating these, substituting into (7) and (8), and canceling out the common tor sin ωt gives the two expressions:

$$\left(-L_1 \omega^2 + \frac{1}{C_1} + \frac{1}{C_3}\right) i_1 - \frac{i_2}{C_3} = 0 \tag{10}$$

$$-\frac{i_1}{\overline{C}_3} + \left(-L_2\omega^2 + \frac{1}{\overline{C}_2} + \frac{1}{\overline{C}_3}\right) i_2 = 0 \tag{11}$$

Let

$$\omega_1^2 = \frac{1}{L_1}\left(\frac{1}{\overline{C}_1} + \frac{1}{\overline{C}_3}\right)$$

$$\omega_2^2 = \frac{1}{L_2}\left(\frac{1}{\overline{C}_2} + \frac{1}{\overline{C}_3}\right) \tag{12}$$

where ω_1 and ω_2 are the individual resonant frequencies of mesh 1 and mesh 2, respectively, (See Figure 24).

Rewrite equations (10) and (11) by substituting equations (12):

$$\left(\omega_1^2 - \omega^2\right) L_1 i_1 = \frac{i_2}{\overline{C}_3} \tag{13}$$

$$\frac{i_1}{\overline{C}_3} = \left(\omega_2^2 - \omega^2\right) L_2 i_2 \tag{14}$$

Divide (13) by (14) to eliminate the currents:

$$\frac{\left(\omega_1^2 - \omega^2\right) L_1}{\frac{1}{\overline{C}_3}} = \frac{\frac{1}{\overline{C}_3}}{\left(\omega_2^2 - \omega^2\right) L_2} \tag{15}$$

Expand equation (15) and collect coefficients of like powers of ω:

$$\omega^4 - \omega^2\left(\omega_1^2 + \omega_2^2\right) + \omega_1^2\,\omega_2^2 - \frac{1}{L_1 L_2 \overline{C}_3^2} = 0$$

The constant term may be rewritten as follows:

$$\omega_1^2\,\omega_2^2 - \frac{1}{L_1 L_2 \overline{C}_3^2} \equiv \omega_1^2\,\omega_2^2\left(1 - \frac{\overline{C}_1\,\overline{C}_2}{(\overline{C}_1 + \overline{C}_3)(\overline{C}_2 + \overline{C}_3)}\right) = \omega_1^2\,\omega_2^2\,(1-k^2) \tag{16}$$

where $k = \dfrac{\sqrt{\overline{C}_1\,\overline{C}_2}}{\sqrt{(\overline{C}_1 + \overline{C}_3)(\overline{C}_2 + \overline{C}_3)}}$ . . . . . , the coefficient of coupling. (16A)

Making this substitution gives the equation

$$\omega^4 - \left(\omega_1^2 + \omega_2^2\right)\omega^2 + \omega_1^2\,\omega_2^2\left(1 - k^2\right) = 0 \tag{17}$$

which has the following positive roots:

$$\omega = \sqrt{\frac{\left(\omega_1^2 + \omega_2^2\right) \pm \sqrt{\left(\omega_1^2 + \omega_2^2\right)^2 - 4\,\omega_1^2\,\omega_2^2\,(1 - k^2)}}{2}} \tag{18}$$

If $\omega_1 = \omega_2 \equiv \omega_0$, then equation (18) becomes

$$\omega = \omega_0 \sqrt{1 \pm k} = \omega_0 \left(1 \pm \frac{k}{2} \pm \ldots\right) \tag{19}$$

by the binomial expansion theorem.

The frequency associated with the negative sign is the frequency at which the two dee-to-ground voltages are 180° out of phase; the frequency corresponding to the positive sign is the one at which the dee-to-ground voltages are in phase.

To determine ω_1 and ω_2 in terms of actual dee capacities, the relations expressed in equations (1) must be substituted into equations (12). The results are as follows:

$$\omega_1^2 = \frac{1}{L_1}\left(\frac{1}{C_1 + \frac{C_2\,C_3}{C_2+C_3}}\right) = \frac{1}{L_1}\left(\frac{1}{C_1 + C_3\left[1 - \left(\frac{C_3}{C_2}\right) + \ldots\right]}\right) \doteq \frac{1}{L_1\,(C_1 + C_3)} \tag{20}$$

$$\omega_2^2 = \frac{1}{L_2}\left(\frac{1}{C_2 + \frac{C_1\,C_3}{C_1+C_3}}\right) = \frac{1}{L_2}\left(\frac{1}{C_2 + C_3\left[1 - \left(\frac{C_3}{C_1}\right) + \ldots\right]}\right) \doteq \frac{1}{L_2\,(C_2 + C_3)} \tag{21}$$

The radian resonant frequencies ω_1 and ω_2, therefore, correspond very closely to the frequencies to which the cyclotron is normally tuned. Grounding one dee, say the west dee, the frequency of the east dee circuit is given by

$$\omega_1^2 = \frac{1}{L_1(C_1 + C_3)}$$

Grounding the east dee the resonant frequency of the west dee circuit is given by

$$\omega_2^2 = \frac{1}{L_2(C_2 + C_3)}.$$

When tuning the cyclotron, the procedure is to adjust $\omega_1 = \omega_2$ by alternately ground-each dee and moving the spider corresponding to the dee circuit being tuned. The frequencies given by equation (19) are the free-running frequencies. For high Q circuits they are very nearly the same as the driving frequencies.

<u>Determination of the Coefficient of Coupling.</u> From equation (19)

$$\omega \doteq \omega_0 \left(1 \pm \frac{k}{2}\right) \tag{22}$$

therefore,

$$\omega_h \doteq \omega_0 \left(1 + \frac{k}{2}\right) \tag{23}$$

$$\omega_L \doteq \omega_0 \left(1 - \frac{k}{2}\right) \tag{24}$$

Subtracting (24) from (23) and solving for k yields

$$k = \frac{\omega_h - \omega_L}{\omega_0} \tag{25}$$

The coefficient of coupling may be approximated, therefore, by measuring these three frequencies.

Determination of the Relative Magnitude and Phase of the Currents Flowing in the Dee Stems.

The circuit in Figure 25 will be used for this discussion. All circuit parameters are considered as lumped constants:

Let; I_1, I_2, I_3 = effective values of the mesh currents
E_1, E_2 = effective values of the dee-to-ground voltages

$$Q_1 = \frac{\omega L_1}{R_1}$$

$$Q_2 = \frac{\omega L_2}{R_2}$$

E = induced voltage from the coupling loop
C_1, C_2 = dee-to-ground capacities
C_3 = dee-to-dee coupling capacity
L_1, L_2 = inductances represented by the dee stems
R_1, R_2 = resistances representing losses in the individual dee circuits

$$\gamma = \frac{\omega}{\omega_0} = \frac{f}{f_0}$$ (both circuits assumed to be tuned to same frequency)

Kirchoff's law applied to each mesh gives three simultaneous linear equations:

$$\left(-j\omega L_1 - R_1 + j\frac{1}{\omega C_1}\right)I_1 + 0 \cdot I_2 + \left(-j\frac{1}{\omega C_1}\right)I_3 = -E \tag{26}$$

$$\left(-j\frac{1}{\omega C_1}\right)I_1 + \left(-j\frac{1}{\omega C_2}\right)I_2 + \left(\frac{1}{C_1} + \frac{1}{C_2} + \frac{1}{C_3}\right)\frac{j}{\omega}I_3 = 0 \tag{27}$$

$$(0)I_1 + \left(-j\omega L_2 - R_2 + j\frac{1}{\omega C_2}\right)I_2 + \left(-j\frac{1}{\omega C_2}\right)I_3 = 0 \tag{28}$$

Consider the general expression

$$Z = R + j\left(\omega L - \frac{1}{\omega C}\right) \tag{29}$$

This may be transformed into an expression involving the Q of the circuit, the ratio of frequencies, and the capacity:

$$Z = \frac{R}{\omega L} \cdot \omega^2 LC \cdot \frac{1}{\omega C} + j\frac{1}{\omega C}(\omega^2 LC - 1)$$

$$Z = \frac{1}{\omega C}\left[\frac{\gamma^2}{Q} + j(\gamma^2 - 1)\right] \tag{30}$$

Equation (30) may be written in a more useful form for this discussion:

$$Z = \frac{j}{\omega C}\left[\left(1 - \frac{j}{Q}\right)\gamma^2 - 1\right] \tag{31}$$

Rewrite equations (26), (27) and (28), substituting (31) in (26) and (28):

$$\frac{j}{\omega C}\left[\left(1 - \frac{j}{Q_1}\right)\gamma^2 - 1\right] I_1 - 0 \cdot I_2 + \left(\frac{j}{\omega C_1}\right) I_3 = +E \tag{32}$$

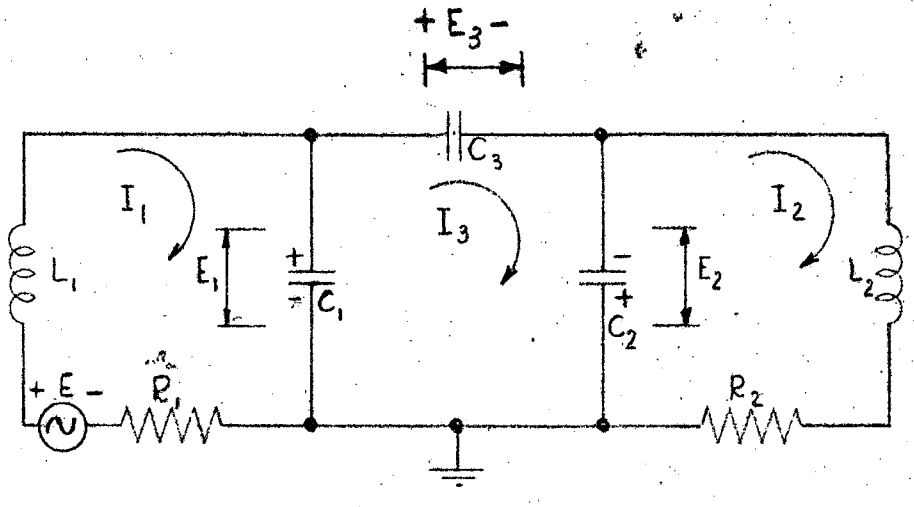

FIG. 25

$$\left(+ j\frac{1}{\omega C_1}\right) I_1 + \left(j\frac{1}{\omega C_2}\right) I_2 - \frac{j}{\omega}\left(\frac{1}{C_1} + \frac{1}{C_2} + \frac{1}{C_3}\right) I_3 = 0 \qquad (33)$$

$$-0 \cdot I_1 + \frac{j}{\omega C_2}\left[\left(1 - \frac{j}{Q_2}\right)\gamma^2 - 1\right] I_2 + \left(j\frac{1}{\omega C_2}\right) I_3 = 0 \qquad (34)$$

These equations may be solved by Crámer's rule for the three mesh currents. The determinant of the coefficients is:

$$\begin{vmatrix} \frac{j}{\omega C_1}\left[\left(1 - \frac{1}{Q_1}\right)\gamma^2 - 1\right] & 0 & +\frac{j}{\omega C_1} \\ +\frac{j}{\omega C_1} & +\frac{j}{\omega C_2} & -\frac{j}{\omega}\left(\frac{1}{C_1} + \frac{1}{C_2} + \frac{1}{C_3}\right) \\ 0 & \frac{j}{\omega C_2}\left[\left(1 - \frac{j}{Q_2}\right)\gamma^2 - 1\right] & \frac{j}{\omega C_2} \end{vmatrix} \equiv D \qquad (35)$$

The determinantal forms of the three mesh currents are:

$$I_1 D = \begin{vmatrix} E & 0 & \frac{j}{\omega C_1} \\ 0 & \frac{j}{\omega C_2} & -\frac{j}{\omega}\left(\frac{1}{C_1} + \frac{1}{C_2} + \frac{1}{C_3}\right) \\ 0 & \frac{j}{\omega C_2}\left[\left(1 - \frac{j}{Q_2}\right)\gamma^2 - 1\right] & \frac{j}{\omega C_2} \end{vmatrix} \qquad (36)$$

$$I_2 D = \begin{vmatrix} \frac{j}{\omega C_1}\left[\left(1 - \frac{j}{Q_1}\right)\gamma^2 - 1\right] & E & \frac{j}{\omega C_1} \\ \frac{j}{\omega C_1} & 0 & -\frac{j}{\omega}\left(\frac{1}{C_1} + \frac{1}{C_2} + \frac{1}{C_3}\right) \\ 0 & 0 & j/\omega C_2 \end{vmatrix} \qquad (37)$$

$$I_3 D = \begin{vmatrix} \frac{j}{\omega C_1}\left[\left(1 - \frac{j}{Q_1}\right)\gamma^2 - 1\right] & 0 & E \\ \frac{j}{\omega C_1} & \frac{j}{\omega C_2} & 0 \\ 0 & \frac{j}{\omega C_2}\left[\left(1 - \frac{j}{Q_2}\right)\gamma^2 - 1\right] & 0 \end{vmatrix} \qquad (38)$$

e complex ratio I_1/I_2 gives the relative magnitude and phase of the circulating currents the dee circuits:

$$\frac{I_1}{I_2} = \frac{-\frac{1}{\omega^2 C_2^2} - \frac{1}{\omega^2 C_2}\left[\left(1 - \frac{j}{Q_2}\right)\gamma^2 - 1\right]\left[\frac{1}{C_1} + \frac{1}{C_2} + \frac{1}{C_3}\right]}{\frac{1}{\omega^2 C_1 C_2}} \tag{38a}$$

The phase angle between the two currents is obtained by taking the ratio of the imaginary component to the real component:

$$\tan \phi = \frac{\frac{\gamma^2}{Q_2}\left(1 + \frac{C_1}{C_2} + \frac{C_1}{C_3}\right)}{\left(1 - \gamma^2\right)\left(1 + \frac{C^1}{C_3}\right) - \gamma^2 \frac{C^1}{C_2}}$$

This may be rearranged to give the more useful form:

$$\tan \phi = \frac{\gamma^2 \left[1 + \frac{C_3}{C_2}\left(\frac{C_1}{C_1 + C_3}\right)\right]}{Q_2 \left\{1 - \gamma^2 \left[1 + \frac{C_3}{C_2}\left(\frac{C_1}{C_1 + C_3}\right)\right]\right\}} \tag{39}$$

When the frequency of the applied voltage E is equal to the resonant frequency of the tuned circuits, the relative phase of the two circulating currents is nearly 180 degrees. This means that the current I_1 has a maximum positive value when I_2 has its maximum negative value, or vice versa. Therefore, I_2 is flowing in a direction opposite to that indicated by the arrow in Figure 25; it is flowing so that the polarity of E_2 is opposite to that shown, or, in other words, so that E_1 and E_2 have at every instant the same polarity.

The relative magnitude of the circulating currents is obtained by finding the absolute magnitude of equation (38a):

$$\left|\frac{I_1}{I_2}\right| = \left\{\left[\left(1 - \gamma^2\right)\left(1 + \frac{C_1}{C_3}\right) - \gamma^2 \frac{C_1}{C_2}\right]^2 + \left[\frac{\gamma^2}{Q_2}\left(1 + \frac{C_1}{C_2} + \frac{C_1}{C_3}\right)\right]^2\right\}^{1/2} \tag{40}$$

<u>Determination of the Relative Magnitude and Phase of the Two Dee-to-Ground Voltages.</u> The expression for the two dee-to-ground potential drops are: (See figure 25)

$$E_1 = j\frac{(I_1 - I_3)}{\omega C_1} \tag{41}$$

$$E_2 = -j\frac{(I_2 - I_3)}{\omega C_2} \tag{42}$$

e ratio of the dee-to-ground voltages is:

$$\frac{E_1}{E_2} = -\frac{I_1 - I_3}{I_2 - I_3}\,\frac{C_2}{C_1} \tag{43}$$

Expanding the determinantal forms of the current equations (36), (37), and (38) and substituting into equation (43), gives a complex expression for this ratio:

$$\frac{E_1}{E_2} = -\frac{\left[\left(1 + \frac{C_2}{C_3}\right)\left(1 - \gamma^2\right) - 1\right] + \frac{j}{Q_2}\,\frac{C_2}{C_3}}{\gamma^2} = -\frac{\frac{C_2}{C_3} - \left(1 + \frac{C_2}{C_3}\right)\gamma^2 + \frac{j}{Q_2}\,\frac{C_2}{C_3}}{\gamma^2} \tag{44}$$

The relative phase of the two voltages is found by taking the ratio of the imaginary term to the real term:

$$\tan\theta = -\frac{1}{Q_2\left[1 - \gamma^2\left(1 + \frac{C_3}{C_2}\right)\right]} \tag{45}$$

The relative magnitude of the dee-to-ground potential drops is obtained by finding the absolute magnitude of equation (45).

CALIBRATION OF THE DEE VOLTMETER

Method of Measuring the Dee-to-Ground Potential. The dee voltage monitoring circuit is shown in Figure 26. The probe p located in the face plate is a copper disc two inches in diameter supported on a spark plug which is screwed into the tank face plate. This small plate faces another plate five inches in diameter which is mounted on the dee; the two plates are spaced two inches apart. By utilizing a large disc for one plate and a small disc for the other plate, the effect of moving the dee is minimized since the probe p sees approximately the same surface for small changes in dee position.

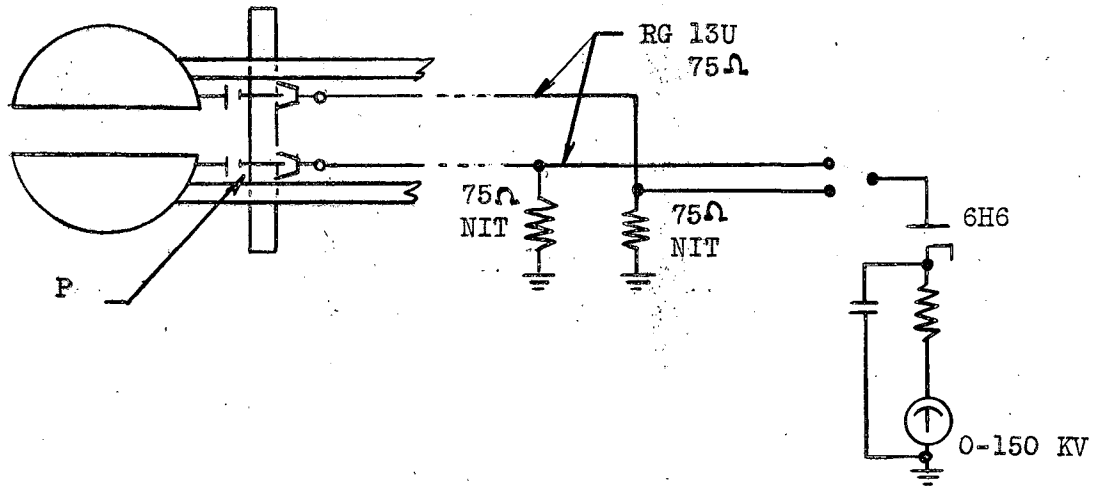

Fig. 26

Two concentric transmission lines connect the probes located on the tank face plate to the indicating circuit located in the control room. The indicating circuit is a simple diode rectifier using a 6H6 tube. The meter is calibrated linearly from 1-150 kilovolts and is adjusted to read the peak dee-to-ground voltage. A switch connected the meter to the circuit desired.

Calibration of the Dee Voltmeter. The booster oscillator is used as a low voltage source of radio frequency for calibration purposes since it is permanently connected to the system and can be tuned from the control room. The procedure is as follows:

A specially built diode voltmeter is connected to the dee by removal of a port near the target chamber. The cap of the diode connects directly to the dee; ground connection is made by a sharp knife-edge.

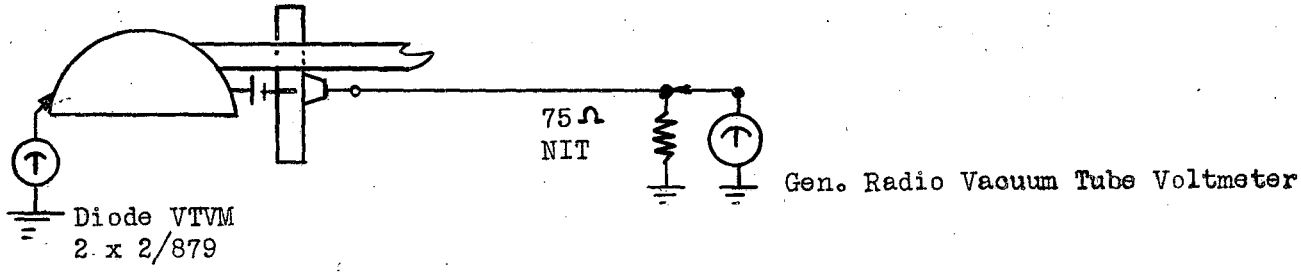

Fig. 27

The operator in the control room tunes the oscillator until the General Radio Vacuum Tube Voltmeter* reads a maximum; by interphone, the operator at the dee is informed exactly when to read the meter there. The frequency and the two meter readings are recorded. The frequency is measured with a Philco Precision Frequency Meter Type BC-221N. Three to five readings are taken; duplication of readings is easily obtained. This procedure is carried out for both dees.

The next step is to check the GRVTVM readings and the other meter readings against known standards (Weston Model 430 and 434, for example). The number obtained by dividing the actual dee voltage by the GRVTVM gives the dee-to-ground voltage per volt on the GRVTVM. When the tank is sealed, pumped down, and the main oscillator turned on, readings on the GRVTVM are again taken. The product of the meter reading by the "dee-volts per volt" factor gives the dee-to-ground voltage. The latest calibration follows:

	ACTUAL DEE VOLTAGE		GENERAL RADIO VTVM		FREQUENCY
	Uncorrected	Corrected	Uncorrected	Corrected	
East	320 peak 320 peak	340 peak 340 peak	.15 rms. .15 rms.	.175 .175	11.862 mc.
West	390 390	417 417	.20 rms. .20 rms.	.222	11.856 mc.

From the data in the table:

East: $\frac{340}{1.414(.175)} = 1376$ peak volts - actual dee voltage per peak on GRVTVM.

West: $\frac{417}{(1.414)(.222)} = 1327$ peak volts actual dee voltage per peak volt on GRVTVM.

*Hereafter referred to as GRVTVM.

n oscillator on:	east:	GRVTVM - 55.5 volts rms.
	west:	GRVTVM - 64.0 volts rms.
Actual dee voltage:	east:	1376(55.5) (1.414) = 108 KV.
	west:	1327 (64) (1.414) = 120 KV.

The cables are then disconnected from the GRVTVM and connected to the indicating unit; the calibrating potentiometers are adjusted so that the desk meter reads 108 KV when switched to the east and 120 KV when switched to the west.

Short Half Life and Bombarding and Measuring Equipment

Purpose: a. Studying the short-lived activities produced by cyclotron bombardment.
b. Obtaining excitation curves for short-lived activities (e.g., the Wigner elements at the light end of the table).

Equipment: The equipment at the present stage of development consists of three essential parts:
a. Target assembly
b. Target transfer apparatus
c. Recording mechanism

Target Assembly. Mark I. (See Fig. 28) Consists of a copper box mounted on a standard cyclotron window assembly with a slide provided so that a target may be put into place and held with a latch. After a short bombardment, the target carriage may be released and it will drop from the box under its own weight. The sample may then be removed to the counter or chemistry room. The minimum time from the end of bombardment to the counter is about 6 seconds so that this type of target can be easily used for periods of order of 10 sec or longer. There is no cooling provided for the target or window because of the usual short duration of bombardment. However, the copper box is constructed so that the target may be bombarded in an atmosphere of helium to eliminate contamination from oxygen and nitrogen recoil activity which has been found to be present in targets bombarded in air.

Mark II. (See Fig. 29) Constructed on the same principle as Mark I, (Fig. 28), this target assembly provides for pneumatic transfer apparatus for transferring the sample to the counter cave. Also, a shutter is provided to control the length of bombardment so that more uniform and absolute data may be taken. The shutter timing is adjustable so that the length of bombardment may be in the range of 0.1 to 3.0 seconds. Aluminum absorbers may be inserted in the shutter to give various beam energies for the determination of the general shape of the excitation curve but, for more accurate data, another unit is being constructed (Mark IV).

To give the record of the length of bombardment, microswitches are activated by the shutter and the signals are recorded on the same film that records the data (see below).

A special window assembly is provided to bring the target closer to the window for proton bombardments. On the 60 inch, protons are obtained as molecular hydrogen (H_2^+) which breaks up on passing through a window into two 9 Mev protons. These protons will then have a sharper radius of curvature than the 38 Mev alphas and will hit the inside edge of the target if it is at any distance from the foil. Initially, Mark II had a standard window assembly and spacer which made the target foil distance about 7 inches. This has been reduced to 4 inches with a new window assembly and, by increasing the deflector voltage, the beam is brought out from the center line and strikes the center of the target.

Mark III. Constructed for special gas bombardments, this target consists of a standard window assembly with a chamber 4 inches in diameter and approximately 12 inches long. The gas is fed

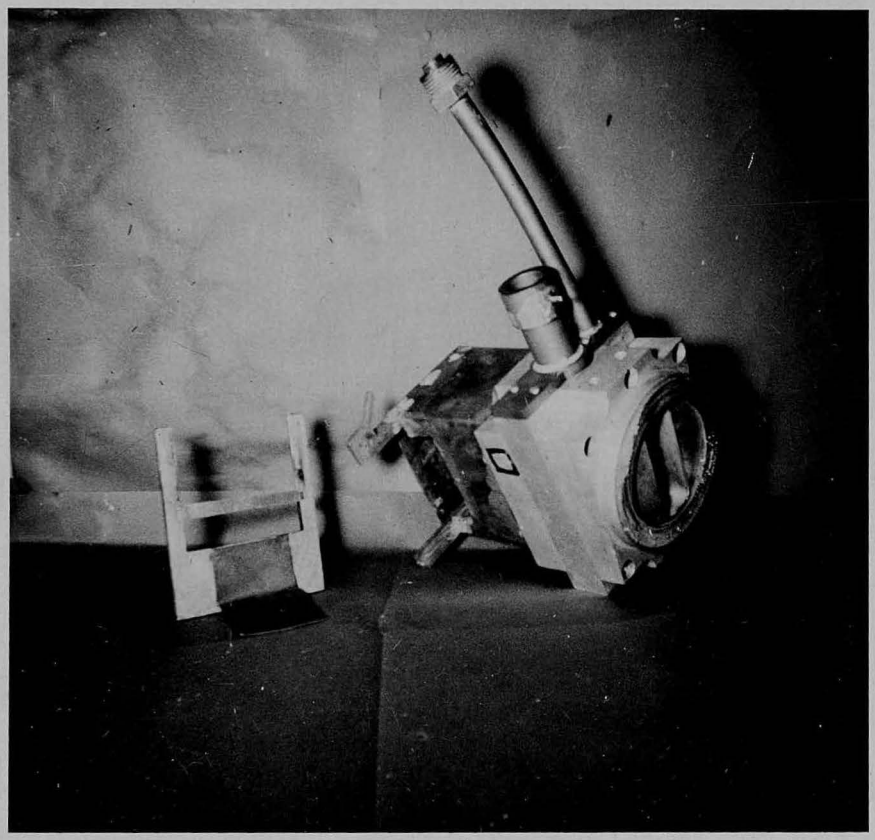

FIG. 28

MARK I

OZ-281

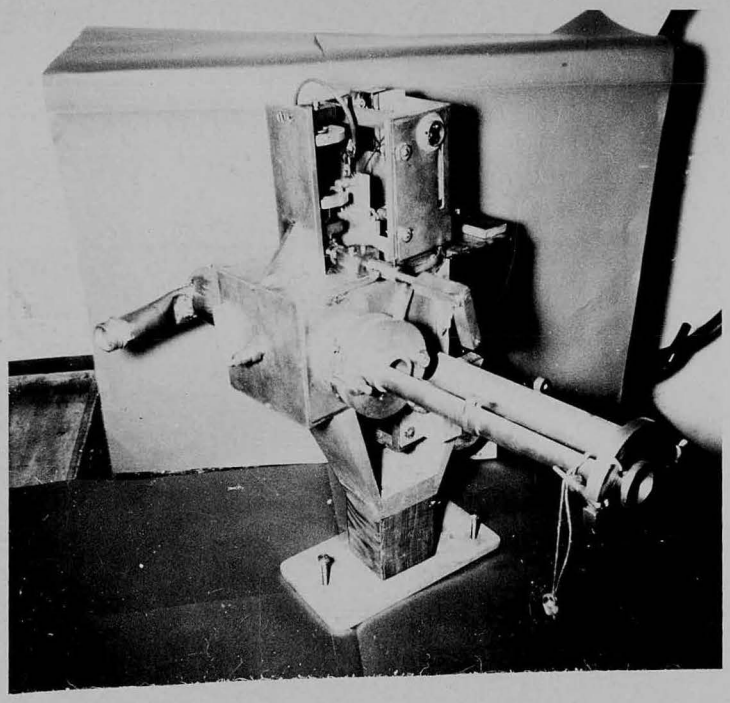

FIG. 29
Mark II

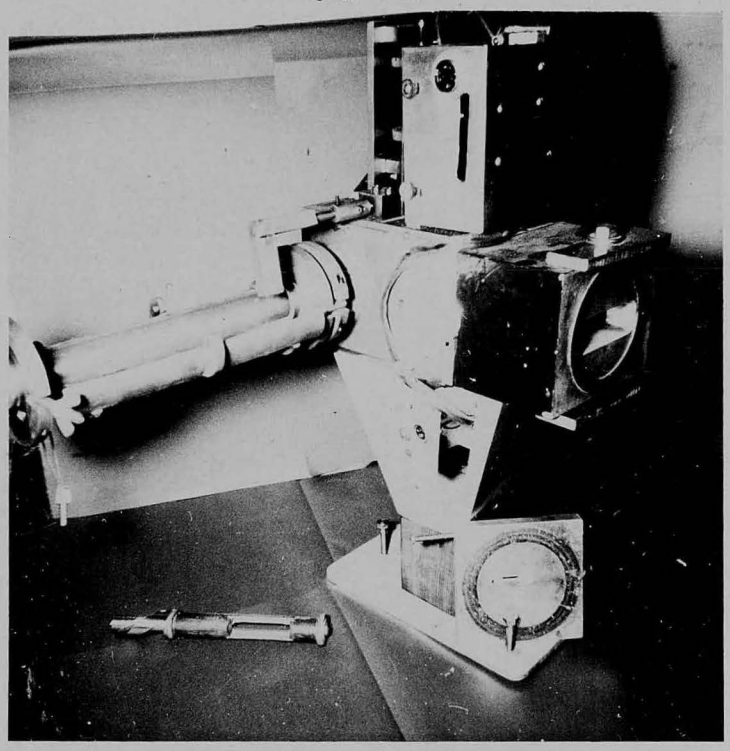

Fig. 30. Mark II showing defining slit and target carriage

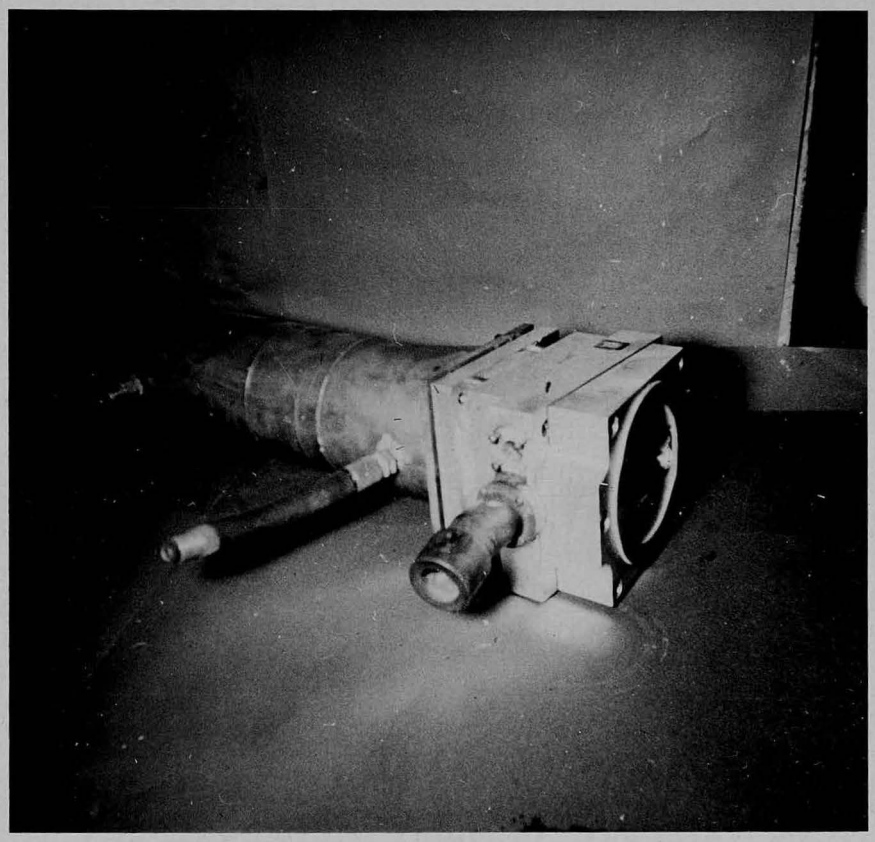

FIG. 31
MARK III

OZ-282

the back end and brought out the front end (beam end). It then passes down a tube into the counter cave. A 1 inch diameter aluminum tube approximately 4 inches in length provides the volume of gas to be counted. This section is isolated by two solenoid valves at the moment counting begins. The estimated time for the gas to pass from the target to the counter is about 1/2 second at about 20 lbs. pressure. The aluminum tube also acts as an absorber for low energy beta activities.

Mark IV. Designed, but as yet not constructed, Mark IV will utilize the shutter and start mechanism of Mark II but will provide a slit system to define the beam so that it impinges exactly on the center of the sample and prevents stray beam from hitting the carriage or the surrounding tube. This is essential if absolute data is to be obtained since the exact quantity of beam striking the sample must be known. Also, a rotating wheel with aluminum absorbers will be provided to permit a measurement of the beam energy to be made prior to or after the bombardment.

Transfer Apparatus. The transfer apparatus consists of a 1 inch inner diameter pipe about 20 feet in length leading from the target assembly outside the water barrier to the counter cave. When the shutter drops, it trips and air solenoid and the compressed air shoots the target carriage down the tube. The transit time is recorded on photographic paper by micro-switches in the tube (see below). The time is in the range of 0.5-0.6 seconds. This can be decreased by a few modifications of the equipment, but to date this has not been necessary since it is possible to measure half lives as short as 0.1-0.2 seconds (e.g., At^{212} - .2 sec alpha emitter). In order to insure a correct orientation of the carriage when it stops under the counter (see Fig. 32), a special head is mounted on the carriage which engages a key in the stop mechanism. Also, a set of 4 springs in the tube slows the carriage down just before it hits the key and prevents it from bouncing back. The carriage is made of polystyrene since, if any stray beam hits it, the resulting activities will be known and are not in a range which will obscure any very short periods.

Measuring and Recording Equipment. For measuring the activity, two counters are in use at the present time for alpha and beta active samples. The alpha counter is a methane counter working either with or without a scale of 64 if desired; the beta counter is a thin window counter (3 mg/cm^2 mica) Scott type with a Richardson scaler (8 and 64). An anthracene counter is also being installed at the present time.

The counter cave consists of concrete walls 16 to 32 inches thick, lined with 1/16 to 1/8 inch of cadmium and 4 inches lead. A cadmium lined paraffin door, which is removable by the overhead crane, and a 3 inch lead door provide access to the counter and target carriage stop mechanism. The cave is located outside the 5 feet thick water tanks of the water barrier. With the activity from "hot" targets nearby and from the cyclotron, the background count in the cave is about 2 counts per second.

A Heiland Recording Oscillograph, Type A401R, and a mechanical register are used to record the data. The oscillograph consists of a bank of six galvanometers, a timing device and a camera with drive motor. The camera uses a photosensitive paper (Eastman #809) which runs at a speed of 7-8 inches per second. The galvanometers put individual traces on the paper and are now utilized as shown in Figure 33. The timer is a vibrating, reed device providing 0.01 sec markers on the paper.

The frequency response of the galvanometers sets an upper limit of about 400-500 pulses per second or counting rates of 25-30,000 c/m without a scaler. This indicates that it is adequate to handle the full range of the present crystal counters with a scaler, and the use of such a counter will make better statistics available than is possible with the ordinary

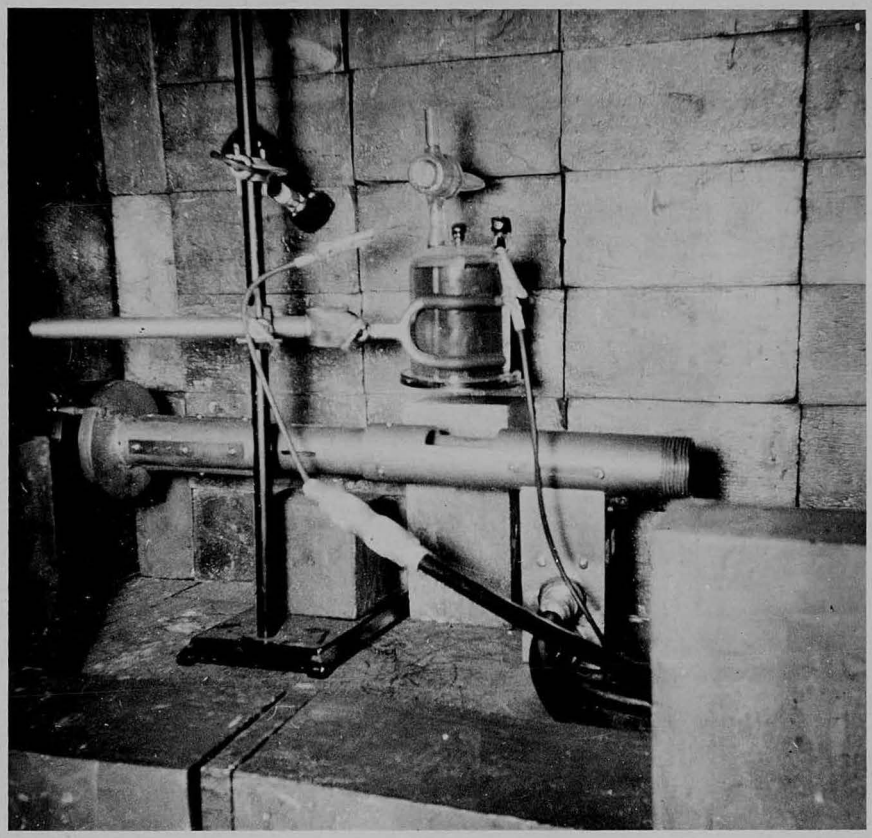

FIG. 32

COUNTER AND TARGET CARRIAGE STOP MECHANISM

OZ-283

tube. At present the equipment is being used to look for and check the periods of and O^{14} and to obtain an excitation curve for At^{212}. The half life of At^{212} was found to be 0.2 seconds.

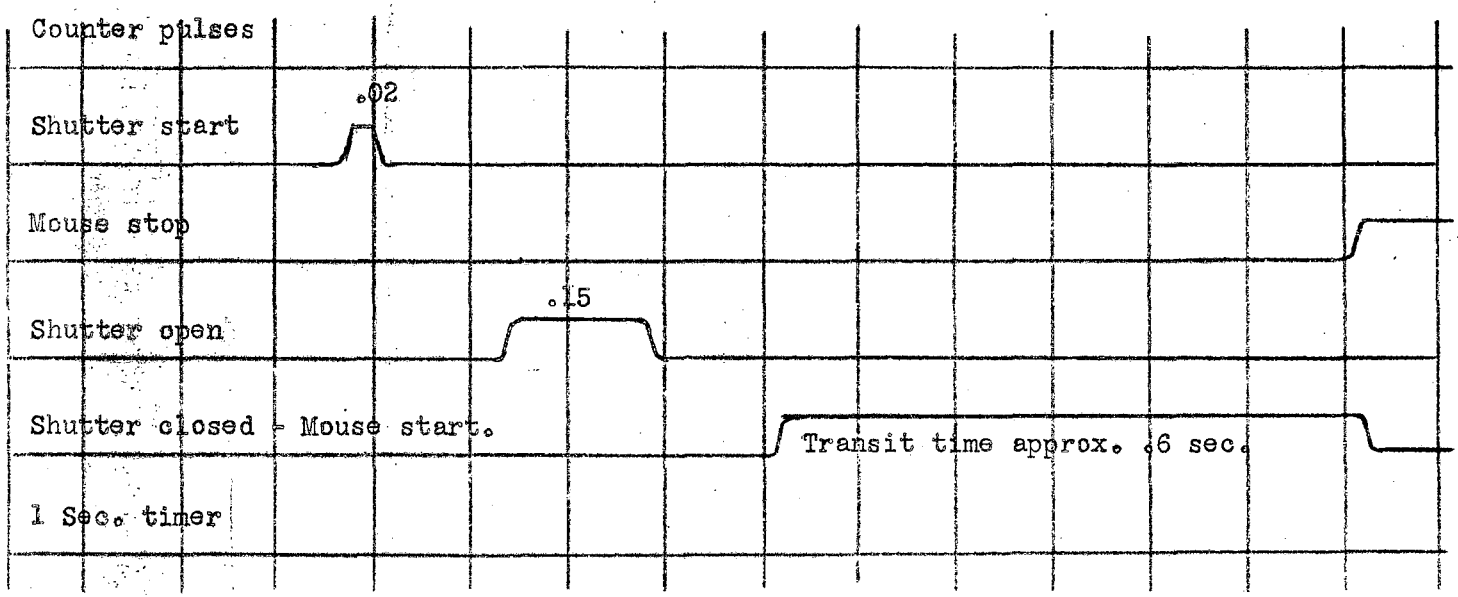

Fig. 33

GENERAL APPEARANCE OF TIMING PULSES ON THE FILM

Selection of Exit Radius for the Cyclotron.

The Energy-Radius Graph. Recently the possibility has been suggested of finding a better beam current at the same energy, by decreasing the radius and raising the magnetic field of the 60 inch cyclotron. The suggestion was based on the fact that for the same energy, the slope of the field $\frac{dH}{dr}$ decreases as the field is raised. An enclosed graph, Fig. 34, shows the relations between H, r, and E for the magnet measurements of May 14, 1946. It was also known that the dee voltage required to accelerate the ion to a given energy is very sensitive to the field slope. For example, a computation of the phase-resonance equation showed that changing the field at the exit radius from 0.97 Ho to 0.95 required an increase in dee voltage of 1.4 Vo, where Vo and Ho are present operating values. Consequently, the above suggestion makes it appear that the same energy could be obtained with less dee voltage, or with more beam current for the same dee voltage (assuming an increase in Vo brings an increase in beam current).

Evaluation of the Radius. To evaluate this scheme means that one must be able to answer the general question on how to choose the exit radius for a cyclotron. The enclosed graph shows that the 60 inch magnet can support circular orbits with maximum energies up to 54 Mev alpha particles but, in this region of maximum energies, the field is in the order of .94 Ho to .89 Ho. The degree to which the maximum energy can be approached in a particle acceleration depends the dee voltage. Using the phase equation, one could compute lines of constant dee voltage the energy-radius graph, and it would then be a simple matter to choose an operating energy and radius. We have assumed that the oscillator frequency can be adjusted to match the ion frequency. If the ions are to be deflected onto a target external to the circular orbit, then the radius choice is further restricted, because the ions are most easily deflected in the

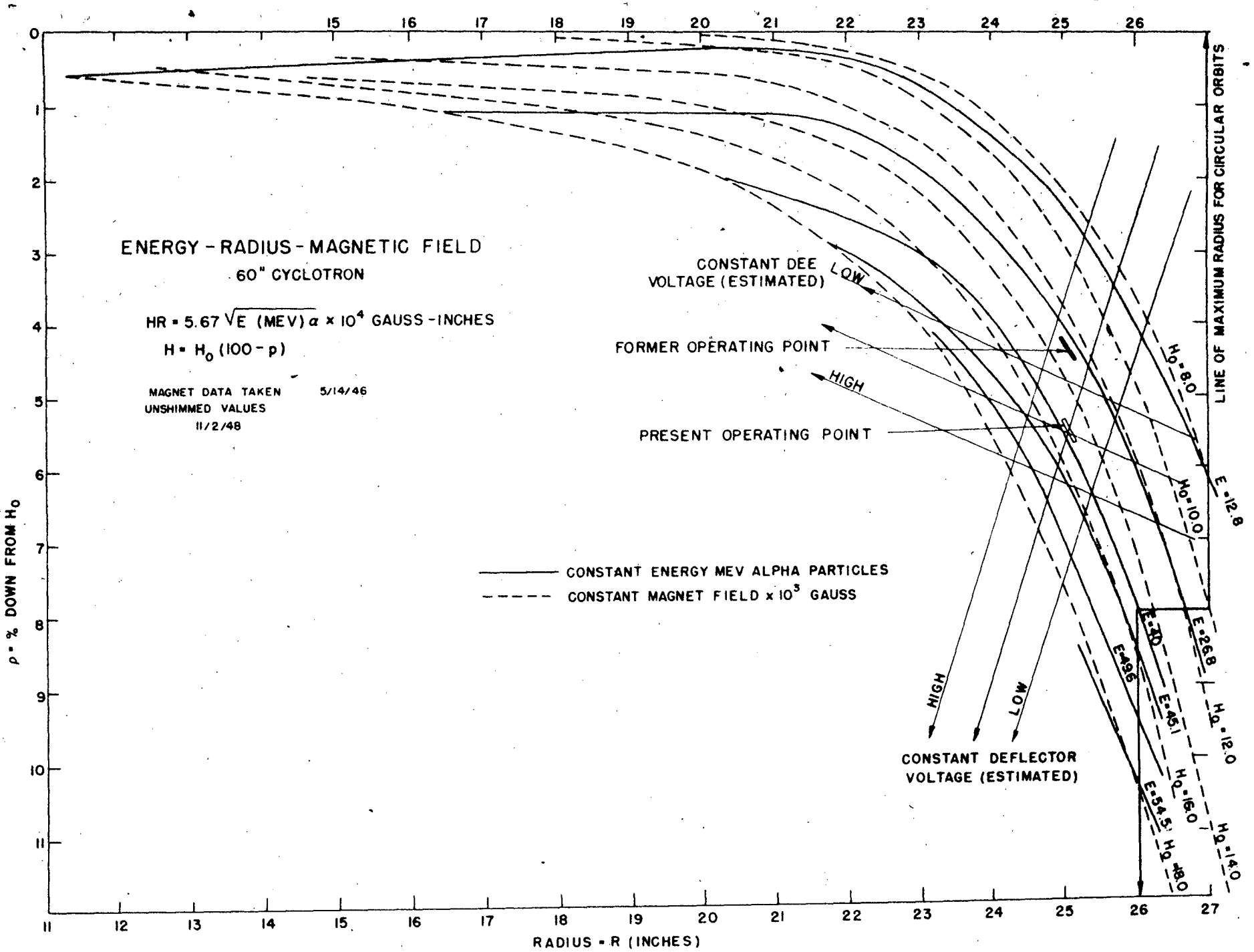
ENERGY - RADIUS - MAGNETIC FIELD
60" CYCLOTRON
HR = 5.67 √E (MEV) α × 10⁴ GAUSS-INCHES
H = H₀ (100 - p)
MAGNET DATA TAKEN 5/14/46
UNSHIMMED VALUES
11/2/48
CONSTANT DEE VOLTAGE (ESTIMATED)
LOW
FORMER OPERATING POINT
HIGH
PRESENT OPERATING POINT
CONSTANT ENERGY MEV ALPHA PARTICLES
CONSTANT MAGNET FIELD x 10³ GAUSS
HIGH
LOW
CONSTANT DEFLECTOR VOLTAGE (ESTIMATED)
LINE OF MAXIMUM RADIUS FOR CIRCULAR ORBITS
H₀ = 8.0
H₀ = 10.0
E = 12.8
E = 26.8
H₀ = 12.0
H₀ = 14.0
H₀ = 16.0
H₀ = 18.0
E = 40
E = 45.1
E = 49.6
E = 54.5
ρ = % DOWN FROM H₀
RADIUS = R (INCHES)

Fig. 34

OZ-323

gion of maximum energy for a particular field, (i.e., a small force at right angles to the orbit, will pull the ion into a region where rapidly (Hr) becomes too small to support a circular orbit). Thus, for a given magnetic field, we have a conflict between the dee voltage and the deflector voltage. The dee voltage limits the maximum energy and the deflector voltage system sets a limit on the minimum energy which can be pulled out of its circular orbit. The exit radius must lie within the overlapping energy range. The deflected ion path has been computed graphically for the 60 inch so one in principal could show lines of constant deflector voltage on the energy-radius graph, assuming a given deflector geometry. The estimated direction and qualitative magnitudes of lines of constant deflector and dee voltage have been sketched on the graph.

Conclusion. In the above we have outlined how a combination graphical-computing method may be used to present the important cyclotron parameters, and from which one should be able to choose the best exit radius. The computation of the values of dee voltage and deflector voltage for a general graph such as is enclosed is rather long even with the aid of a small computing machine, but it should be emphasized that the procedure is known and has been used. At present, there is not enough computed data to specify the range of allowable radii for the 60 inch cyclotron.

3. Synchrotron

Marvin Martin

The past quarter has been devoted to rebuilding the synchrotron in an attempt to correct the suspected reasons for failure to obtain a betatron beam. The three possible causes are believed to be (1) lack of a satisfactory vacuum, (2) insufficient uniformity of the magnetic field, and (3) the existence of an insulating coating on the vacuum chamber walls. Two of these troubles were corrected by installing the fused silica doughnut in place of the plastic vacuum chamber formerly used. A pressure lower than 10^{-5} mm. of mercury has been obtained in the silica vacuum chamber which, according to betatron experience, should be entirely adequate in this machine. The inside of the doughnut has been carefully coated with a palladium film giving a surface resistivity of approximately 20 ohms which is recommended by those experienced in betatron operation.

The adjustment of the magnetic field has proved to be a very difficult problem. Numerous methods of compensation for the azimuthal phase variations were tried and it was discovered that most of the errors were introduced by a short lived residual field caused by the necessity for flux crossing the plane of laminations. The time required for this residual field to become smooth was greater than a half period of the 60 cycle magnet frequency. Considerable improvement, however, was possible by using the first half-cycle for injection, thereby allowing the interval between magnet pulses (nine 60-cycle periods) for this residual field to decay. In addition to the substantial gain made by using the first half-cycle, a number of radial wires above and below the gap have been used to smooth out local variations in the field. These corrections have resulted in reducing the total variations to .4 gauss at the time of injection (8 gauss). The peak magnet excitation has been reduced to 5000 gauss in order to make this compensation easier. Since reassembly of the magnet with the above corrections, a considerable increase in the intensity of electrons making one revolution has been noted.

Recent experiments have been concerned with the problem of investigating a phosphorescence in the anthracene-lucite detector. It is now believed that this phosphorescence results from electron bombardment of the lucite rod. A new detector has been made in which the lucite is protected from electron bombardment and will be tested in the immediate future.

Further injector development has resulted in a gun which will hold 120 kilovolts in the test tank. This gun will be installed in the synchrotron immediately and should considerably improve the performance of the machine since during observations to date, it has been noted that increased injection energy has greatly increased the signal amplitude for one turn electrons.

Following installation of these improvements, additional attempts will be made to observe a betatron beam by adjusting the betatron flux and making minor changes in the azimuthal magnetic field variations. The resonant cavity and oscillator will not be installed in the machine until after a betatron beam has been observed.

4. Linear Accelerator

L. Alvarez

The initial performance of the accelerator was described somewhat over a year ago. At that time, the operation was very erratic, and the beam current was about 10^{-11} ampere. The reliability of operation now corresponds to that of an average cyclotron. 32 Mev protons are available about 95 per cent of the time the Van de Graaff injector is operating, indicating that the high frequency part of the accelerator is remarkably free from trouble. The beam current now averages 10^{-9} ampere. A program to increase this by a factor of 100 or more now under way involves four features: (1) The focusing grids have been made more transparent, (2) the duty cycle of operation is being increased, (3) the entering ions are being bunched into a smaller phase angle by radiofrequency techniques, and (4) a new ion source is being installed. (When the improvement factors of these four programs are multiplied together, the result is of the order of 10^3.)

The main source of difficulty with the Van de Graaff has been repeated failure of the direct current generator in the shell. During the past month this generator has been replaced by a 400-cycle alternator. At the same time, the machine, including the accelerating column, is being thoroughly cleaned.

RECEIVED